Development of Anisotropic Polymeric Substrates for Tendon Tissue Engineering

A thesis submitted to the National University of Ireland Galway for the Degree of Doctor of Philosophy

By

Andrew English

February 2015

Network of Excellence for Functional Biomaterials

National University of Ireland, Galway

Research Supervisor: Dr Dimitrios Zeugolis

Table of Contents

List of Appendices

List of Figures

Chapter 1

Figure 2.6: Scanning electron micrographs of random and aligned orientated electro-spun scaffolds (a and b respectively). Scanning electron micrographs of mono-dispersed microspheres embedded within aligned orientated electro-spun scaffolds (c). Scanning electron (d) and optical (e) micrographs of three-dimensional aligned nano-structured composites.

Figure 2.7: Stress-strain curves of dry and wet aligned and random orientated electro-spun fibrous mats. Aligned electro-spun mats in dry and wet state exhibited a region of rising stress, followed by a region of decreasing stress, whilst random electro-spun mats in dry and wet state revealed a region of rising stress, followed by a region of constant gradient and then a region of decreasing stress, which persisted up to fracture.

Figure 2.8: Fibre orientation resulted in different deformation mechanisms. Aligned orientated electro-spun mats (a) exhibited a split fracture mode, whilst random orientated electro-spun mats (b) displayed a delayed split fracture mode.

Figure 2.9: alamarBlue® metabolic activity assay results for bovine tenocytes over a 7 day culture period. No significant difference in metabolic activity of bovine tenocytes was observed among the different scaffold conformations by day 7 ($p>0.05$). * indicates significant difference.

Figure 2.10: Bovine tenocytes were seeded on solvent casted and random orientated electro-spun mats exhibited a random cytoskeleton and nuclei orientation for all time points. However, when the bovine tenocytes were seeded on aligned orientated electro-spun mats, they appeared to orientate perpendicularly to the substrate

topography. The actin cytoskeleton of the cells was stained red with rhodamine-conjugated phalloidin; nuclei were stained blue with DAPI. Arrows indicate the orientation of the substrate topography.

Chapter 3

Figure 3.1: For the tendon model, we induced an incision to the side of the leg (A) to expose the tendon by moving the skin (B). Using a 2 mm in diameter punch biopsy, we created a wound at the centre of the tendon, where the structured substrates were then inserted (C). The implants were secured using a PLGA film (D) and wounds were closed using biodegradable sutures (E).

Figure 3.2: For the subcutaneous model, incisions were created on the back. The substrates were then inserted subcutaneously and wounds were closed using biodegradable sutures.

Figure 3.3: AFM analysis of isotropic (A) and structured (B, C, D) substrates. Quantification of isotropic control roughness, groove width, line width and groove depth (E).

Figure 3.4: DAPI (blue) and rhodamine-conjugated phalloidin (red) indicates that tenocytes aligned parallel to the substrate topography of groove depths of ~317 nm and ~1988 nm, whilst a random morphology was observed on isotropic substrates and substrates with groove depth of ~37 nm.

Figure 3.5: Tenocyte alignment to the substrate topography further confirmed when the angle of cells parallel to the underlying topography was between 0 – 20 ° on substrates with groove depth of ~317 nm and ~1988 nm (A). Substrates with groove depth of ~317 nm and ~1988 nm induced the highest cytoskeleton elongation (C). No significant difference was observed in cellular area (B) and nuclei aspect ratio (D) as a function of surface topography.

Figure 3.6: No significant difference in cell viability was detected as a function of topography and time in culture.

Figure 3.7: No significant difference in cell metabolic activity was detected as a function of topography and time in culture.

Figure 3.8: No significant difference in cell proliferation was detected as a function of topography and time in culture.

Figure 3.9: Gene analysis demonstrates an overall gene upregulation at day 1 only on cells seeded on ~1988 nm in depth substrates, whilst at day 10 substrates with groove depth ~317 nm and ~1988 nm had more upregulated genes than substrates with groove depth of ~37 nm. At day 10, bone sialoprotein and aggrecan were upregulated on all substrates.

Figure 3.10: Histological examination at the tendon repair site showed a disorganised collagen fibre pattern for all implanted anisotropic substrates.

Figure 3.11: In a subcutaneous model, the structured substrates did not induce parallel to the substrate topography host cell orientation.

List of Tables

Chapter 1

Chapter 2

Chapter 3

Acknowledgements

Foremost, I would like to sincerely thank Dr Dimitrios Zeugolis for his support and patience throughout this project. My sincere thanks also go to the rest of Dr Zeugolis's group for their support and help over the course of this project.

I would also like to thank all the members, staff and students of the Network of Excellence for Functional Biomaterials. I would like to specifically thank Dr Carolyn Holladay, Ms Ayesha Azeem, Mr Abhigyan Satyam and Mr Pramod Kumar.

This project would not have been possible without the support of our collaborators, to whom I am sincerely grateful. I would like to acknowledge Alan Hynes from CCAN (Collaborative Centre for Applied Nanotechnology) and Niall Rooney from Proxy Biomedical. For the help with the nano imprinting, I would like to thank Prof Graham Cross and Dr Bhawana Tripathi from the Centre for Research on Adaptive Nanostructures and Nanodevices. Also, for their support with the gene analysis, I would like to thank Dr Graham Riley and Dr Eleanor Jones from the University of East Anglia, UK.

I would like to thank my family and friends and specifically my brothers, John and David, all the Richardson clan and all the O'Connors, who were always supportive and encouraging through my studies.

Finally, I would like to thank my partner Orla. Thank you for supporting me for the last few years.

List of Abbreviations

BSA	Bovine Serum Albumin
CTRL	Control
DAPI	4’,6-Diamidino-2-phenylindole
DHT	Dehydrothermal
DMEM	Dulbecco’s modified Eagle’s medium
DMSO	Dimethyl Sulfoxide
DPPA	Diphenylphosphoryl azide
ECM	Extra Cellular Matrix
EDC 1-	Ethyl-3-[3-dimethylaminopropyl]carbodiimide hydrochloride
EDTA	Ethylenediaminetetraacetic Acid
EtOH	Ethanol
FBS	Foetal Bovine Serum
FITC	Fluorescein isothiocyanate
GAGs	Glycosaminoglycans
GTA	Glutaraldehyde
HBSS	Hanks Balanced Salt Solution
HMDC	Hexamethylene diisocyanate
IMS	Industrial methylated spirit
MMC	Macromolecular Crowding
mRNA	Messenger Ribonucleic acid
NHS	*N*-hydroxysulfosuccinimide
PBS	Phosphate-buffered saline
PCL	Polycaprolactone
PDMS	Polydimethylsiloxane

PLA	Poly(lactic acid) or polylactide
PLGA	Poly(glycolide-co-lactide)
PMMA	Poly(methyl methacrylate)
RPM	Rotations per minute
SEM	Scanning Electron Microscope
UV	Ultraviolet

Abstract

Tendon injuries and degenerative conditions constitute an unmet clinical need with pharmacological strategies and tissue grafts failing to recapitulate native tendon function. Advancements in bioengineering have enabled the development of various scaffold fabrication technologies, using natural or synthetic in origin polymers that closely imitate the native tendon anisotropic architecture. Anisotropic collagen sponges, extruded collagen fibres, isoelectric focused collagen fibres, electro-spun polymeric fibres and imprinted polymeric substrates are at the forefront of scientific and technological research and innovation. Herein, we ventured to assess whether one-step functionalisation of electro-spun fibres with nano / micro particles is possible and whether anisotropic imprinted substrates can maintain tenogenic phenotype *in vitro* and promote functional neotissue formation *in vivo*.

Starting with electro-spinning, mechanical evaluation demonstrated that aligned orientated electro-spun fibres exhibited significant higher stress at break values than their random aligned counterparts and random orientated electro-spun fibres exhibited significant higher strain at break values than the aligned orientated scaffolds. While maintaining fibre structure, a co-deposition method of spraying and electro-spinning was developed that enabled the incorporation of microspheres within the three-dimensional structure of the scaffold. Of significant importance is that bovine tenocytes aligned perpendicular to the fibre orientation, possibly due to the absence of mechanical tension.

With respect to imprinting, it is still unclear whether surface topography can be translated into a clinically functional response *in vivo* at the tissue / device interface. Herein, we demonstrated that anisotropic substrates with groove depth of ~317 nm and ~1988 nm promoted human tenocyte alignment parallel to underlined topography

in vitro. However, none of the topographies assessed (~37 nm, ~317 nm and ~1988 nm groove depth) induced parallel to the substrate cellular orientation in a subcutaneous model and none of the topographies promoted directional tenogenesis *in vivo*. Further, the rigid poly(lactic-co-glycolic acid) substrate used induced trans-differentiation towards chondrogenic / osteogenic lineage, as evidenced by gene analysis. Collectively, these data indicate that two-dimensional imprinting technologies are useful tools for *in vitro* cell phenotype maintenance, rather than for directional neotissue formation, should multifactorial approaches that consider both surface topography and substrate rigidity are established.

Overall, both electro-spinning and imprinting technologies show great promise for tendon repair and regeneration. Imprinting could be the ideal technology for cell phenotype maintenance *in vitro*, as we can closely control architectural features. Although it was not investigated here, electro-spinning is the ideal technology for *in vivo* positive outcomes, as the three-dimensional architecture would allow directional tissue formation within the fibrous construct.

Keywords

Electro-spun polymeric fibres; Nano- and micro- particles; Imprinted polymeric substrates; Tendon repair and regeneration

Chapter 1

Introduction

Sections of this chapter have been published at:

Cigognini, D., Lomas, A., Kumar, P., Satyam, A., **English, A.**, Azeem, A., Pandit, A., Zeugolis, D.* *Engineering in vitro microenvironments for cell-based therapies and drug discovery*. Drug Discovery Today, Vol. 18, No. 21-22, pp. 1099-1108, 2013.

Lomas, A., **English, A.**, Biggs, M., Pandit, A., Zeugolis, D.I. *Engineering anisotropic 2D and 3D structures for tendon repair*, in Tendon regeneration: Understanding tissue physiology and development to engineer functional substitutes. Elsevier Science. Editors: Reis, R.L., Gomes, M.E., Rodrigues, M.T.

1.1. Introduction

Tendons are dense connective tissues that join muscle to bone and play a vital role in overall joint stability and function. Collagen type I fibrils are described as long crystals that are arranged in an anisotropic fashion [1-8]. These collagen fibrils are organised into primary, secondary and tertiary bundles, responsible for the mechanical resilience of the tissue (**Table 1.1**). Primary fibre bundles consist of a collection of fibrils with diameters of around 1-4 μm [9]. Secondary fibre bundles group together the sub-fascicles into larger units of approximately 150-1000 μm in diameter [10], which are then grouped into tertiary fibre bundles of diameter 1000-3000 μm [11]. The diameter of the bundles is directly related to the macroscopic size of the tendon; small tendons like the flexors and extensors have small diameter bundles, whilst large tendons, such as the Achilles, have thicker fibre bundles [12]. Endotenon divides the bundles of collagen fibrils into areas that can be supplied with blood and nutrients. Further, endotenon is made up of a criss-cross pattern of collagen types I and III and high concentrations of glycosaminoglycan molecules that due to their water-holding capacity, allow tendon fascicles glide over each other [12].

Injuries to tendons and ligaments are some of the most frequently encountered disorders presented in the clinic and can range in severity from a small sprain to complete rupture. Due to the inherent poor healing properties of tendons, injuries frequently result in long-term disability, which leads to development of degenerative disorders in later life. In USA, over 75,000 Achilles tendon ruptures, 55,000 rotator cuff injuries and over 5 million new cases of tennis elbow are diagnosed annually, with associated healthcare costs to run into the billions of dollars [13]. Tissue grafts are considered the gold standard in large tendon injuries. However, such materials have failed to restore full function due to mechanical failure at graft / tissue interface

and the formation of fibrous adhesions preventing the repaired tendon from gliding correctly [14, 15]. As the world population increases and ages, tendon injuries will become even more prevalent, placing a further burden on already stretched healthcare systems, making the development of novel strategies to manage all types of tendon injuries and degenerative conditions imperative. To this end, anisotropic scaffolds, in form of sponges, fibres and imprinted substrates, alone [16, 17] or in combination with cells [18-20] are at the forefront of scientific and technological research and innovation for tendon repair and regeneration.

Table 1.1: Mechanical properties of human tendons are evidently dependent on the anatomical location and the age of the patient. High load bearing tendons (e.g. Achilles) have higher ultimate strain and stress than low load bearing tendons (e.g. supraspinatus). Ultimate stress is also reduced as the age is increased.

Tendon	Patient / Donor age	Ultimate load (N)	Ultimate strain (%)	Ultimate Tensile Stress (UTS) (MPa)	Reference
Achilles	36 - 50 79 - 100	3534 ± 919 2735 ± 1371	21 22	73 48	[21]
Rotator cuff	28 - 98	662 ± 223	≥ 11	30 ± 14	[22, 23]
Patellar	29 - 50 64 - 93	3855 ± 550 3346 ± 1167	14 ± 6 15 ± 5	65 ± 16 54 ± 10	[24, 25]
Extensor	22 - 78	2914 ± 644	9 ± 1	66 ± 12	[26]
Tibialis	15 - 45 56 - 65	3062 ± 699 3004 ± 603	20 ± 5 20 ± 6	127 ± 28 111 ± 16	[27]

1.2. Anisotropic Sponges

Freeze-drying has the capacity to produce biomaterials with an interconnected porous structure. Collagen / glycosaminoglycans (GAGs) sponges were the first scaffolds produced and since then, they have been used for several clinical targets including, skin, bone, tooth, muscle and cartilage [28-35]. In combination with bone marrow stem cells, collagen sponges enhanced neotissue formation with mechanical properties of approximately 75% of the normal tissue [36]. However, due to the random porosity of the porous structure, mechanical stimulation is essential [37]. To this end, moulds; unidirectional temperature gradients during the freeze-drying process (**Figure 1.1**); particle/porogen leaching; and centrifugation followed by freeze-drying have been shown to induce anisotropic morphology [38-54]. Anisotropic collagen / GAG scaffolds with elongated pores induced physiological elongated tendon cell morphology [55]. Further, a highly porous core surrounded by a high-density shell collagen / GAG conformation significantly increased the mechanical properties of the scaffold, making it suitable for tendon repair [56]. In general, problems with low mechanical resilience and non-uniform cell mediated contraction, which result in phenotypic losses *in vitro* and disorganised tissue formation *in vivo*, imposed the need for alternative scaffold fabrication technologies.

Figure 1.1: Temperature gradient freeze drying technique to fabricate anisotropic collagen sponges. A) Illustrates the random porous structure of typical collagen sponge and B) illustrates the degree of alignment introduced to the sponge using the modified temperature gradient technique [56].

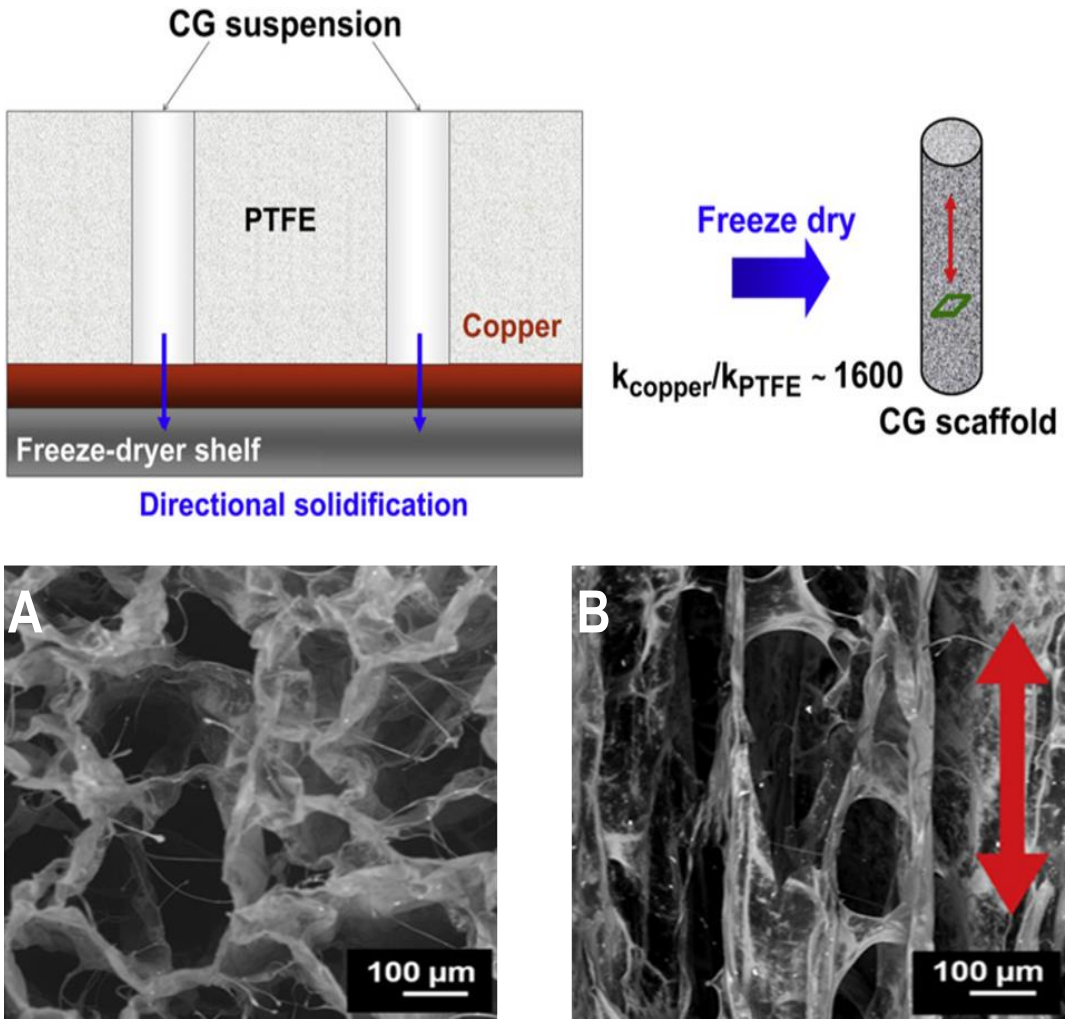

1.3. Anisotropic Self-assembled Fibres

Collagen micro-fibres can be produced through extrusion in a series of phosphate buffers and cross-linking solutions maintained 37 °C (**Figure 1.2**) [57, 58]. The produced fibres, similar to native tendon, have diameter range 50 to 650 μm; and are comprised of structurally aligned and highly crystalline collagen fibrils [59-63]. To enhance the mechanical properties of the produced fibres, numerous chemical, physical and biological cross-linking methods have been assessed over the years (**Table 1.2**), resulting in materials with similar mechanical properties to the native tissue [64, 65]. Subject to the cross-linking method employed, fibres with crevices and ridges along the longitudinal fibre axis are produced that facilitate bidirectional cell attachment, migration and growth (**Figure 1.3**) [66, 67]. Functionalisation strategies, based on transglutaminase, have also been used as means to enhance the bioactivity of the fibres [68]. When extruded collagen fibres were used in a rabbit Achilles tendon model, they were rapidly integrated with the repairing tissue and allowed the formation of aligned connective tissue similar to that of autologous tendon graft and almost identical to normal tendon [69, 70]. Further, when these fibres were used in a canine anterior cruciate ligament model, they were completely remodelled and integrated into the host tissue after 12 weeks implantation [71]. In a rabbit anterior cruciate ligament model, these fibres produced a crimped neoligament tissue at 20 weeks post implantation, with failure loads 2-4 times the pre implanted levels [72]. In an ovine model, it was demonstrated that integration is subject to the cross-linking method employed [73], imposing the need for the development of biocompatible cross-linking methods.

Isoelectric focusing has also been used to produce aligned collagen fibres with characteristic D periodicity, piezoelectricity and mechanical properties (**Table 1.2**) proportional to native tendon fibres [74-77]. *In vitro* evaluation of isoelectrically produced collagen fibres induce directional cell growth of tendon-derived fibroblasts and bone marrow stem cells [78]. Further, these fibres have been shown to induce tenogenic differentiation of bone marrow stem cells, even in the absence of growth factors [79]. *In vivo* in a rabbit patellar tendon defect model was promising, as the implanted fibres did not induce severe inflammation and were integrated into the native tendon over a period of 8 months [80]. It is expected that scalability issues would be addressed in the years to come, bringing these technologies to clinical setting.

Figure 1.2: Demonstrates the fabrication technique use to generate collagen fibres. By combining single fibres into bundles anisotropic fibrous scaffold are generated.

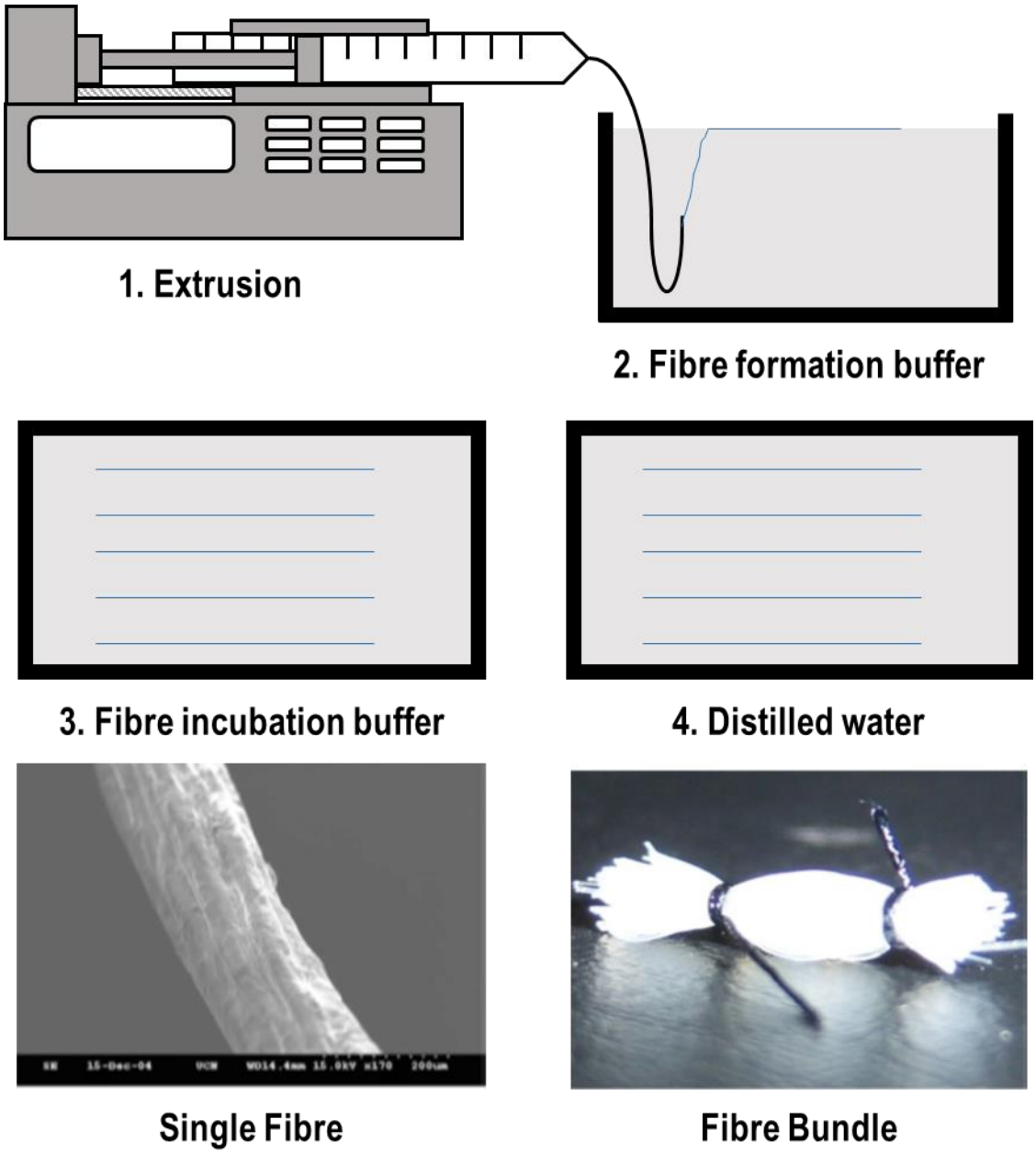

Table 1.2: Mechanical properties of self-assembled collagen fibres produced through extrusion and isoelectric focusing, as a function of various cross-linking methods.

Fabrication Method	Cross-linker	Fibre Diameter (μm)	Maximum Stress (MPa)	Maximum Strain (%)	Reference
Extrusion	Non-Cross-linked	298	3	33	[64]
	0.625% Genipin	340	7	40	
	EDC/NHS	373	3	54	
	DPPA	310	5	44	
	HMDC	336	17	45	
	DHT	264	2.46	26	
	UV	252	3	21	
	Myrica rubra	205	28	15	[65]
	0.625% Genipin	118	34	13	[67].
	EDC/NHS	228	3	10	
	PEG	119	19	8	

	EDC	215	5	23	[81]
	EDC/NHS	137	10	23	
Isoelectric focussing	0.1% Genipin	62	21	6	[77]
	2% Genipin	56	55	9	

Figure 1.3: Non-cross-linked fibres (CTRL) exhibit the smoothest surface topography; glutaraldehyde cross-linked fibres (GTA) exhibit the roughest surface topography; and 4-star poly(ethylene glycol) ether tetrasuccinimidyl glutarate (PEG) fibres exhibit intermediate smoothness / roughness. Using skin fibroblasts (7 days in culture), it is evidenced that only CTRL and PEG fibres support cell growth and cellular elongation along the longitudinal fibre axis. Green: Cytoskeleton; Red: Nuclei [67].

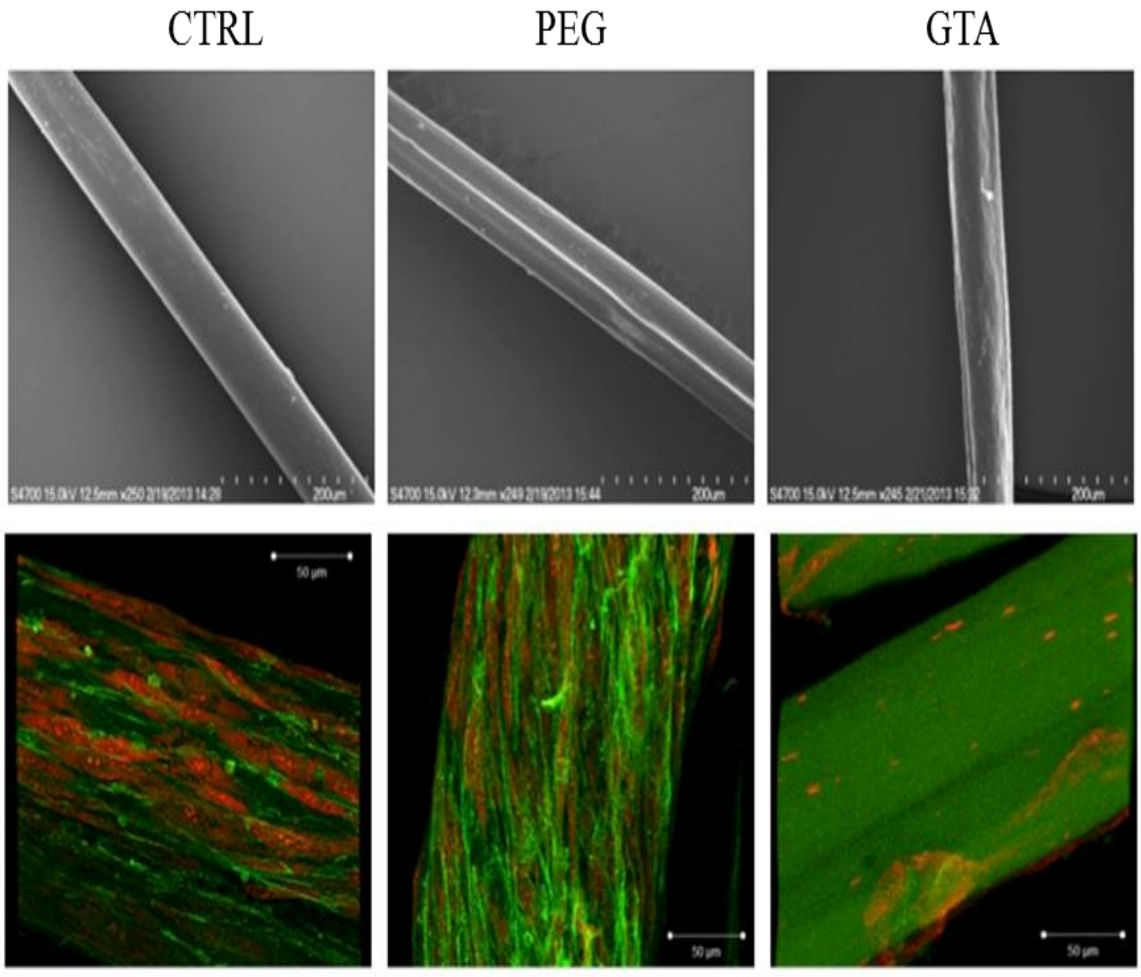

1.4. Anisotropic Electro-spun Fibres

Electro-spinning is a highly versatile polymer processing technique for forming non-woven fibrous mats, originally developed by Lord Rayleigh in the 19th century for the textile industry. Over the next 100 years a number of researchers have worked on optimising, perfecting and understanding the electro-spinning process [82, 83] for various applications, including textiles, catalysis, energy and filtration [84-89]. The first paper of electro-spinning in the field of tissue engineering was published in 2001 [90], and since then it has become a reference scaffold fabrication technology for numerous clinical targets, including skin [91-93] and cartilage [94-100], given the inherent capacity of the process to create nano- to micro- scale fibres of controlled spatial orientation and to incorporate therapeutics / biologics with controlled release capacity [101-108]. Incorporation of a rotating collector (**Figure 1.4**) in the fabrication process was considered a developmental landmark, as aligned fibrous constructs were materialised, creating an artificial hierarchical biomimicry, suitable for soft tissue repair, such as neural [109-115], blood vessel [116] and corneal [117, 118], musculoskeletal applications [119], such as bone [120-135], tendon [136-139] and bone-tendon interface [140] and cancer cell migration [141, 142]. Such aligned scaffolds, as opposed to randomly orientated scaffolds, have been shown to maintain tendon-derived cell phenotype, as evidenced by physiological elongated cellular morphology and tenogenic protein and gene expression. The aligned scaffolds also demonstrate similar to native tendon mechanical properties (**Table 1.3**). To increase further mechanical resilience, without compromising structural anisotropy and cellular function, sacrificial fibres / removable ice-crystals [143, 144], knitting [145] and twisting [146] have been proposed.

Figure 1.4: A) Shows the electro-spinning set up for creating randomly orientation fibrous scaffolds. The fibres are collected on the grounded stationary collector plate. B) Aligned electro-spun scaffolds are fabricated by the incorporation of a rotational collector.

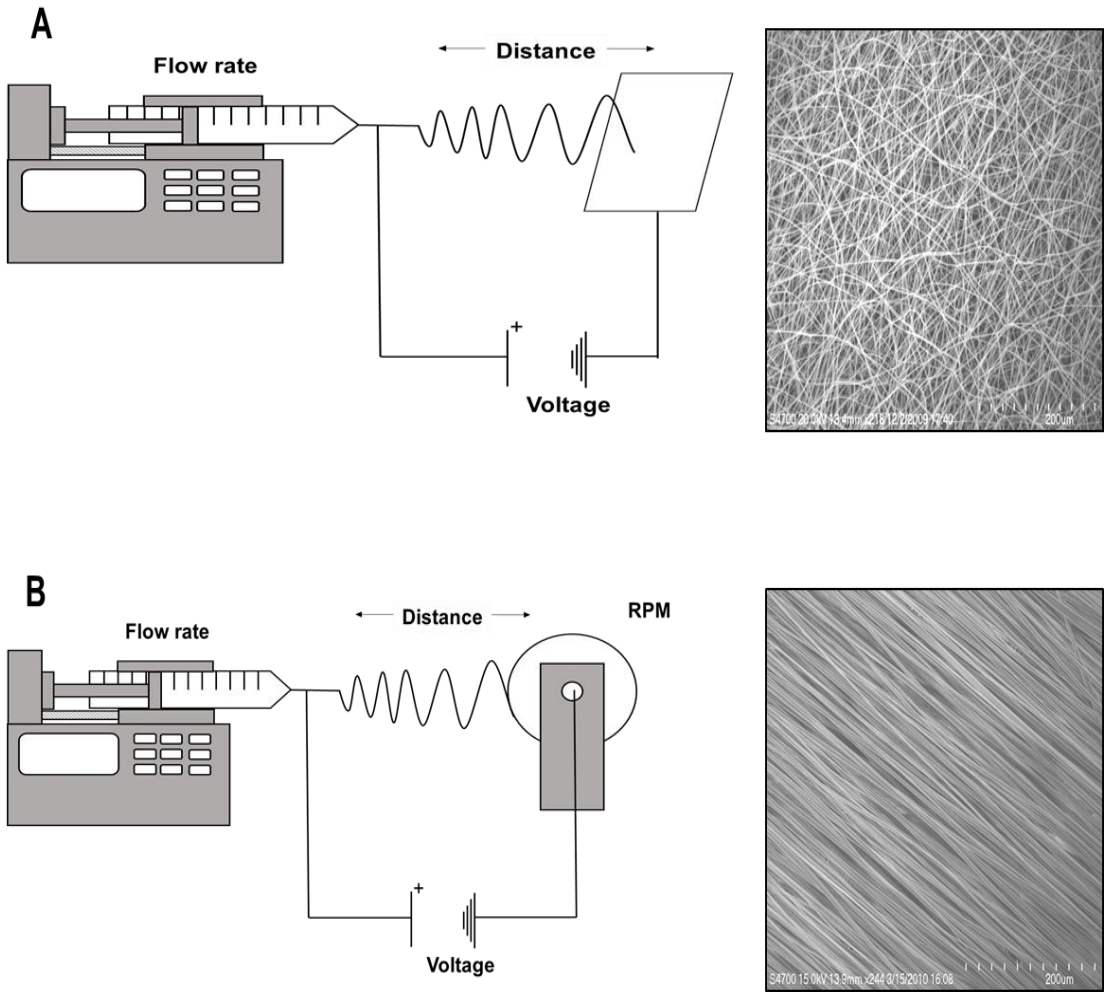

Table 1.3: Representative examples of mechanical properties of electro-spun scaffolds, as a function of polymer, conformation and functionalisation.

Material	Orientation	Functionalisation	Fibre diameter (nm)	Ultimate stress (MPa)	Reference
PCL	Aligned	No	≤ 500	5	[146]
	Random			0.5	
PLGA	Aligned	No	615	12	[147]
	Random		568	4	
PLA	Aligned	No	430	25	[136]
	Random		450	2	
Collagen	Random	No	Not stated	19	[148]

Specifically to tendon repair, *in vitro* studies using rotator cuff fibroblasts demonstrated cell orientation and matrix deposition conformed to the anisotropic organisation of the electro-spun scaffold, while providing significantly higher mechanical properties than that of randomly orientated scaffolds [147]. Anisotropic electro-spun scaffolds induced bidirectional human tendon stem/progenitor cell morphology, hindered osteogenesis, as evidenced by alkaline phosphatase activity and alizarin red staining, and induced significantly higher tendon-specific gene expression than on the random fibres in both normal and osteogenic culture media. Further, the anisotropic architecture increased collagen production and induced an organised deposition of collagen matrix after 1 week *in vivo* [136]. Anisotropic electro-spun collagen fibres, although integrated and induced neotissue bidirectional orientation in a rabbit Achilles large defect model, they were only half of the mechanical properties of the uninjured tissue [148], which is not surprising, given that the electro-spinning process induces collagen denaturation [62, 149]. However, functionalisation with extracellular matrix molecules and growth factors induced tenogenic differentiation of mesenchymal progenitor cells [150], adipose-derived stem cells [151, 152], skeletal muscle-derived cells [153] and skin fibroblasts under static mechanical strain [154], with the latter showing promising results even in large (porcine) model [155].

Multi-hierarchical scaffolds have been produced combining additive manufacturing and electro-spinning. The additive manufacturing produces large size pores, essential for cell and mass transportation, whilst the fibrous component provides suitable structures for cell attachment; the potential of such materials has been demonstrated for bone-ligament [156] and muscle-tendon [157] tissue engineering. Electro-spun fibres have also been combined with hydrogels contained cells / and or biologics for

more effective localised delivery for various clinical targets [158-160], including tendon [161]. However, the complexity of such devices poses questions with respect to the commercialisation potential of such scaffolds. It is also worth pointing out that the necessity of alignment has been questioned, as a recent study demonstrated that fibre diameter is more crucial than alignment for mesenchymal stem cell differentiation towards tenogenic lineage [162]. Further, other studies have suggested that mechanical loading may be necessary for tenogenic phenotype maintenance / tenogenic differentiation of stem cells, as has been suggested previously [163-165]. It is evidenced that electro-spinning has significantly improved our knowledge in tendon tissue engineering and we are expecting to see this technology in clinic within this decade. Nonetheless, the inability to create constructs with precise special control has triggered investigations into imprinting.

1.5. Anisotropic Imprinted Substrates

Numerous lithography polymer processing technologies have been developed over the years that offer the ability to create substrates with precise control of dimensional features down to nano-scale (**Table 1.4**). For example, optical lithography involves selectively exposing a light sensitive material to a light using a mask with the desired features, then the substrate is etch with solvents to remove either the exposed (positive photoresist) or unexposed (negative photoresist) regions [166, 167]. Alternatively, focused ion beam lithography creates patterns by direct impingement of a small spot onto a substrate [168, 169]. The great benefit of imprint lithography is that it allows for the precise addition of a surface topography to a wide range of materials, while maintaining specific physicochemical properties. However, photolithography is limited in applications in tissue engineering, where specific material properties are required, such as adsorption and functionalities [170]. Soft lithography involves creating a master mould by casting liquid polymer precursor, such as poly(dimethyl siloxane), against a topographically patterned mould. Then the master mould is used to create the substrate, the resultant substrates have the reversed pattern. In principle, the ultimate limit can be pushed to less than 0.5 nm. Nano-imprinting lithography utilises a thermoplastic polymer film, which is heated above its glass transition temperature and then a rigid mould is pressed into the film. After the polymer has cooled below its glass transition temperature, the polymer film is removed. Nano-imprinting lithography has been used to create features as small as 5 nm (**Figure 1.5**) [171-173].

Table 1.4: Advantages and disadvantages of various lithography technologies.

Method	Minimum feature size	Common materials used	Advantages	Disadvantages	Reference
Optical	$\leq 0.1\ \mu$m	Silicon	Large areas are possible	High cost of masks with sub-micron feature size	[174]
Ion beam	≤ 10 nm	PMMA, aluminium fluoride	No requirement for a photoresist mask	Slow processing time for large areas	[175, 176]
Soft	0.5 nm	PDMS, Hydrogels	Mould scan be reused	Moulds are required	[177, 178]
Nano-imprint	5 nm	Amorphous metals, Silicon	Low cost, high throughput, high resolution process	Only certain materials can be used	[179]

Figure 1.5: Illustrates the imprinting lithography technique.

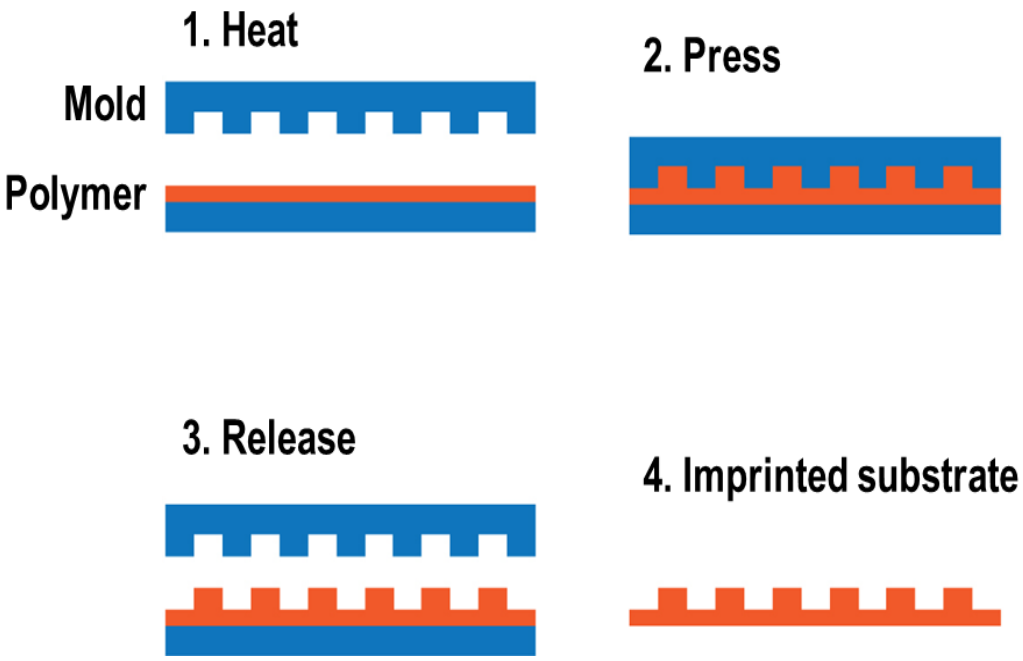

Anisotropic arrays of various topographical patterns (**Figure 1.6**) have been shown to be potent tools in maintaining phenotype of primary cells, such as osteocytes [180, 181] and to differentiate stem cells towards osteogenic [181-187] or tenogenic [188] lineage. Anisotropic grooved substrates have been used to study the effect of substrate topography on cellular morphology, adhesion, motility and phenotype on a range of permanently differentiated and stem cells [189-191]. With the ability to create anisotropic topographies on the same size scale as those found in tendon, imprinted substrates have been used to investigate the relationship between substrate topography and tendon cell behaviour / phenotype maintenance. Groove widths smaller than the width of the cells not only promote alignment and elongation, but also maintain tendon cell phenotype. Further, cell with lost phenotype, regained expression of tenogenic markers, when they were grown on structured substrates [192]. Grooves that are larger than the dimensions of the cell, on the other hand, have no beneficial effect on phenotype maintenance [193]. Although a lab-on-chip technology allows simultaneously assessment of numerous topographies [183], the unlimited number of potential features prohibits identification of the optimal surface topography to maintain cellular phenotype *in vitro*. To address this issue, tendon slices were used as stamps to imprint true tendon topography on synthetic substrates and subsequently used to effectively differentiate stem cells towards tenogenic lineage [194]. Despite the very promising *in vitro* results to-date, imprinted substrates have failed to induce directional tissue formation in bone [195] setting, suggesting that three-dimensional configuration is essential for recapitulation of native tissue function *in vivo*.

Figure 1.6: Topographical features ranging from the micro- to nano- scale can modulate cellular morphology and cellular adhesion through the reinforcement of focal adhesions. Tenocytes cultured on 2 µm wide anisotropic grooves exhibit contact guidance mediated cellular and focal adhesion alignment. Focal adhesion formation is perturbed in osteoblast cells cultured on 120 nm diameter pits. Conversely, focal adhesion formation is enhanced in neuroblastoma cells cultured on 20 nm diameter pillars. Red: actin, Green: paxillin, Blue: nuclei [180].

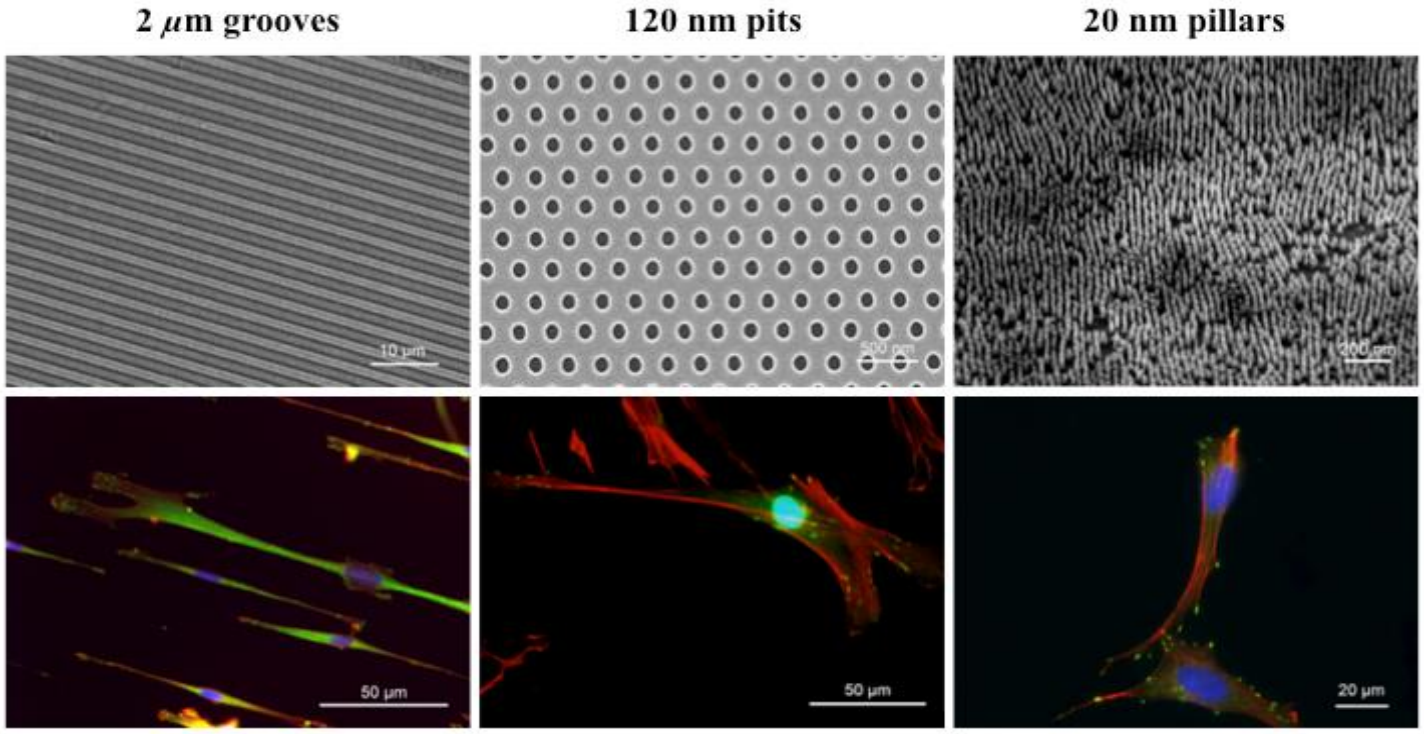

1.6. Project Objectives

Electro-spinning and imprinting lithography technologies are at forefront of scientific and technological research and innovation. However, the full potential of these technologies has yet to be realised in tendon tissue engineering and regenerative medicine. Herein, we ventured to validate the following hypotheses:

Phase I:

Hypothesis:

Electro-spun constructs, with functionalisation capacity, can be fabricated to provide topographical guidance to permanently differentiated cells.

Objectives:

1. Fabrication of electro-spun scaffolds with random and anisotropic architectural features.
2. Fabrication of electro-spun scaffolds constructs with functionalisation capacity, with the ability to tailor the temporal release while not affecting structural integrity.
3. Structural (orientation), biophysical (mechanical) and biological (cellular morphology and metabolic activity) assessment of the produced scaffolds.

Phase II:

Hypothesis:

There is an optimal anisotropically ordered topography that will facilitate maintenance of fundamental cellular functions *in vitro* and directional neotissue formation *in vivo*.

Objectives:

1. Fabricate anisotropically ordered substrates with topographical features ranging from nano- to micro- scale.
2. Evaluate tenocyte response to the structured substrates by assessing cell-shape parameters (e.g. alignment, elongation, and shape) and cellular functions (e.g. metabolic activity, viability and phenotype).
3. Assess neotissue formation using a rat patellar tendon model.

1.7. References

[1] Brodsky Doyle B, Hukins DWL, Hulmes DJS, Miller A, White S, Woodhead Galloway J. Low angle X-ray diffraction studies on stained rat tail tendons. Biochimica et Biophysica Acta (BBA) - Protein Structure 1978;535:25-32.

[2] Orgel JPRO, Irving TC, Miller A, Wess TJ. Microfibrillar structure of type I collagen in situ. Proc Natl Acad Sci U S A 2006;103:9001-9005.

[3] Wang JHC, Jia FY, Gilbert TW, Woo SLY. Cell orientation determines the alignment of cell-produced collagenous matrix. Journal of Biomechanics 2003;36:97-102.

[4] Cox G, Kable E, Jones A, Fraser I, Manconi F, Gorrell MD. 3-Dimensional imaging of collagen using second harmonic generation. Journal of Structural Biology 2003;141:53-62.

[5] Williams RM, Zipfel WR, Webb WW. Interpreting Second-Harmonic Generation Images of Collagen I Fibrils. Biophysical Journal 2005;88:1377–1386.

[6] Campagnola PJ, Loew LM. Second-harmonic imaging microscopy for visualizing biomolecular arrays in cells, tissues and organisms. Nat Biotechnol 2003;21:1356-1360.

[7] Theodossiou TA, Thrasivoulou C, Ekwobi C, Becker DL. Second harmonic generation confocal microscopy of collagen type I from rat tendon cryosections. Biophysical Journal 2006;91:4665-4677.

[8] Stoller P, Kim BM, Rubenchik AM, Reiser KM, Da Silva LB. Polarization-dependent optical second-harmonic imaging of a rat-tail tendon. J Biomed Opt 2002;7:205-214.

[9] Rhee SH, Suetsugu Y, Tanaka J. Biomimetic configurational arrays of hydroxyapatite nanocrystals on bio-organics. Biomaterials 2001;22:2843-2847.

[10] Butler DL, Gooch C, Kinneberg KR, Boivin GP, Galloway MT, Nirmalanandhan VS, Shearn JT, Dyment NA, Juncosa-Melvin N. The use of mesenchymal stem cells in collagen-based scaffolds for tissue-engineered repair of tendons. Nature Protocols 2010;5:849-863.

[11] Wang JH. Mechanobiology of tendon. Journal of Biomechanics 2006;39:1563-1582.

[12] Kannus P. Structure of the tendon connective tissue. Sc J Med Sc Sp 2000;10:312-320.

[13] Chen J, Xu J, Wang A, Zheng M. Scaffolds for tendon and ligament repair: Review of the efficacy of commercial products. Expert Review of Medical Devices 2009;6:61-73.

[14] Boyer MI, Goldfarb CA, Gelberman RH. Recent progress in flexor tendon healing. The modulation of tendon healing with rehabilitation variables. Journal of Hand Therapy 2005;18:80-86.

[15] P. Sharma NM. Tendinopathy and tendon injury: The future. Disability and Rehabilitation 2008;30:1733-1745.

[16] Lomas A, Ryan C, Sorushanova A, Shologu N, Sideri A, Tsioli V, Fthenakis G, Tzora A, Skoufos I, Quinlan L, O'Laighin G, Mullen A, Kelly J, Kearns S, Biggs M, Pandit A, Zeugolis D. The past, present and future in scaffold-based tendon treatments. Adv Drug Deliv Rev In Press.

[17] Kew S, Gwynne J, Enea D, Abu-Rub M, Pandit A, Zeugolis D, Brooks R, Rushton N, Best S, Cameron R. Regeneration and repair of tendon and ligament tissue using collagen fibre biomaterials. Acta Biomater 2011;7:3237-3247.

[18] Spanoudes K, Gaspar D, Pandit A, Zeugolis D. The biophysical, biochemical, and biological toolbox for tenogenic phenotype maintenance in vitro. Trends Biotechnol 2014;32:474-482.

[19] Gaspar D, Spanoudes K, Holladay C, Pandit A, Zeugolis D. Progress in cell-based therapies for tendon repair. Adv Drug Deliv Rev In Press.

[20] Abbah S, Spanoudes K, O'Brien T, Pandit A, Zeugolis D. Assessment of stem cell carriers for tendon tissue engineering in pre-clinical models. Stem Cell Res Ther 2014;5:38.

[21] Lewis G, Shaw KM. Tensile properties of human tendo achillis: Effect of donor age and strain rate. The Journal of Foot and Ankle Surgery 1997;36:435-445.

[22] Reilly P, Amis AA, Wallace AL, Emery RJ. Mechanical factors in the initiation and propagation of tears of the rotator cuff. Quantification of strains of the supraspinatus tendon in vitro. Journal of Bone and Joint Surgery 2003;85:594-599.

[23] Halder A, Zobitz ME, Schultz F, An KN. Mechanical properties of the posterior rotator cuff. Clinical Biomechanics 2000;15:456-462.

[24] Johnson GA, Tramaglini DM, Levine RE, Ohno K, Choi NY, Woo SL. Tensile and viscoelastic properties of human patellar tendon. J Orthop Res 1994;12:796-803.

[25] Hashemi J, Chandrashekar N, Slauterbeck J. The mechanical properties of the human patellar tendon are correlated to its mass density and are independent of sex. Clinical Biomechanics 2005;20:645-652.

[26] Donahue TL, Gregersen C, Hull ML, Howell SM. Comparison of viscoelastic, structural, and material properties of double-looped anterior cruciate ligament grafts made from bovine digital extensor and human hamstring tendons. Journal of Biomechanical Engineering 2001;123:162-169.

[27] Greaves LL, Hecker AT, Brown CH, Jr. The effect of donor age and low-dose gamma irradiation on the initial biomechanical properties of human tibialis tendon Allografts. American journal of sports medicine 2008;36:1358-1366.

[28] Yannas IV, Lee E, Orgill DP, Skrabut EM, Murphy GF. Synthesis and characterization of a model extracellular matrix that induces partial regeneration of adult mammalian skin. Proc Natl Acad Sci U S A 1989;86:933-937.

[29] Maruguchi T, Maruguchi Y, Suzuki S, Matsuda K, Toda K-I, Isshiki N. A new skin equivalent: Keratinocytes proliferated and differentiated on collagen sponge containing fibroblasts. Plastic and Reconstructive Surgery 1994;93:537-544.

[30] Glowacki J, Mizuno S, Greenberger JS. Perfusion Enhances Functions of Bone Marrow Stromal Cells in Three-Dimensional Culture. Cell Transplantation 1998;7:319-326.

[31] Kim B-S, Nikolovski J, Bonadio J, Smiley E, Mooney DJ. Engineered smooth muscle tissues: Regulating cell phenotype with the scaffold. Experimental Cell Research 1999;251:318-328.

[32] Fujisato T, Sajiki T, Liu Q, Ikada Y. Effect of basic fibroblast growth factor on cartilage regeneration in chondrocyte-seeded collagen sponge scaffold. Biomaterials 1996;17:155-162.

[33] Speer DP, Chvapil M, Volz RG, Holmes MD. Enhancement of healing in osteochondral defects by collagen sponge implants. Clinical Orthopeadics and Relatated Research 1979;144:326-335.

[34] Sumita Y, Honda MJ, Ohara T, Tsuchiya S, Sagara H, Kagami H, Ueda M. Performance of collagen sponge as a 3-D scaffold for tooth-tissue engineering. Biomaterials 2006;27:3238-3248.

[35] Silver FH, Pins G. Cell growth on collagen: A review of tissue engineering using scaffolds containing extracellular matrix. Journal of Long Term Effects of Medical Implants 1992;2:67-80.

[36] Juncosa-Melvin N, Shearn JT, Boivin GP, Gooch C, Galloway MT, West JR, Nirmalanandhan VS, Bradica G, Butler DL. Effects of mechanical stimulation on the biomechanics and histology of stem cell-collagen sponge constructs for rabbit patellar tendon repair. Tissue Eng 2006;12:2291-2300.

[37] Juncosa-Melvin N, Matlin KS, Holdcraft RW, Nirmalanandhan VS, Butler DL. Mechanical stimulation increases collagen type I and collagen type III gene expression of stem cell-collagen sponge constructs for patellar tendon repair. Tissue Eng 2007;13:1219-1226.

[38] Faraj KA, van Kuppevelt TH, Daamen WF. Construction of collagen scaffolds that mimic the three-dimensional architecture of specific tissues. Tissue Eng 2007;13:2387-2394.

[39] Davidenko N, Gibb T, Schuster C, Best S, Campbell J, Watson C, Cameron R. Biomimetic collagen scaffolds with anisotropic pore architecture. Acta Biomater 2012;8:667-676.

[40] Keeney M, Collin E, Pandit A. Multi-channelled collagen-calcium phosphate scaffolds: Their physical properties and human cell response. Tissue Eng Part C 2009;15:265-273.

[41] Zhu J, Xiong Y, Zeng C, Qiang N, Quan D, Wan J. Elastic chitosan conduits with multiple channels and well defined microstructure. Int J Biol Macromol 2012;51:105-112.

[42] Francis N, Hunger P, Donius A, Riblett B, Zavaliangos A, Wegst U, Wheatley M. An ice-templated, linearly aligned chitosan-alginate scaffold for neural tissue engineering. J Biomed Mater Res A 2013;101:3493-3503.

[43] Kasoju N, Kubies D, Kumorek M, Kriz J, Fabryova E, Machova L, Kovarova J, Rypacek F. Dip TIPS as a facile and versatile method for fabrication of polymer foams with controlled shape, size and pore architecture for bioengineering applications. PLoS One 2014;9:e108792.

[44] Yook S, Jung H, Park C, Shin K, Koh Y, Estrin Y, Kim H. Reverse freeze casting: A new method for fabricating highly porous titanium scaffolds with aligned large pores. Acta Biomater 2012;8:2401-2410.

[45] Deville S. Freeze-casting of porous ceramics: A review of current achievements and issues. Adv Eng Mater 2008;10:155-169.

[46] Lu H, Ko Y, Kawazoe N, Chen G. Cartilage tissue engineering using funnel-like collagen sponges prepared with embossing ice particulate templates. Biomaterials 2010;31:5825-5835.

[47] Ko Y, Kawazoe N, Tateishi T, Chen G. Preparation of chitosan scaffolds with a hierarchical porous structure. J Biomed Mater Res B 2010;93:341-350.

[48] Ko Y, Grice S, Kawazoe N, Tateishi T, Chen G. Preparation of collagen-glycosaminoglycan sponges with open surface porous structures using ice particulate template method. Macromol Biosci 2010;10:860-871.

[49] Harley B, Hastings A, Yannas I, Sannino A. Fabricating tubular scaffolds with a radial pore size gradient by a spinning technique. Biomaterials 2006;27:866-874.

[50] Byette F, Bouchard F, Pellerin C, Paquin J, Marcotte I, Mateescu M. Cell-culture compatible silk fibroin scaffolds concomitantly patterned by freezing conditions and salt concentration. Polymer Bulletin 2011;67:159-175.

[51] Alizadeh M, Abbasi F, Khoshfetrat A, Ghaleh H. Microstructure and characteristic properties of gelatin/chitosan scaffold prepared by a combined freeze-drying/leaching method. Mater Sci Eng C 2013;33:3958-3967.

[52] Jamalpoor Z, Mirzadeh H, Joghataei M, Zeini D, Bagheri-Khoulenjani S, Nourani M. Fabrication of cancellous biomimetic chitosan-based nanocomposite scaffolds applying a combinational method for bone tissue engineering. J Biomed Mater Res A In Press.

[53] He X, Kawazoe N, Chen G. Preparation of cylinder-shaped porous sponges of poly(L-lactic acid), poly(DL-lactic-co-glycolic acid), and poly(ε-caprolactone). Biomed Res Int 2014;2014:106082.

[54] Zhang H, Hussain I, Brust M, Butler M, Rannard S, Cooper A. Aligned two- and three-dimensional structures by directional freezing of polymers and nanoparticles. Nat Mater 2005;4:787-793.

[55] Caliari SR, Harley BA. The effect of anisotropic collagen-GAG scaffolds and growth factor supplementation on tendon cell recruitment, alignment, and metabolic activity. Biomaterials 2011;32:5330-5340.

[56] Caliari SR, Ramirez MA, Harley BAC. The development of collagen-GAG scaffold-membrane composites for tendon tissue engineering. Biomaterials 2011;32:8990-8998.

[57] Kato YP, Christiansen DL, Hahn RA, Shieh S-J, Goldstein JD, Silver FH. Mechanical properties of collagen fibres: A comparison of reconstituted and rat tail tendon fibres. Biomaterials 1989;10:38-42.

[58] Zeugolis DI, Paul RG, Attenburrow G. Engineering extruded collagen fibers for biomedical applications. Journal of Applied Polymer Science 2008;108:2886-2894.

[59] Zeugolis DI, Paul RG, Attenburrow G. Factors influencing the properties of reconstituted collagen fibers prior to self-assembly: Animal species and collagen extraction method. J Biomed Mater Res A 2008;86A:892-904.

[60] Zeugolis DI, Paul RG, Attenburrow G. Extruded collagen fibres for tissue-engineering applications: Influence of collagen concentration and NaCl amount. J Biomater Sci Polym Ed 2009;20:219-234.

[61] Zeugolis DI, Paul RG, Attenburrow G. Post-self-assembly experimentation on extruded collagen fibres for tissue engineering applications. Acta Biomater 2008;4:1646-1656.

[62] Zeugolis DI, Khew ST, Yew ESY, Ekaputra AK, Tong YW, Yung L-YL, Hutmacher DW, Sheppard C, Raghunath M. Electro-spinning of pure collagen nano-fibres - Just an expensive way to make gelatin? Biomaterials 2008;29:2293-2305.

[63] Daly WT, Yao L, Abu-rub MT, O'Connell C, Zeugolis DI, Windebank AJ, Pandit AS. The effect of intraluminal contact mediated guidance signals on axonal mismatch during peripheral nerve repair. Biomaterials 2012;33:6660-6671.

[64] Zeugolis DI, Paul GR, Attenburrow G. Cross-linking of extruded collagen fibers-A biomimetic three-dimensional scaffold for tissue engineering applications. J Biomed Mater Res A 2009;89A:895-908.

[65] Zeugolis DI, Paul RG, Attenburrow G. The influence of a natural cross-linking agent (Myrica rubra) on the properties of extruded collagen fibres for tissue engineering applications. Materials Science & Engineering C 2010;30:190-195.

[66] Cornwell K, Downing B, Pins G. Characterizing fibroblast migration on discrete collagen threads for applications in tissue regeneration. J Biomed Mater Res A 2004;71:55-62.

[67] Sanami M, Sweeney I, Shtein T, Miraftab M, Shoseyov O, O'Dowd C, Pandit A, Zeugolis D. The influence of poly(ethylene glycol) ether tetrasuccinimidyl glutarate on the structural, physical and biological properties of collagen fibres. J Biomed Mater Res B Submitted.

[68] Zeugolis D, Panengad P, Yew E, Sheppard C, Phan T, Raghunath M. An in situ and in vitro investigation for the transglutaminase potential in tissue engineering. J Biomed Mater Res A 2010;92:1310-1320.

[69] Goldstein JD, Tria AJ, Zawadsky JP, Kato YP, Christiansen D, Silver FH. Development of a reconstituted collagen tendon prosthesis. A preliminary implantation study. Journal of Bone and Joint Surgery 1989;71:1183-1191.

[70] Kato YP, Dunn MG, Zawadsky JP, Tria AJ, Silver FH. Regeneration of Achilles tendon with a collagen tendon prosthesis. Results of a one-year implantation study. Journal of Bone and Joint Surgery 1991;73:561-574.

[71] Cavallaro JF, Kemp PD, Kraus KH. Collagen fabrics as biomaterials. Biotechnol Bioeng 1994;43:781-791.

[72] Dunn MG, Tria AJ, Kato YP, Bechler JR, Ochner RS, Zawadsky JP, Silver FH. Anterior cruciate ligament reconstruction using a composite collagenous prosthesis. A biomechanical and histologic study in rabbits. American journal of sports medicine 1992;20:507-515.

[73] Enea D, Gwynne J, Kew S, Arumugam M, Shepherd J, Brooks R, Ghose S, Best S, Cameron R, Rushton N. Collagen fibre implant for tendon and ligament biological augmentation. In vivo study in an ovine model. Knee Surgery, Sports Traumatology, Arthroscopy 2013;21:1783-1793.

[74] Cheng X, Gurkan UA, Dehen CJ, Tate MP, Hillhouse HW, Simpson GJ, Akkus O. An electrochemical fabrication process for the assembly of anisotropically oriented collagen bundles. Biomaterials 2008;29:3278-3288.

[75] Denning D, Abu-Rub MT, Zeugolis DI, Habelitz S, A. P, Fertala A, Rodriguez BJ. Electromechanical properties of dried tendon and iso-electrically focused collagen hydrogels. Acta Biomater 2012;8:3073-3079.

[76] Abu-Rub MT, Billiar KL, van Es MH, Knight A, Rodriguez BJ, Zeugolis DI, McMahon S, Windebank AJ, Pandit A. Nano-textured self-assembled aligned collagen hydrogels promote directional neurite guidance and overcome inhibition by myelin associated glycoprotein. Soft Matter 2011;7:2770-2781.

[77] Alfredo Uquillas J, Kishore V, Akkus O. Genipin crosslinking elevates the strength of electrochemically aligned collagen to the level of tendons. J Mech Behav Biomed Mater 2012;15:176-189.

[78] Gurkan UA, Cheng X, Kishore V, Uquillas JA, Akkus O. Comparison of morphology, orientation, and migration of tendon derived fibroblasts and bone marrow stromal cells on electrochemically aligned collagen constructs. J Biomed Mater Res A 2010;94:1070-1079.

[79] Kishore V, Bullock W, Sun X, Van Dyke WS, Akkus O. Tenogenic differentiation of human MSCs induced by the topography of electrochemically aligned collagen threads. Biomaterials 2012;33:2137-2144.

[80] Kishore V, Uquillas JA, Dubikovsky A, Alshehabat MA, Snyder PW, Breur GJ, Akkus O. In vivo response to electrochemically aligned collagen bioscaffolds. J Biomed Mater Res B 2011.

[81] Enea D, Henson F, Kew S, Wardale J, Getgood A, Brooks R, Rushton N. Extruded collagen fibres for tissue engineering applications: Effect of crosslinking

method on mechanical and biological properties. J Mater Sci Mater Med 2011;22:1569-1578.

[82] Shin YM, Hohman MM, Brenner MP, Rutledge GC. Experimental characterization of electrospinning: The electrically forced jet and instabilities. Polymer 2001;42:09955-09967.

[83] Tan SH, Inai R, Kotaki M, Ramakrishna S. Systematic parameter study for ultra-fine fiber fabrication via electrospinning process. Polymer 2005;46:6128-6134.

[84] Huang Z-M, Zhang YZ, Kotaki M, Ramakrishna S. A review on polymer nanofibers by electrospinning and their applications in nanocomposites. Composites Science and Technology 2003;63:2223-2253.

[85] Yan S, Jian G, Zachariah M. Electrospun nanofiber-based thermite textiles and their reactive properties. ACS Appl Mater Interfaces 2012;4:6432-6435.

[86] Doshi J, Reneker D. Electrospinning process and applications of electrospun fibers. J Electrostatics 1995;35:151-160.

[87] Chronakis I. Novel nanocomposites and nanoceramics based on polymer nanofibers using electrospinning process—A review. J Materials Processing Technology 2005;167:283-293.

[88] Wu H, Hu L, Rowell M, Kong D, Cha J, McDonough J, Zhu J, Yang Y, McGehee M, Cui Y. Electrospun metal nanofiber webs as high-performance transparent electrode. Nano Letters 2010;10:4242-4248.

[89] Dai Y, Liu W, Formo E, Sun Y, Xia Y. Ceramic nanofibers fabricated by electrospinning and their applications in catalysis, environmental science, and energy technology. Polym Advanc Technol 2011;22:326-338.

[90] Huang L, Nagapudi K, Apkarian R, Chaikof E. Engineered collagen-PEO nanofibers and fabrics. J Biomater Sci Polym Ed 2001;12:979-993.

[91] Norouzi M, Shabani I, Ahvaz H, Soleimani M. PLGA/gelatin hybrid nanofibrous scaffolds encapsulating EGF for skin regeneration. J Biomed Mater Res A In Press.

[92] Hodgkinson T, Yuan X, Bayat A. Electrospun silk fibroin fiber diameter influences in vitro dermal fibroblast behavior and promotes healing of ex vivo wound models. J Tissue Eng 2014;5:doi: 10.1177/2041731414551661.

[93] Jeong L, Kim M, Jung J, Min B, Park W. Effect of silk fibroin nanofibers containing silver sulfadiazine on wound healing. Int J Nanomedicine 2014;9:5277-5287.

[94] Li W, Danielson K, Alexander P, Tuan R. Biological response of chondrocytes cultured in three-dimensional nanofibrous poly(epsilon-caprolactone) scaffolds. J Biomed Mater Res A 2003;67:1105-1114.

[95] Li W, Jiang Y, Tuan R. Chondrocyte phenotype in engineered fibrous matrix is regulated by fiber size. Tissue Eng 2006;12:1775-1785.

[96] Yang W, Yang F, Wang Y, Both S, Jansen J. In vivo bone generation via the endochondral pathway on three-dimensional electrospun fibers. Acta Biomater 2013;9:4505-4512.

[97] Garrigues N, Little D, Sanchez-Adams J, Ruch D, Guilak F. Electrospun cartilage-derived matrix scaffolds for cartilage tissue engineering. J Biomed Mater Res A 2014;102:3998-4008.

[98] Gomez-Sanchez C, Kowalczyk T, Ruiz-De-Eguino G, Lopez-Arraiza A, Infante A, Rodriguez C, Kowalewski T, Sarrionandia M, Aurrekoetxea J. Electrospinning of poly(lactic acid)/polyhedral oligomeric silsesquioxane nanocomposites and their potential in chondrogenic tissue regeneration. J Biomater Sci Polym Ed 2014;25:802-825.

[99] Dahlin R, Kinard L, Lam J, Needham C, Lu S, Kasper F, Mikos A. Articular chondrocytes and mesenchymal stem cells seeded on biodegradable scaffolds for the repair of cartilage in a rat osteochondral defect model. Biomaterials 2014;35:7460-7469.

[100] Liu X, Liu S, Liu S, Cui W. Evaluation of oriented electrospun fibers for periosteal flap regeneration in biomimetic triphasic osteochondral implant. J Biomed Mater Res B 2014;102:1407-1414.

[101] Chang J, Fujita S, Tonami H, Kato K, Iwata H, Hsu S. Cell orientation and regulation of cell-cell communication in human mesenchymal stem cells on different patterns of electrospun fibers. Biomed Mater 2013;8:055002.

[102] Fuller K, Pandit A, Zeugolis D. The multifaceted potential of electro-spinning in regenerative medicine. Pharmaceut Nanotechnol 2014;2:23-34.

[103] Baker S, Atkin N, Gunning P, Granville N, Wilson K, Wilson D, Southgate J. Characterisation of electrospun polystyrene scaffolds for three-dimensional in vitro biological studies. Biomaterials 2006;27:3136-3146.

[104] Pham Q, Sharma U, Mikos A. Electrospinning of polymeric nanofibers for tissue engineering applications: A review. Tissue Eng 2006;12:1197-1211.

[105] Ji W, Yang F, van den Beucken JJJP, Bian Z, Fan M, Chen Z, Jansen JA. Fibrous scaffolds loaded with protein prepared by blend or coaxial electrospinning. Acta Biomater 2010;6:4199-4207.

[106] Jiang H, Hu Y, Zhao P, Li Y, Zhu K. Modulation of protein release from biodegradable core–shell structured fibers prepared by coaxial electrospinning. J Biomed Mater Res B 2006;79B:50-57.

[107] Liu W, Thomopoulos S, Xia Y. Electrospun nanofibers for regenerative medicine. Adv Healthc Mater 2012;1:10-25.

[108] Chew S, Wen Y, Dzenis Y, Leong K. The role of electrospinning in the emerging field of nanomedicine. Curr Pharm Des 2006;12:4751-4770.

[109] Schnell E, Klinkhammer K, Balzer S, Brook G, Klee D, Dalton P, Mey J. Guidance of glial cell migration and axonal growth on electrospun nanofibers of poly-epsilon-caprolactone and a collagen/poly-epsilon-caprolactone blend. Biomaterials 2007;28:3012-3025.

[110] Yang F, Murugan R, Wang S, Ramakrishna S. Electrospinning of nano/micro scale poly(L-lactic acid) aligned fibers and their potential in neural tissue engineering. Biomaterials 2005;26:2603-2610.

[111] Mohtaram N, Ko J, King C, Sun L, Muller N, Jun M, Willerth S. Electrospun biomaterial scaffolds with varied topographies for neuronal differentiation of human induced pluripotent stem cells. J Biomed Mater Res A In Press.

[112] Yao L, O'Brien N, Windebank A, Pandit A. Orienting neurite growth in electrospun fibrous neural conduits. J Biomed Mater Res B 2009;90:483-491.

[113] Yang F, Murugan R, Wang S, Ramakrishna S. Electrospinning of nano/micro scale poly(L-lactic acid) aligned fibers and their potential in neural tissue engineering. Biomaterials 2005;26:2603-2610.

[114] Chew S, Mi R, Hoke A, Leong K. The effect of the alignment of electrospun fibrous scaffolds on Schwann cell maturation. Biomaterials 2008;29:653-661.

[115] Chew S, Mi R, Hoke A, Leong K. Aligned protein-polymer composite fibers enhance nerve regeneration: A potential tissue-engineering platform. Adv Funct Mater 2007;17:1288-1296.

[116] Xu C. Aligned biodegradable nanofibrous structure: a potential scaffold for blood vessel engineering. Biomaterials 2004;25:877-886.

[117] Wu J, Du Y, Watkins S, Funderburgh J, Wagner W. The engineering of organized human corneal tissue through the spatial guidance of corneal stromal stem cells. Biomaterials 2012;33:1343-1352.

[118] Wu J, Du Y, Mann M, Yang E, Funderburgh J, Wagner W. Bioengineering organized, multilamellar human corneal stromal tissue by growth factor supplementation on highly aligned synthetic substrates. Tissue Eng Part A 2013;19:2063-2075.

[119] Li WJ, Mauck RL, Cooper JA, Yuan X, Tuan RS. Engineering controllable anisotropy in electrospun biodegradable nanofibrous scaffolds for musculoskeletal tissue engineering. Journal of Biomechanics 2007;40:1686-1693.

[120] Sefcik L, Neal R, Kaszuba S, Parker A, Katz A, Ogle R, Botchwey E. Collagen nanofibres are a biomimetic substrate for the serum‐free osteogenic differentiation of human adipose stem cells. J Tissue Eng Regen Med 2008;2:210-220.

[121] Pişkin E, Işoğlu I, Bölgen N, Vargel I, Griffiths S, Çavuşoğlu T, Korkusuz P, Güzel E, Cartmell S. In vivo performance of simvastatin‐loaded electrospun spiral‐wound polycaprolactone scaffolds in reconstruction of cranial bone defects in the rat model. J Biomed Mater Res A 2009;90:1137-1151.

[122] Jose M, Thomas V, Xu Y, Bellis S, Nyairo E, Dean D. Aligned bioactive multi-component nanofibrous nanocomposite scaffolds for bone tissue engineering. Macromol Biosci 2010;10:433-444.

[123] Sell S, Wolfe P, Garg K, McCool J, Rodriguez I, Bowlin G. The use of natural polymers in tissue engineering: A focus on electrospun extracellular matrix analogues. Polymers 2010;2:522-553.

[124] Wang Y, Gao R, Wang P, Jian J, Jiang X, Yan C, Lin X, Wu L, Chen G, Wu Q. The differential effects of aligned electrospun PHBHHx fibers on adipogenic and osteogenic potential of MSCs through the regulation of PPARgamma signaling. Biomaterials 2012;33:485-493.

[125] Lyu S, Huang C, Yang H, Zhang X. Electrospun fibers as a scaffolding platform for bone tissue repair. J Orthop Res 2013;31:1382-1389.

[126] Ji W, Yang F, Ma J, Bouma M, Boerman O, Chen Z, van den Beucken J, Jansen J. Incorporation of stromal cell-derived factor-1α in PCL/gelatin electrospun membranes for guided bone regeneration. Biomaterials 2013;34:735-745.

[127] Liao S, Nguyen L, Ngiam M, Wang C, Cheng Z, Chan C, Ramakrishna S. Biomimetic nanocomposites to control osteogenic differentiation of human mesenchymal stem cells. Adv Healthc Mater 2014;3:737-751.

[128] Thibault R, Mikos A, Kasper F. Scaffold/Extracellular matrix hybrid constructs for bone-tissue engineering. Adv Healthc Mater 2013;2:13-24.

[129] Shin S, Purevdorj O, Castano O, Planell J, Kim H. A short review: Recent advances in electrospinning for bone tissue regeneration. J Tissue Eng 2012;3:2041731412443530.

[130] Ma J, He X, Jabbari E. Osteogenic differentiation of marrow stromal cells on random and aligned electrospun poly(L-lactide) nanofibers. Ann Biomed Eng 2011;39:14-25.

[131] Liao S, Murugan R, Chan C, Ramakrishna S. Processing nanoengineered scaffolds through electrospinning and mineralization suitable for biomimetic bone tissue engineering. J Mech Behav Biomed Mater 2008;1:252-260.

[132] Ekaputra A, Zhou Y, Cool S, Hutmacher D. Composite electrospun scaffolds for engineering tubular bone grafts. Tissue Eng Part A 2009;15:3779-3788.

[133] Kolambkar Y, Peister A, Ekaputra A, Hutmacher D, Guldberg R. Colonization and osteogenic differentiation of different stem cell sources on electrospun nanofiber meshes. Tissue Eng Part A 2010;16:3219-3230.

[134] Martins A, Alves da Silva M, Faria S, Marques A, Reis R, Neves N. The influence of patterned nanofiber meshes on human mesenchymal stem cell osteogenesis. Macromol Biosci 2011;11:978-987.

[135] Kolambkar Y, Dupont K, Boerckel J, Huebsch N, Mooney D, Hutmacher D, Guldberg R. An alginate-based hybrid system for growth factor delivery in the functional repair of large bone defects. Biomaterials 2011;32:65-74.

[136] Yin Z, Chen X, Chen J, Shen W, Hieu Nguyen T, Gao L, Ouyang H. The regulation of tendon stem cell differentiation by the alignment of nanofibers. Biomaterials 2010;31:2163-2175.

[137] Cao D, Liu W, Wei X, Xu F, Cui L, Cao Y. In vitro tendon engineering with avian tenocytes and polyglycolic acids: A preliminary report. Tissue Eng 2006;12:1369-1377.

[138] Xu L, Cao D, Liu W, Zhou G, Zhang W, Cao Y. In vivo engineering of a functional tendon sheath in a hen model. Biomaterials 2010;31:3894-3902.

[139] Deng D, Wang W, Wang B, Zhang P, Zhou G, Zhang W, Cao Y, Liu W. Repair of Achilles tendon defect with autologous ASCs engineered tendon in a rabbit model. Biomaterials 2014;35:8801-8809.

[140] Kolluru P, Lipner J, Liu W, Xia Y, Thomopoulos S, Genin G, Chasiotis I. Strong and tough mineralized PLGA nanofibers for tendon-to-bone scaffolds. Acta Biomater 2013;9:9442-9450.

[141] Jain A, Betancur M, Patel G, Valmikinathan C, Mukhatyar V, Vakharia A, Pai S, Brahma B, MacDonald T, Bellamkonda R. Guiding intracortical brain tumour cells

to an extracortical cytotoxic hydrogel using aligned polymeric nanofibres. Nat Mater 2014;13:308-316.

[142] Nelson M, Short A, Cole S, Gross A, Winter J, Eubank T, Lannutti J. Preferential, enhanced breast cancer cell migration on biomimetic electrospun nanofiber 'cell highways'. BMC Cancer 2014;14:doi: 10.1186/1471-2407-1114-1825.

[143] Baker BM, Gee AO, Metter RB, Nathan AS, Marklein RA, Burdick JA, Mauck RL. The potential to improve cell infiltration in composite fiber-aligned electrospun scaffolds by the selective removal of sacrificial fibers. Biomaterials 2008;29:2348-2358.

[144] Simonet M, Schneider OD, Neuenschwander P, Stark WJ. Ultraporous 3D polymer meshes by low-temperature electrospinning: Use of ice crystals as a removable void template. Polymer Engineering & Science 2007;47:2020-2026.

[145] Sahoo S, Ouyang H, Goh JC, Tay TE, Toh SL. Characterization of a novel polymeric scaffold for potential application in tendon/ligament tissue engineering. Tissue Eng 2006;12:91-99.

[146] Bosworth LA, Alam N, Wong JK, Downes S. Investigation of 2D and 3D electrospun scaffolds intended for tendon repair. J Mater Sci Mater Med 2013;24:1605-1614.

[147] Moffat KL, Kwei AS, Spalazzi JP, Doty SB, Levine WN, Lu HH. Novel nanofiber-based scaffold for rotator cuff repair and augmentation. Tissue Eng Part A 2009;15:115-126.

[148] Oryan A, Moshiri A, Parizi Meimandi A, Silver IA. A long-term in vivo investigation on the effects of xenogenous based, electrospun, collagen implants on the healing of experimentally-induced large tendon defects. Journal of Musculoskeletal & Neuronal Interactions 2013;13:353-367.

[149] Yang L, Fitié C, van der Werf K, Bennink M, Dijkstra P, Feijen J. Mechanical properties of single electrospun collagen type I fibers. Biomaterials 2008;29:955-962.

[150] Sahoo S, Toh SL, Goh JC. A bFGF-releasing silk/PLGA-based biohybrid scaffold for ligament/tendon tissue engineering using mesenchymal progenitor cells. Biomaterials 2010;31:2990-2998.

[151] Chainani A, Hippensteel KJ, Kishan A, Garrigues NW, Ruch DS, Guilak F, Little D. Multilayered electrospun scaffolds for tendon tissue engineering. Tissue Eng Part A 2013;19:2594-2604.

[152] James R, Kumbar S, Laurencin C, Balian G, Chhabra A. Tendon tissue engineering: Adipose-derived stem cell and GDF-5 mediated regeneration using electrospun matrix systems. Biomedical Mater 2011;6:025011.

[153] Chen B, Wang B, Zhang W, Zhou G, Cao Y, Liu W. In vivo tendon engineering with skeletal muscle derived cells in a mouse model. Biomaterials 2012;33:6086-6097.

[154] Deng D, Liu W, Xu F, Yang Y, Zhou G, Zhang W, Cui L, Cao Y. Engineering human neo-tendon tissue in vitro with human dermal fibroblasts under static mechanical strain. Biomaterials 2009;30:6724-6730.

[155] Liu W, Chen B, Deng D, Xu F, Cui L, Cao Y. Repair of tendon defect with dermal fibroblast engineered tendon in a porcine model. Tissue Eng 2006;12:775-788.

[156] Samavedi S, Guelcher S, Goldstein A, Whittington A. Response of bone marrow stromal cells to graded co-electrospun scaffolds and its implications for engineering the ligament-bone interface. Biomaterials 2012;33:7727-7735.

[157] Ladd M, Lee S, Stitzel J, Atala A, Yoo J. Co-electrospun dual scaffolding system with potential for muscle–tendon junction tissue engineering. Biomaterials 2011;32:1549-1559.

[158] Ekaputra A, Prestwich G, Cool S, Hutmacher D. The three-dimensional vascularization of growth factor-releasing hybrid scaffold of poly (epsilon-caprolactone)/collagen fibers and hyaluronic acid hydrogel. Biomaterials 2011;32:8108-8117.

[159] Çakmak S, Çakmak A, Gümüşderelioğlu M. RGD-bearing peptide-amphiphile-hydroxyapatite nanocomposite bone scaffold: An in vitro study. Biomed Mater 2013;8:045014.

[160] Butcher A, Offeddu G, Oyen M. Nanofibrous hydrogel composites as mechanically robust tissue engineering scaffolds. Trends Biotechnol 2014;32:564-570.

[161] Samavedi S, Vaidya P, Gaddam P, Whittington A, Goldstein A. Electrospun meshes possessing region-wise differences in fiber orientation, diameter, chemistry and mechanical properties for engineering bone-ligament-bone tissues. Biotechnol Bioeng 2014;111:2549-2559.

[162] Cardwell R, Dahlgren L, Goldstein A. Electrospun fibre diameter, not alignment, affects mesenchymal stem cell differentiation into the tendon/ligament lineage. J Tissue Eng Regen Med 2014;8:937-945.

[163] Wang W, Deng D, Li J, Liu W. Elongated cell morphology and uniaxial mechanical stretch contribute to physical attributes of niche environment for MSC tenogenic differentiation. Cell Biol Int 2013;37:755-760.

[164] Bosworth L, Rathbone S, Bradley R, Cartmell S. Dynamic loading of electrospun yarns guides mesenchymal stem cells towards a tendon lineage. J Mech Behav Biomed Mater 2014;39:175-183.

[165] Lee C, Shin H, Cho I, Kang Y, Kim I, Park K, Shin J. Nanofiber alignment and direction of mechanical strain affect the ECM production of human ACL fibroblast. Biomaterials 2005;26:1261-1270.

[166] Yang Y, Leong KW. Nanoscale surfacing for regenerative medicine. Wiley Interdisciplinary Reviews: Nanomedicine and Nanobiotechnology 2010;2:478-495.

[167] Wu B, Kumar A. Extreme ultraviolet lithography: A review. Journal of Vacuum Science & Technology B 2007;25:1743-1761.

[168] Bagnaninchi PO, Yang Y, Zghoul N, Maffulli N, Wang RK, Haj AJE. Chitosan microchannel scaffolds for tendon tissue engineering characterized using optical coherence tomography. Tissue Eng 2007;13:323-331.

[169] Vieu C, Carcenac F, Pépin A, Chen Y, Mejias M, Lebib A, Manin-Ferlazzo L, Couraud L, Launois H. Electron beam lithography: Resolution limits and applications. Applied Surface Science 2000;164:111-117.

[170] Truskett VN, Watts MP. Trends in imprint lithography for biological applications. Trends Biotechnol 2006;24:312-317.

[171] Guo LJ. Recent progress in nanoimprint technology and its applications. Journal of Physics D: Applied Physics 2004;37:R123.

[172] Austin MD, Ge H, Wu W, Li M, Yu Z, Wasserman D, Lyon SA, Chou SY. Fabrication of 5nm linewidth and 14nm pitch features by nanoimprint lithography. Applied Physics Letters 2004;84:5299-5301.

[173] Hu W, Yim EK, Reano RM, Leong KW, Pang SW. Effects of nanoimprinted patterns in tissue-culture polystyrene on cell behavior. J Vac Sci Technol A 2005;23:2984-2989.

[174] Ito T, Okazaki S. Pushing the limits of lithography. Nature 2000;406:1027-1031.

[175] Masson JF, Murray-Methot MP, Live LS. Nanohole arrays in chemical analysis: Manufacturing methods and applications. Analyst 2010;135:1483-1489.

[176] Utke I, Hoffmann P, Melngailis J. Gas-assisted focused electron beam and ion beam processing and fabrication. Journal of Vacuum Science & Technology B 2008;26:1197-1276.

[177] Zorlutuna P, Annabi N, Camci-Unal G, Nikkhah M, Cha JM, Nichol JW, Manbachi A, Bae HJ, Chen SC, Khademhosseini A. Microfabricated biomaterials for engineering 3D tissues. Advanced Materials 2012;24:1782-1804.

[178] Huh D, Hamilton GA, Ingber DE. From 3D cell culture to organs-on-chips. Trends Cell Biol 2011;21:745-754.

[179] Kumar G, Tang HX, Schroers J. Nanomoulding with amorphous metals. Nature 2009;457:868-872.

[180] Biggs M, Richards R, Gadegaard N, Wilkinson C, Oreffo R, Dalby M. The use of nanoscale topography to modulate the dynamics of adhesion formation in primary osteoblasts and ERK/MAPK signalling in STRO-1+ enriched skeletal stem cells. Biomaterials 2009;30:5094-5103.

[181] Lamers E, Walboomers X, Domanski M, te Riet J, van Delft F, Luttge R, Winnubst L, Gardeniers H, Jansen J. The influence of nanoscale grooved substrates on osteoblast behavior and extracellular matrix deposition. Biomaterials 2010;31:3307-3316.

[182] Dalby M, Gadegaard N, Tare R, Andar A, Riehle M, Herzyk P, Wilkinson C, Oreffo R. The control of human mesenchymal cell differentiation using nanoscale symmetry and disorder. Nat Mater 2007;6:997-1003.

[183] Unadkat H, Hulsman M, Cornelissen K, Papenburg B, Truckenmuller R, Post G, Uetz M, Reinders M, Stamatialis D, van Blitterswijk C, de Boer J. An algorithm-

based topographical biomaterials library to instruct cell fate. Proc Natl Acad Sci U S A 2011;108:16565-16570.

[184] Watari S, Hayashi K, Wood J, Russell P, Nealey P, Murphy C, Genetos D. Modulation of osteogenic differentiation in hMSCs cells by submicron topographically-patterned ridges and grooves. Biomaterials 2012;33:128-136.

[185] Cabezas M, Eichelsdoerfer D, Brown K, Mrksich M, Mirkin C. Combinatorial screening of mesenchymal stem cell adhesion and differentiation using polymer pen lithography. Methods Cell Biol 2014;119:261-276.

[186] Biggs M, Richards R, Gadegaard N, McMurray R, Affrossman S, Wilkinson C, Oreffo R, Dalby M. Interactions with nanoscale topography: Adhesion quantification and signal transduction in cells of osteogenic and multipotent lineage. J Biomed Mater Res A 2009;91:195-208.

[187] Nandakumar A, Truckenmuller R, Ahmed M, Damanik F, Santos D, Auffermann N, de Boer J, Habibovic P, van Blitterswijk C, Moroni L. A fast process for imprinting micro and nano patterns on electrospun fiber meshes at physiological temperatures. Small 2013;9:3405-3409.

[188] Wojciak B, Crossan J, Curtis A, Wilkinson C. Grooved substrata facilitate in vitro healing of completely divided flexor tendons. J Mater Sci Mater Med 1995;6:266-271.

[189] Yim E, Reano R, Pang S, Yee A, Chen C, Leong K. Nanopattern-induced changes in morphology and motility of smooth muscle cells. Biomaterials 2005;26:5405-5413.

[190] Yim EKF, Leong KW. Significance of synthetic nanostructures in dictating cellular response. Nanomedicine: Nanotechnology, Biology and Medicine 2005;1:10-21.

[191] Crouch AS, Miller D, Luebke KJ, Hu W. Correlation of anisotropic cell behaviors with topographic aspect ratio. Biomaterials 2009;30:1560-1567.

[192] Zhu J, Li J, Wang B, Zhang WJ, Zhou G, Cao Y, Liu W. The regulation of phenotype of cultured tenocytes by microgrooved surface structure. Biomaterials 2010;31:6952-6958.

[193] Kapoor A, Caporali EHG, Kenis PJA, Stewart MC. Microtopographically patterned surfaces promote the alignment of tenocytes and extracellular collagen. Acta Biomater 2010;6:2580-2589.

[194] Tong W, Shen W, Yeung C, Zhao Y, Cheng S, Chu P, Chan D, Chan G, Cheung K, Yeung K, Lam Y. Functional replication of the tendon tissue microenvironment by a bioimprinted substrate and the support of tenocytic differentiation of mesenchymal stem cells. Biomaterials 2012;33:7686-7698.

[195] Azeem A, English A, Kumar P, Satyam A, Biggs M, Jones E, Tripathi B, Basu N, Henkel J, Vaquette C, Rooney N, Riley G, O'Riordan A, Cross G, Ivanovski S, Hutmacher D, Pandit A, Zeugolis D. The influence of anisotropic nano- to micro-topography on in vitro and in vivo osteogenesis. Nanomedicine In Press.

Chapter 2

Anisotropic Electro-spun Fibres, with Functionalisation Capacity, for Directional Cell Growth

Sections of this chapter have been published at:

English, A., Azeem, A., Gaspar, D.A., Keane, K., Kumar, P., Keeney, M., Rooney, N., Pandit, A., Zeugolis, D.I. *Preferential cell response to anisotropic electro-spun fibrous scaffolds under tension-free conditions*. Journal of Materials Science: Materials in Medicine, Vol. 23, No. 1, pp. 137-148, 2012.

2.1. Introduction

Nature shows strong preference for bottom up design to build hierarchically ordered tissues. In the case of tendon, for example, cells synthesise procollagen with intact pro-peptide extensions. Following or during secretion, specific propeptide cleavage by specific proteinases takes place, which triggers the spontaneous quarter-staggered assembly of collagen molecules to elongated collagen fibrils. Following fibril formation, the lysyl-oxidase cross-linking pathway takes place in a head-to-tail fashion to form fibres that will subsequently form fibre bundles and finally a tendon unit [1]. This naturally engineered collagen conveys load bearing functionality to tissues such as tendon and bone [2], whilst in the case of cornea the high degree of structural organisation and alignment facilitates transparency [3]. To successfully build biomimetic tissue equivalents that will repair or replace injured or degenerated tissues, it is essential to recapitulate this fundamental structural hierarchy.

A number of nano- and micro- fabrication technologies are available to-date to build biomimetic three dimensional tissue analogues [4, 5]. Among them, electro-spinning has emerged as a scaffold fabrication technique that enables production of fibres that closely imitate the length and diameter of native collagen fibres. The use of extracellular matrix biopolymers has been restricted, as harsh solvents are often required to perform electro-spinning successfully. [6, 7]. To-date, numerous polymers have been utilised to produce scaffolds of various topographies for neural [8, 9], tendon [10, 11], bone [12, 13], cartilage [14, 15] and cardiovascular [16, 17] applications.

Biomaterials design has evolved from basic constructs that match structural and mechanical properties, to biofunctional materials that aim to incorporate instructive signals into scaffolds and to modulate cellular functions such as proliferation,

differentiation and morphogenesis [18, 19]. Indeed, the emerging field of tissue engineering requires accurate delivery of bioactive and/or therapeutic molecules to a specific location. To this end, the use of polymeric delivery vehicles in the form of micro- or nano-spheres/particles to encapsulate the active molecules and maintain a sustained localised delivery to the target site is attractive [20-22].

Despite the significant strides that have been achieved, the influence of scaffold topography on the biomechanical properties and cell response has not been fully investigated. Moreover, functionalisation of electro-spun scaffolds is primarily carried out through blending the polymer and the molecule of interest together. However, such method offers little control over the release of the loaded molecules; may jeopardise the mechanical properties of the scaffold; and is also characterised by limited miscibility between the solution containing the molecule of interest and the solvent used to dissolve the polymer [23, 24]. Thus, herein we ventured to evaluate the influence of various scaffolds topographies on the mechanical properties of the scaffolds and evaluate bovine tenocytes, response as a function of topography. In addition, we developed a technique that enables simultaneous electro-spinning and micro-sphere spraying and allows the incorporation of microspheres within the three-dimensional structure of the scaffold.

2.2. Materials and Methods

2.2.1. Materials

Poly(glycolide-co-lactide) 85/15 (PLGA) was purchased from Purac Biomaterials (Gorinchem, Netherlands). AlamarBlue® cell metabolic activity kit was purchased from BioSource International, Invitrogen (Dun Laoghaire, Ireland). Tissue culture consumables were purchased from Sarstedt (Wexford, Ireland) and Nunc (Roskilde, Denmark). All other materials were purchased from Sigma Aldrich (Wicklow, Ireland), unless otherwise stated.

2.2.2. Electro-spinning Optimisation

To evaluate optimal settings of the three main parameters (voltage, flow rate, and diameter) each parameter was assessed independently of the rest. While each parameter setting was altered, the remaining parameters were unchanged. This method determines the effect each of the tested parameters had on the fibre confirmation. To evaluate fibre diameter and fibre alignment each setting was allowed to run for a short period of time, for a sufficient quantity of fibres to be collected to carry out the analysis.

2.2.2.1. Fibre Diameter

The fibre average diameter of the different constructs was evaluated using SEM images. Three samples were cut from each construct with three images of each sample captured. 27 fibres were measured in micrographs obtained at random locations.

2.2.2.2. Fibre Alignment by Fast Fourier Transform (FFT)

Fast Fourier Transform (FFT) algorithm was employed to quantitatively assess the orientation of the electro-spun fibres. This method converts the spatial information from SEM images into a mathematically defined domain. The resultant FFT frequency distribution pattern reflects the degree of alignment of the fibrous scaffold. This distribution plot is analysed by placing a circular projection on the FFT output image and conducting a radial summation of pixel intensity for each degree between 0° and 360°, using Image J. The alignment present in the original image is evident, in the resultant graph, in terms of the height and overall shape of the peak present in the FFT plot. A sharp peak indicates a high degree of alignment; whereas a wide peak indicates random orientation.

The alignment of the fibres was calculated using the same SEM images that were used to calculate the fibre diameter. Each image was cropped to remove edge distortions on the image that could interfere with the measurements. The Fast Fourier Transform (FFT) algorithm on Image Pro software was used to analyse the alignment of the fibres in each the SEM images. The FFT algorithm converts the spatial information from the images into a mathematically defined frequency domain, which can map the change in the pixel intensity. Using Image J oval profile plug-in the information from the FFT graph was converted to excel data.

2.2.3. Scaffold Fabrication

The electro-spinning set-up consisted of a high voltage power supply (Gamma High Voltage, USA), a syringe pump (NE-1000, New Era Pump Systems Inc., USA) and a custom-made circular drum (10 cm in diameter) covered with aluminium foil, which acted as a collector. 8% w/v PLGA solution in chloroform was prepared after

overnight orbital stirring using a Stuart® SB3 rotator (Biddy Scientific Limited, UK) **(Figure 1.4)**. Polymer solutions were loaded into a 10 ml syringe (BD and Company, Ireland) fitted with an 18G stainless steel needle (BD and Company, Ireland). Upon application of high voltage between the needle and the collector (18cm distance), the solvent was evaporated and the fibres were collected on the drum. At 1300 rpm aligned fibrous mats were obtained, whilst at 200 rpm non-aligned fibrous mats were obtained. Solvent casted PLGA (8% w/v in chloroform) was used as control scaffold with no topographical features (i.e. smooth surface). The polymer solution was gently poured into aluminium foil trays, avoiding bubble formation. The trays were covered with another layer of aluminium foil to control the evaporation rate of the solvent.

2.2.4. Functionalisation using Microspheres

PLGA microspheres were fabricated using a single-emulsion solvent evaporation technique as has been described before [25]. Briefly, using a T25 digital UltraTurrax® homogenizer, 40 ml of 4% v/w PLGA/chloroform solution was gradually added to a stirring 300 ml solution of 0.5 % polyvinyl alcohol. The resulting emulsion was stirred for 6 hours at 600 rpm and hardened spheres were subsequently collected. The sphere solution was then centrifuged at 1200 rpm for 5 min. The spheres were re-suspended in isopropyl alcohol and placed into spray bottles. To embed the spheres into the electro-spun mats, the rotating drum was sprayed with the sphere solution during the electro-spinning process (**Figure 2.1**).

Figure 2.1: Illustrates the process of incorporating microspheres into the electro-spun scaffolds.

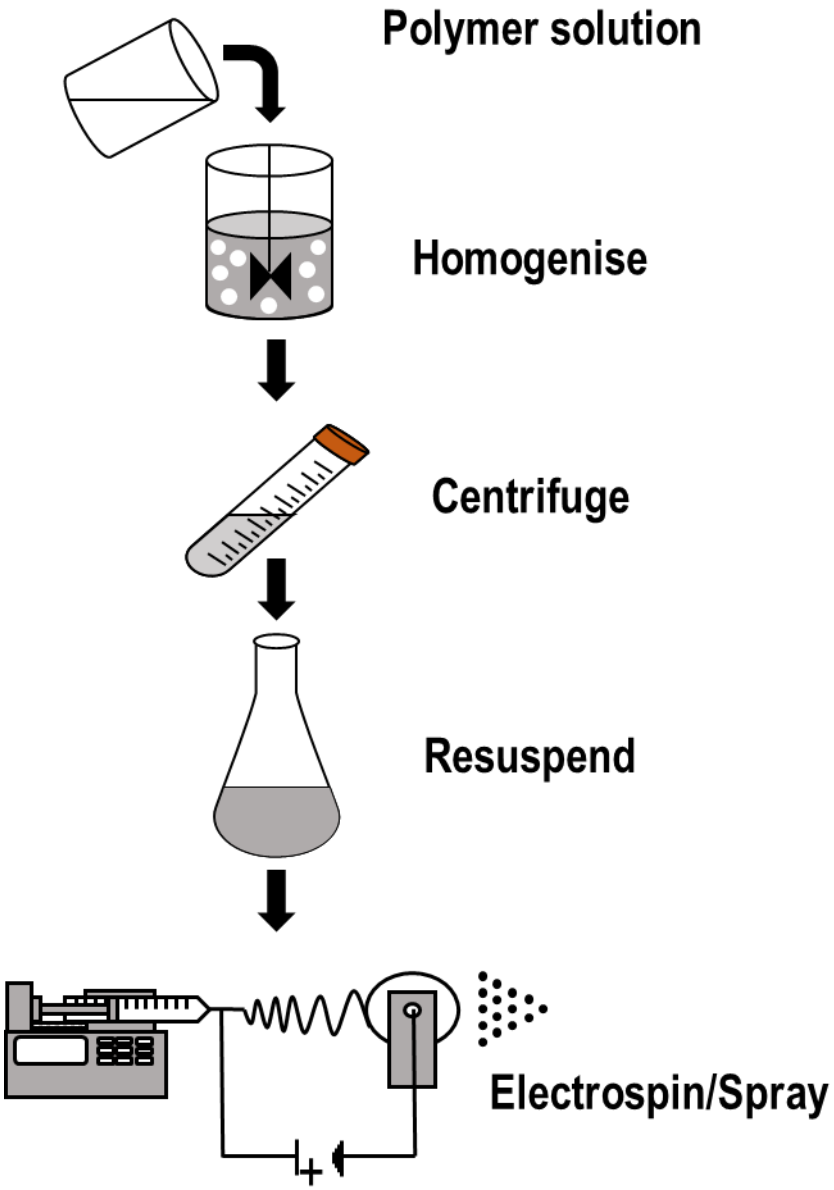

2.2.5. Scanning Electron Microscopy Analysis

The morphology of the produced scaffolds was evaluated using a low voltage, high resolution Scanning Electron Microscope (SEM; S-4700 Hitachi Scientific Instruments, Berkshire, UK) after gold sputtering (Emitech K-550X Sputter Coater, Emitech Ltd., Ashford, Kent, UK).

2.2.6. Biophysical Evaluation

Stress-strain curves of dry and wet electro-spun PLGA mats were determined in uniaxial tension using a Zwich Z2.5 Universal Mechanical Tester (Bratislava, Slovakia) at a crosshead speed of 10 mm/min using a 100 N load cell, as has been described previously [26-29]. To avoid damaging the electro-spun mats during handling, the mats were mounted on a paper frame as has been described before [30, 31]. The gauge length was determined by the vertical dimension of the window in the frame (3 cm in length). Frames containing specimen mats were then placed between the upper and lower grips of the Zwich. The sides of the frame were then cut leaving the specimen intact. The width of the samples was fixed at 1 cm. The thickness of the samples was determined using a digital micro-meter (Tresna, Essen, Germany with an accuracy of 1 μm; three readings were taken for each sample. Results obtained with electro-spun mats that broke at contact points with the grips were rejected. The following definitions were used to calculate the mechanical data: stress at break was defined as the load at complete failure divided by the original cross-sectional area (engineering stress); strain at break was defined as the increase in fibre length required to cause failure divided by the original length and Young's modulus of samples was calculated from slope of the stress strain curve in the linear region and the initial

sample geometry. Prior to wet testing, dry electro-spun mats were equilibrated in PBS (0.01M; pH 7.4) at room temperature overnight.

2.2.7. Bovine Tenocyte Isolation

Bovine hind limbs were sourced from a local abattoir. Using aseptic techniques the tendons were isolated from the surrounding fascia and tenocytes were isolated as has been described previously [32]. Briefly, the limbs were washed with PBS and prepared for incision. The skin was then washed further with 70% ethanol. With disposable scalpel each layer of skin and soft tissue was released and retracted. The tendon was then transected a quarter away from the insertion and musculotendinous junction. The tendons were subsequently placed into sterile Hanks Balanced Salt Solution (HBSS) and stored in ice. Following that, the tendons were placed into a Petri dish with a small volume of ice cold HBSS and diced to approximately 2 mm by 2 mm pieces. The tendon pieces were then digested with filtered 0.15% collagenase solution into 50 ml centrifuge tubes. The solution was stored under agitation in an incubator maintained at 37 °C and 5% CO_2 overnight. The following day, the solution was passed through a nylon mesh cell strainer to remove any matrix debris or undigested material and filtrate-centrifuged at 1200 rpm for 5 minutes. The cell pellet was re-suspended in culture media and seeded into 175 cm^2 tissue culture flasks. Bovine tenocytes were then cultured as described below.

2.2.8. Culture of Bovine Tenocytes

Freshly isolated bovine tenocytes were cultured in Dulbecco's modified Eagle's medium (DMEM) supplemented with 10% Foetal Bovine Serum (FBS) and 1% penicillin/streptomycin in 75 cm^2 flasks. The bovine tenocyte culture was maintained

at 37 °C in a humidified 5% CO_2 incubator until they were approximately 80% confluent with media being changed every 2-3 days. At passage 3, 1.5 x 10^4 cells/cm^2 cells were seeded on the various scaffolds conformations (PLGA aligned and randomly orientated electro-spun mats and solvent cast films) for 2, 4 and 7 days.

2.2.9. Cell Metabolic Activity

Cell metabolic activity was determined using alamarBlue® cell metabolic assay at predetermined time depending on cell type (mentioned above for the different cell types). Briefly, alamarBlue® dye was diluted with Hank's Balance Salt Solution to make a 10% (v/v) alamarBlue® solution. Media was removed from each well and 0.5 ml alamarBlue® solution was added to each well. Depending on cell type after an incubation time of between 1-4 hours at 37 °C, the absorbance was measured at wavelengths of 550 and 595 nm using a microplate reader (Varioskan Flash, Thermo Scientific). The level of metabolic activity was calculated using the simplified method of calculating per cent reduction, according to the supplier's protocol. The metabolic activity of cells at solvent cast film at day 2 was considered as 100%.

2.2.10. Cell Fluorescent Labelling

Cell attachment, spreading and alignment were assessed using immunofluorescent images. Briefly, the cells were fixed with 4% paraformaldehyde for 15 minutes, permeabilised with 0.2% TritonX, and the nucleus was stained with 4',6-Diamidino-2-phenylindole (DAPI, Molecular Probes) for 5 minutes. The actin cytoskeleton of the cells was then stained with rhodamine-conjugated phalloidin (Molecular Probes) for 1h. Images were captured at 10x magnification using an inverted BX51 Olympus fluorescence microscope.

2.2.11. Statistical Analysis

Numerical data is expressed as mean ± SD. Analysis was performed using statistical software (MINITAB™ version 16, Minitab, Inc., State College PA, USA). Two sample t-test for pair wise comparisons was employed after confirming the following assumptions: (a) the distribution from which each of the samples was derived was normal (Anderson-Darling normality test); and (b) the variances of the population of the samples were equal to one another (Bartlett's and Levene's tests for homogenicity of variance). Non-parametric statistics were utilised when either or both of the above assumptions were violated and consequently Mann-Whitney test for two samples was carried out. Statistical significance was accepted at $p<0.05$.

2.3. Results

2.3.1. Electro-spinning Optimisation

2.3.1.1. Fibre Diameter

A range of voltages, 8 kV – 20 kV, was evaluated. The effect the voltage had on fibre diameter is illustrated in **Figure 2.2**; voltage of 20 kV produced the smallest fibres, with an average diameter of 2.1 μm. From our results, it is demonstrated that voltage has a proportional relationship with fibre diameter. From the graph, it can be seen that with an increase in voltage, there is a decrease in the average fibre diameter. An increase from 10 kV – 20 kV gives a reduction of average fibre diameter of approximately 1 μm.

Figure 2.3 displays the average fibre diameter produced versus rotational speed of the drum. The range of fibres produced by this range of parameters is 1.8 μm – 2.3 μm. The results obtained from this study do not vary linearly with rpm. The lowest standard deviation, of 0.34 μm, was produced by a rotational speed of 1300 rpm. The highest standard deviation, of 1.23 μm, was produced by a rotational speed of 754 rpm. With the two lowest rotational speed, standard deviations of above 30% of the average fibre diameter was produced.

Figure 2.4 shows the effect of the flow rate on fibre diameter. These results show that the smallest fibres, with average fibre diameter 1.6 μm, were produced by flow rate of 0.03 ml/min. The other two flow rates (0.05 ml/min and 0.07 ml/min) produced fibres with an average fibre size of 2.1 μm. The lowest standard deviation, of 0.38 μm, was produced by a flow rate of 0.05 ml/min. The highest standard deviation, of 0.79 μm, was produced by a flow rate of 0.07 ml/min.

Figure 2.2: Shows the graph of the average diameter produced with various voltages. Data is represented as mean ± standard deviation.

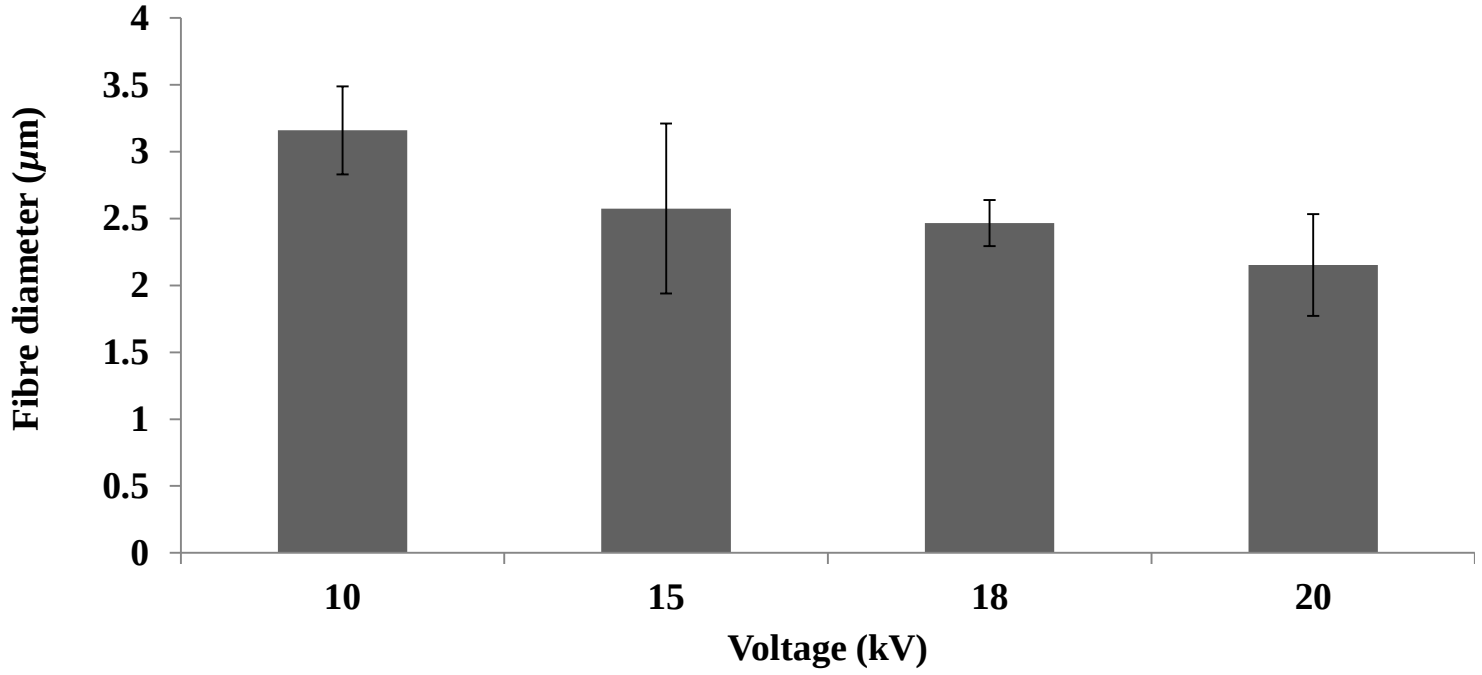

Figure 2.3: Shows the fibre diameter for each rpm. Data is represented as mean ± standard deviation.

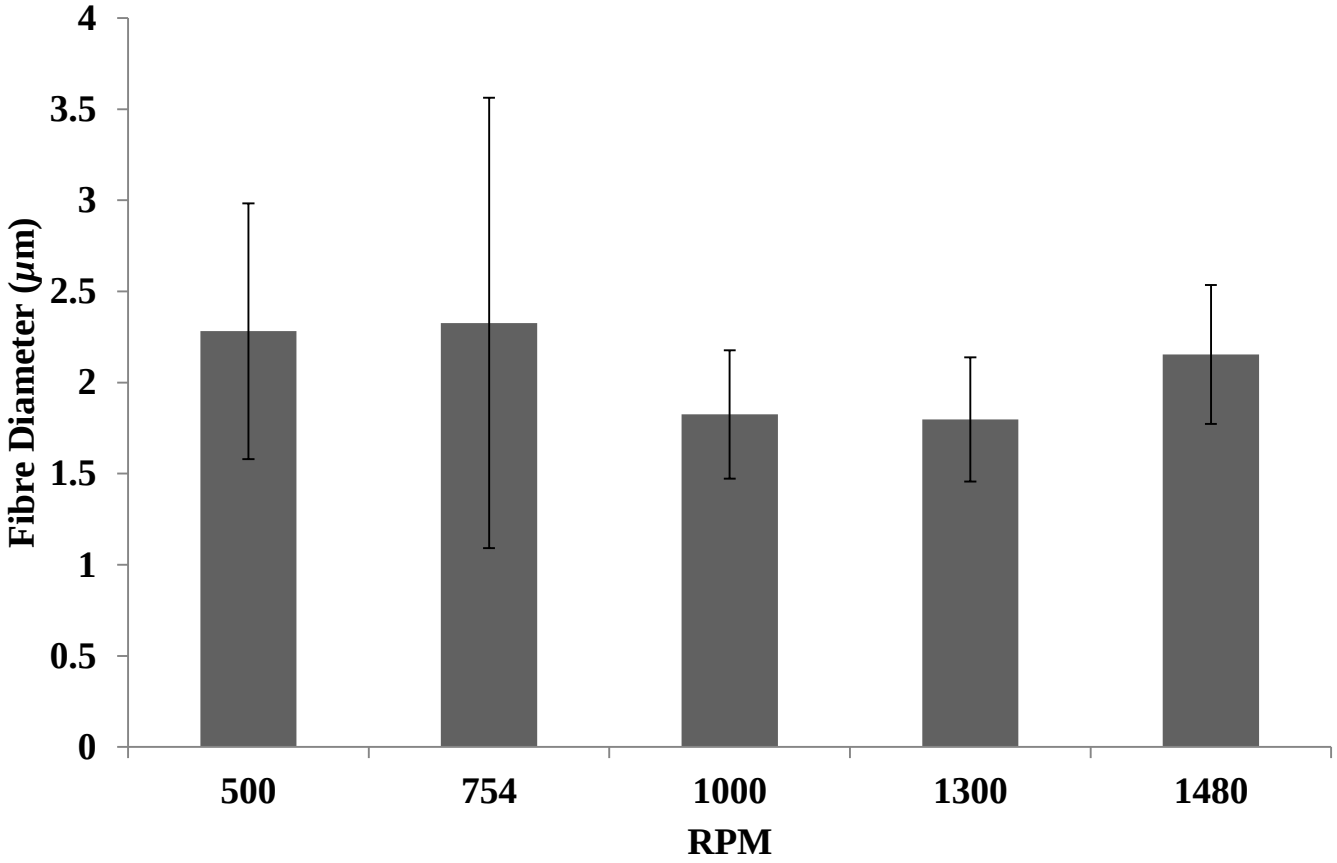

Figure 2.4: Shows the fibre diameter for each flow rate. Data is represented as mean ± standard deviation.

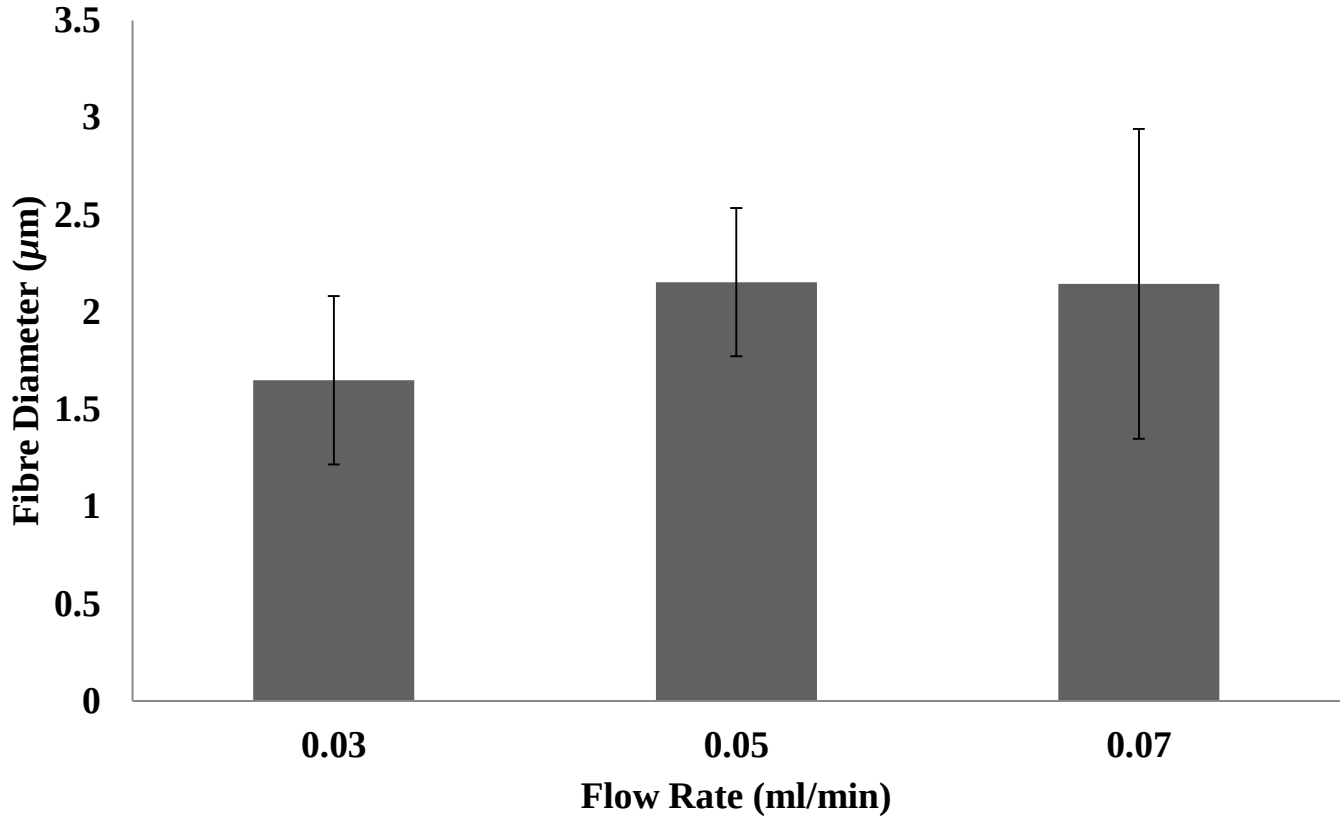

2.3.1.2. Fibre Alignment

Figure 2.5 shows the results from the RPM study. The change in rpm generates a large change in alignment. By examining the SEM images it was noticed that high rotational speeds, such as 1480, 1300, and 1000 rpm all produced highly aligned fibrous scaffolds. While decreasing the rpm further to 745 and 500 rpm produced less aligned scaffolds. From examining the FFT graphs the degree of alignment becomes apparent. The data retrieved from 745 rpm and 500 rpm produced erratic peaks due to the low degree of alignment. Although 1000 rpm did produce aligned scaffolds the location of a second peak at approximately 108° indicates inconsistency across all locations tested. The narrow and tall peaks produced at a speed of 1300 rpm indicate this as the optimal speed for consistent alignment.

Figure 2.5: Fibre alignment versus rotational speed. (A-E) Scanning electron microscope images of fibres produced at a speed 1480 rpm, 1300 rpm, 1000 rpm, 745 rpm and 500 rpm of respectively. (F) Fast Fourier transform of the fibre alignment.

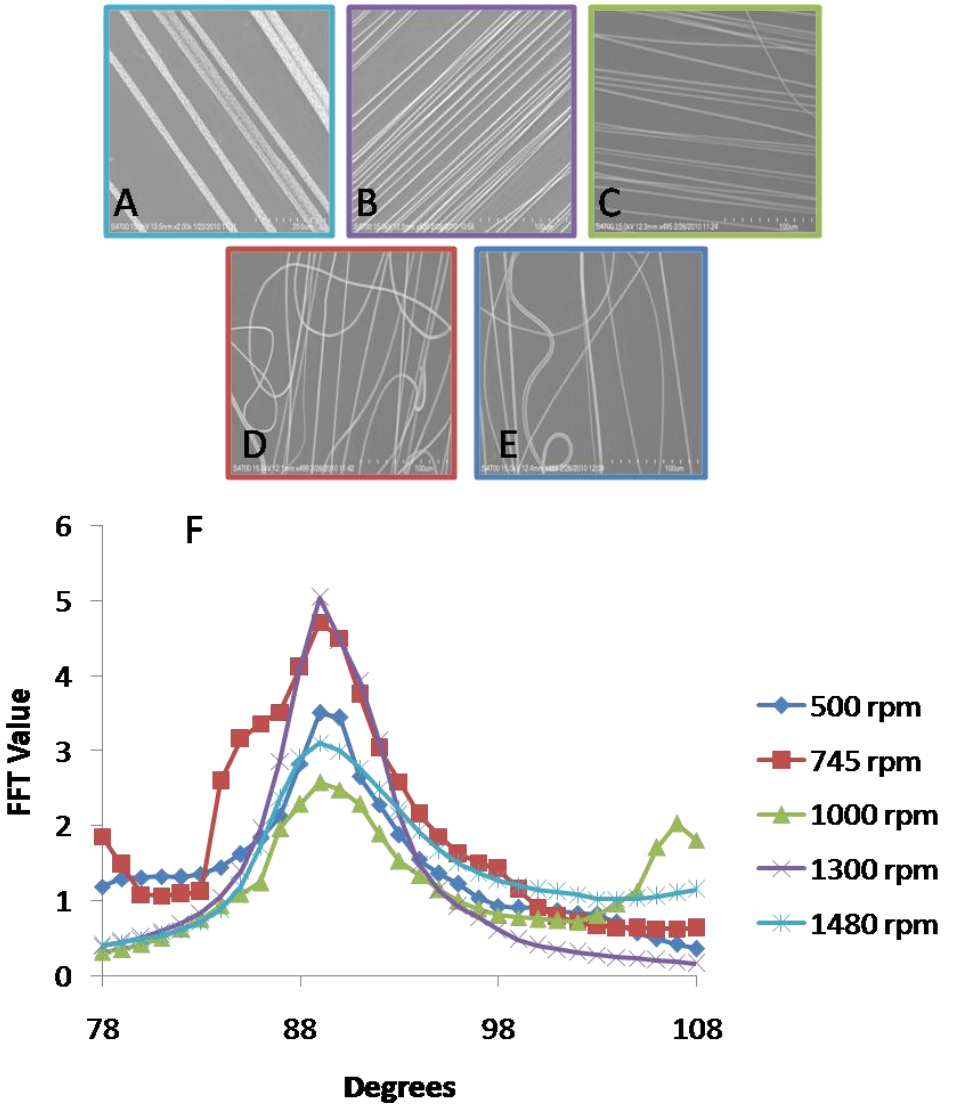

2.3.2. Scaffold Morphology

SEM analysis revealed that all electro-spun mats were composed of uniform random and aligned oriented fibres (**Figure 2.6a** and **Figure 2.6b** respectively) Mono-dispersed microspheres were also produced and successfully incorporated into the produced aligned orientated electro-spun mats (**Figure 2.6c**). Continuous electro-spinning gave rise to a three-dimensional scaffold (**Figure 2.6d** and **Figure 2.6e**).

Figure 2.6: Scanning electron micrographs of random and aligned orientated electro-spun scaffolds (a and b respectively). Scanning electron micrographs of mono-dispersed microspheres embedded within aligned orientated electro-spun scaffolds (c). Scanning electron (d) and optical (e) micrographs of three-dimensional aligned nano-structured composites.

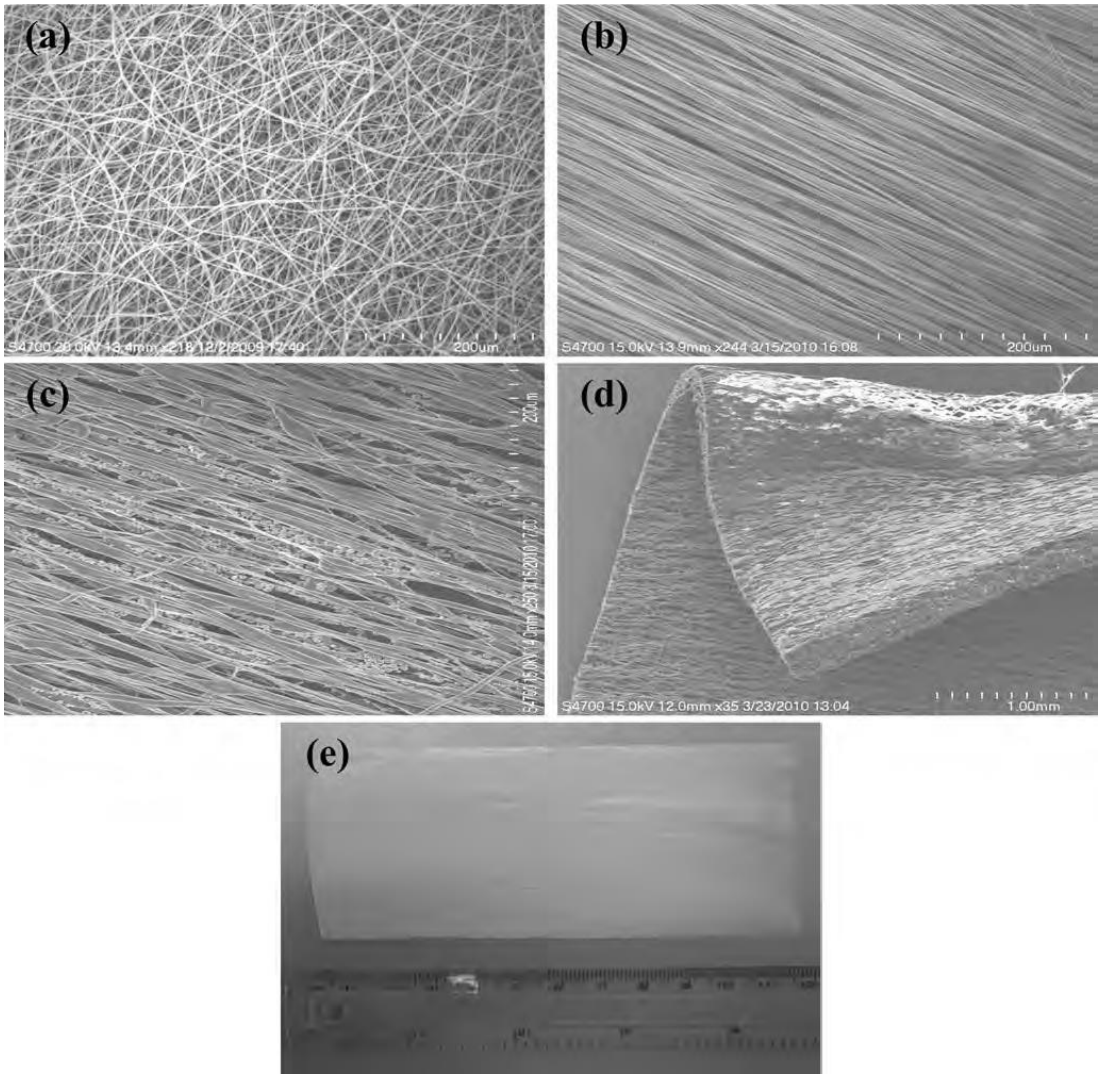

2.3.3. Biophysical Analysis

Uniaxial tensile tests of aligned orientated electro-spun mats in both wet and dry state exhibited stress-strain curves consisting of a region of steeply rising stress, followed by a region of decreasing stress up to the point of fracture (**Figure 2.7**). Uniaxial tensile tests of randomly orientated electro-spun mats in both wet and dry state exhibited stress-strain curves consisted of a region of steeply rising stress, followed by a region of constant gradient and then a region of decreasing stress, which persisted up to the point of fracture (**Figure 2.7**). These distinct deformation mechanisms can be visually observed in **Figure 2.8**, where aligned electro-spun mats exhibited a split fracture mode, whilst their random orientated counterparts demonstrated a delayed split fracture mode.

Figure 2.7: Stress-strain curves of dry and wet aligned and random orientated electro-spun fibrous mats. Aligned electro-spun mats in dry and wet state exhibited a region of rising stress, followed by a region of decreasing stress, whilst random electro-spun mats in dry and wet state revealed a region of rising stress, followed by a region of constant gradient and then a region of decreasing stress, which persisted up to fracture.

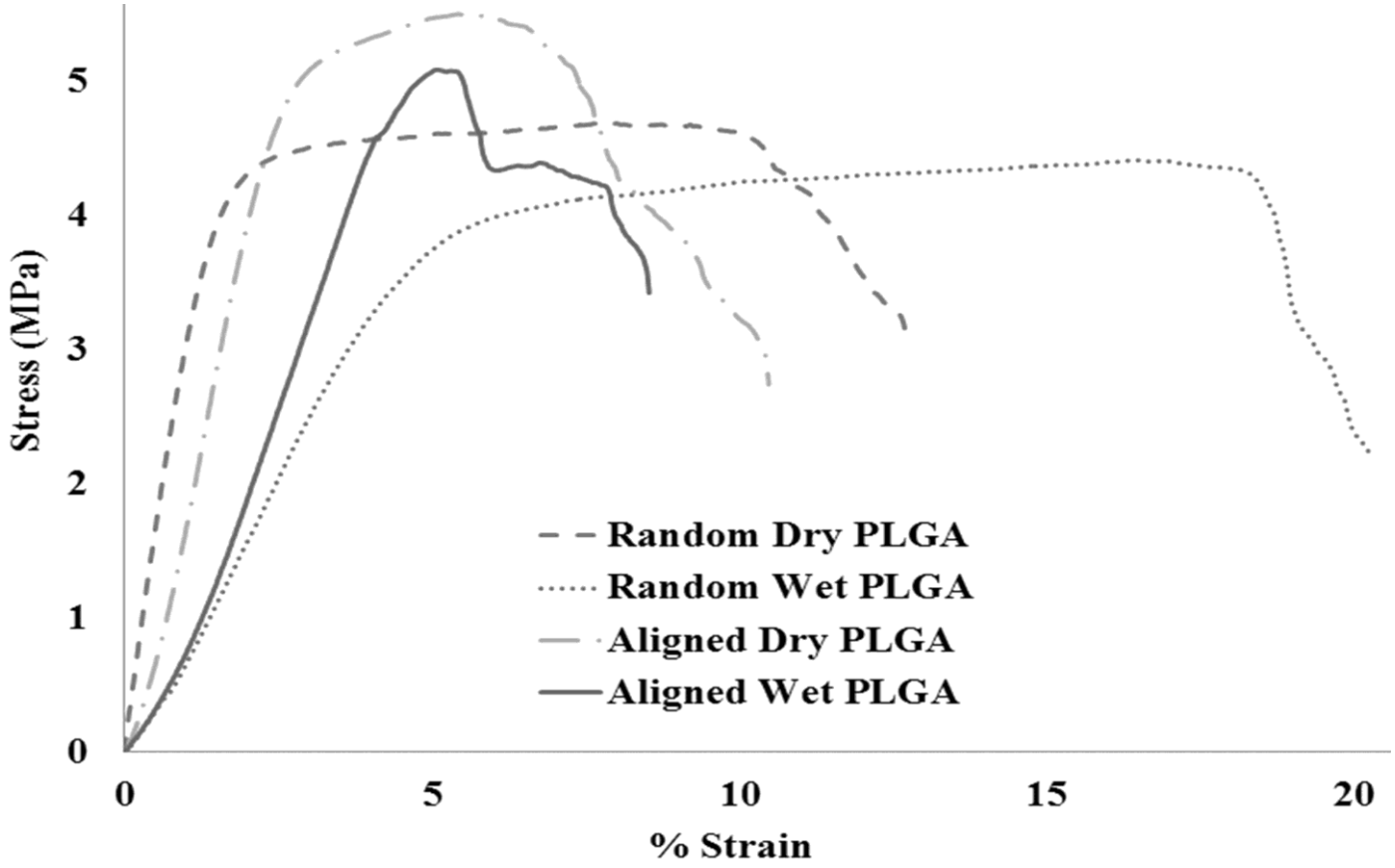

Figure 2.8: Fibre orientation resulted in different deformation mechanisms. Aligned orientated electro-spun mats (a) exhibited a split fracture mode, whilst random orientated electro-spun mats (b) displayed a delayed split fracture mode.

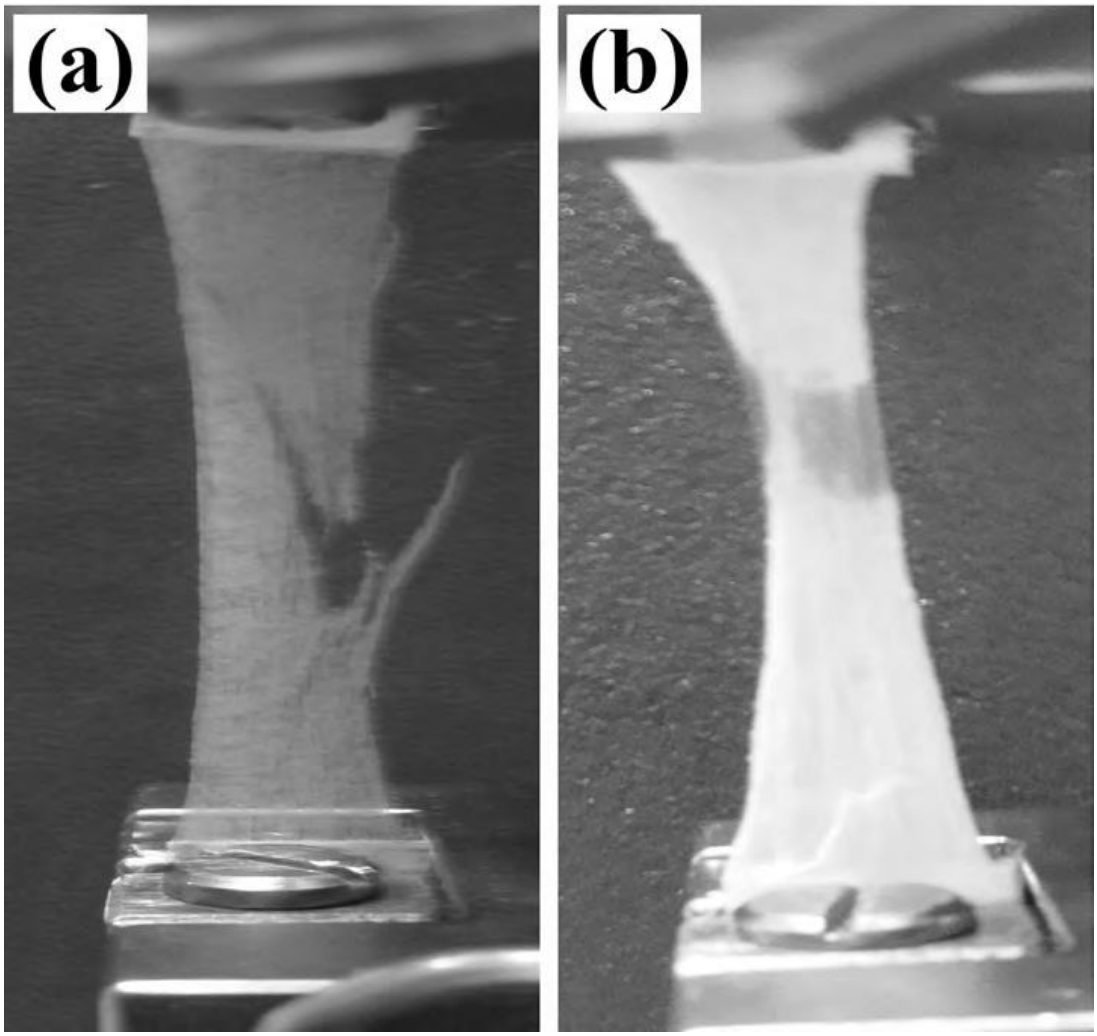

Table 2.1 summarises the mechanical properties of the electro-spun mats produced in this study. In the dry state, random and aligned orientated electro-spun mats demonstrated no significant difference in thickness, stress at break and modulus values (p>0.05), whilst significant difference in strain at break values was observed (p<0.001). In the wet state, random and aligned orientated electro-spun mats demonstrated no significant difference in thickness (p>0.05), whilst significant difference was observed between stress and strain at break and modulus values (p<0.006).

Table 2.1: Mechanical properties of dry and wet random and aligned orientated PLGA electro-spun mats. Sample number n in parentheses; SD: standard deviation.

Scaffold Conformation and State	Thickness (μm) ± SD	Stress at Break (MPa) ± SD	% Strain ± SD	Modulus (MPa) ± SD
Random Dry PLGA Mats (n = 5)	38.40 ± 2.70	3.14 ± 1.15	17.09 ± 2.20	1.61 ± 0.69
Aligned Dry PLGA Mats (n = 5)	37.80 ± 5.03	3.20 ± 0.42	10.38 ± 1.34	1.69 ± 0.78
Random Wet PLGA Mats (n = 4)	43.00 ± 8.25	2.66 ± 0.44	23.66 ± 7.67	0.96 ± 0.46
Aligned Wet PLGA Mats (n = 6)	33.72 ± 5.47	3.98 ± 0.61	9.32 ± 1.07	1.71 ± 0.56

2.3.4. Biological Evaluation

Cell-matrix interactions between different cell-types and different substrates were studied *in vitro* by seeding bovine tenocytes on the produced scaffolds for various time periods. **Figure 2.9** shows results of the alamarBlue® metabolic activity assay. At day 2 and 4, bovine tenocytes seeded on solvent casted films exhibited significant higher metabolic activity than cells seeded on either of the electro-spun mats ($p<0.001$). However, no significant difference in metabolic activity was observed among the different scaffold conformations by day 7 ($p>0.05$).

Bovine tenocytes exhibited a random cytoskeleton and nuclei conformation, when they were seeded on solvent casted films and random orientated electro-spun mats for all the time points evaluated. However, they appeared to orientate perpendicularly to the substrate topography, when they were seeded onto aligned orientated electro-spun mats (**Figure 2.10**).

Figure 2.9: alamarBlue® metabolic activity assay results for bovine tenocytes over a 7 day culture period. No significant difference in metabolic activity of bovine tenocytes was observed among the different scaffold conformations by day 7 (p>0.05). * indicates significant difference.

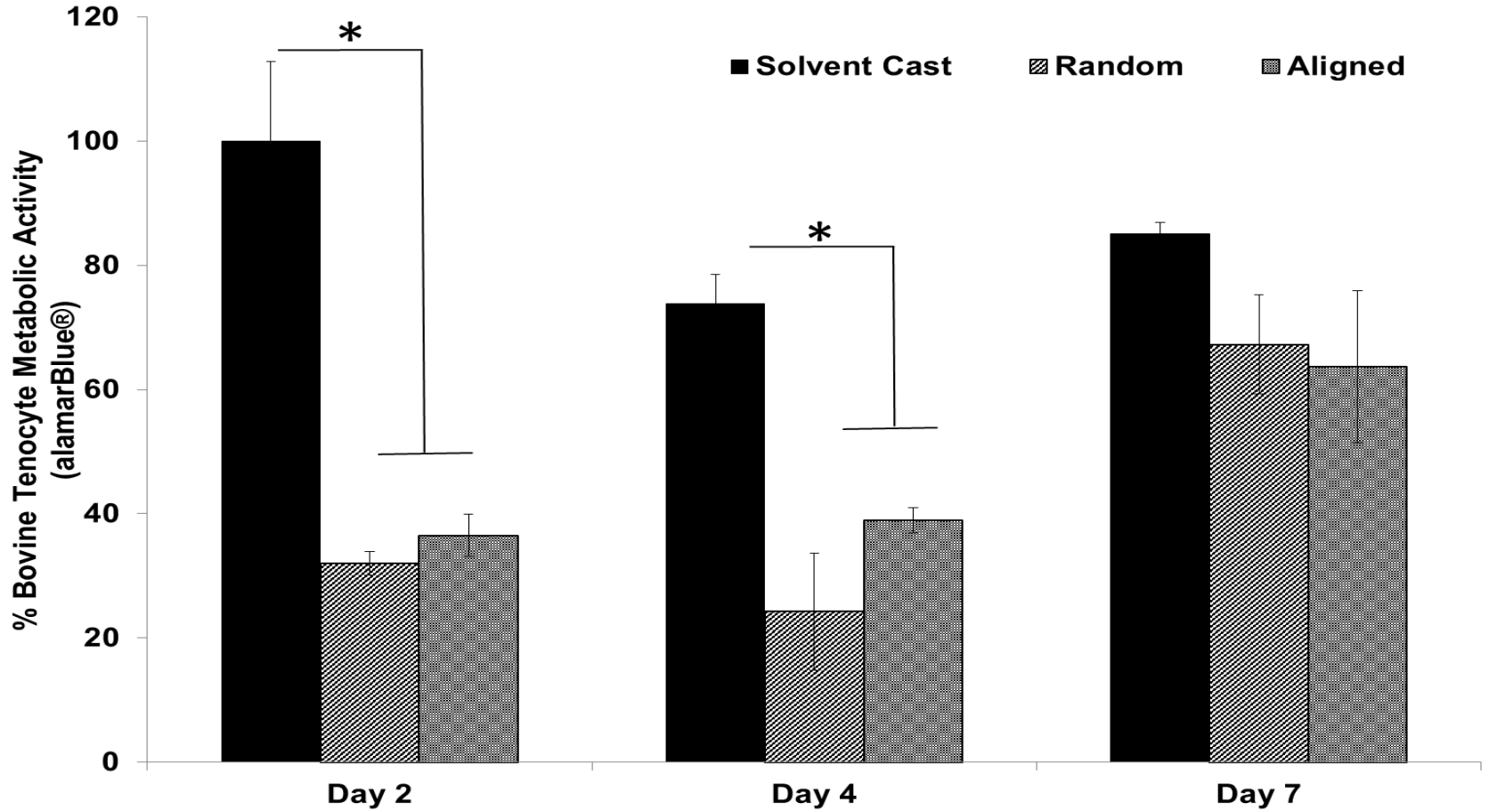

Figure 2.10: Bovine tenocytes were seeded on solvent casted and random orientated electro-spun mats exhibited a random cytoskeleton and nuclei orientation for all time points. However, when the bovine tenocytes were seeded on aligned orientated electro-spun mats, they appeared to orientate perpendicularly to the substrate topography. The actin cytoskeleton of the cells was stained red with rhodamine-conjugated phalloidin; nuclei were stained blue with DAPI. Arrows indicate the orientation of the substrate topography.

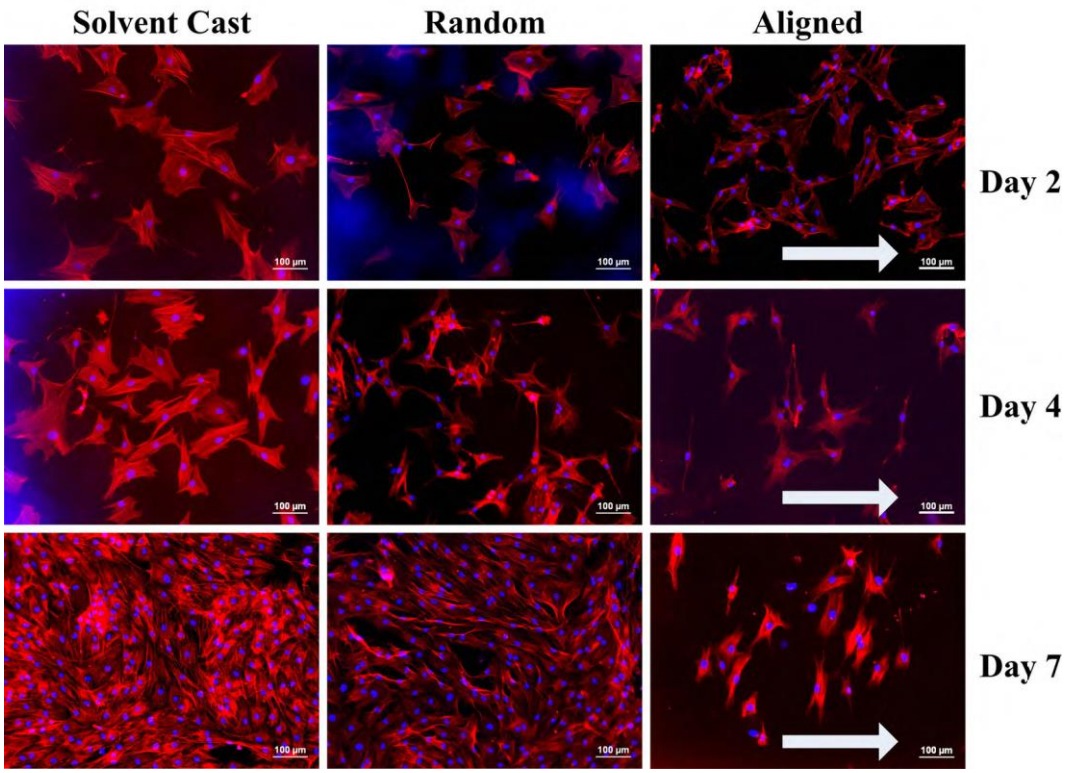

2.4. Discussion

Nano-scale technologies are emerging as powerful tools for tissue engineering and biological studies due to their ability to operate on the same small scale as all functions involved in the growth, development and ageing of the human body [33]. Biomaterials design is now required to include topographical cues, since topography offer control over cellular functions such as growth, directional cell motility, tissue development, angiogenesis and immune response [34-45]. The rationale of this approach is to mimic the complex topographies found in native tissue *in vitro* [18, 46, 47]. Biomaterials are also required to accurate deliver bioactive and/or therapeutic molecules to a specific location in order to protect the typically labile molecules and to positively interact with host and enhance tissue repair and regeneration [48-50]. Herein, we evaluate the effect of electro-spinning- and solvent casting- induced topographies on the metabolic activity and alignment of bovine tenocytes and we describe a method consisting of electro-spinning and spraying to introduce a further element of functionality to the three-dimensional scaffold.

Starting with the biomechanical analysis, we found that uniaxial tensile tests of all scaffolds evaluated in this study produced stress-strain curves similar to those reported for semi-crystalline polymers that yield and undergo plastic flow [51]. Aligned and random orientated scaffolds exhibited a region of reduced stress that lasted until failure. Although it was not investigated during the current study, this yielding mechanism would imply some form of flow occurring within the fibrous structure, possibly inter-fibrillar slippage. *In vivo*, this mechanism is very important in the tensile deformation of connective tissues such as tendon, skin and pericardium [52-54]. Similar stress-strain curves have also been reported previously for collagen-based biomaterials [55-62] and nano-fibrous meshes [63-65]. Although the electro-spun

mats produced in this study were characterised by mechanical properties do not closely match those of native tissues, such as anterior cruciate ligament, Achilles tendon and skin and implantable devices [60, 66-74] aligned electro-spun scaffolds are shown to be slightly stronger than the randomly orientated counterparts.

Continuing with the biological analysis, we observed that the metabolic activity of bovine tenocytes seeded on different scaffolds increased as a function of time. Given that increasing metabolic activity is an indicator of cell proliferation, these results indicate that all scaffold conformations can support cell growth. Although there no significant difference was observed in metabolic activity bovine tenocytes seeded on aligned and random orientated electro-spun mats. Fluorescent labelling of the cell cytoskeleton indicates the cellular orientation of the tenocytes. Of significant importance is the observation that bovine tenocytes aligned perpendicularly to the substrate topography. In previous studies, primary tenocytes had aligned parallel to the substrate topography either when grooves bigger than the cells were used or when applied load had been used along the fibre axis [75-78]. In vivo, tenocytes are elongated in shape cells arranged in a unicellular row in the space between adjacent tendon fibres [79-82], which are exposed to repeated tensile forces [83-87]. The combination of aligned collagen fibres and repeated loading may be responsible for the aligned conformation of these cells. However, when only one of these parameters is available, such as topography in the current study, we observe that the cells align perpendicularly to the underlying topography.

The emerging field of tissue engineering requires accurate delivery of bioactive and/or therapeutic molecules to a specific location. Glycosaminoglycans and proteoglycans [88-90] or bioactive molecules such as growth factors or hormones are traditionally used to enhance biological functions of biomaterials [91-94]. However, such

molecules are typically labile; the biologic half-lives of platelet-derived growth factor, basic fibroblast growth factor, and vascular endothelial growth factor are 2, 3, and 50 min, respectively, when intravenously administered [95]. As a result, the use of polymeric delivery vehicles has been advocated to encapsulate such bioactive molecules and maintain a sustained localised delivery to the target site. Current approaches to functionalise electro-spun mats are primarily based on mixing the polymer from which the scaffold is to be made with the bioactive molecule. However, this approach may affect the mechanical properties of the fibres as well as the fibre structure [23, 24]. While maintaining fibre orientation and structure we developed a co-deposition technique, whereby spinning and spraying occur simultaneously. During the deposition of electro-spun fibres, microspheres are also sprayed and trapped within the three dimensional scaffold. Microspheres are a versatile delivery vehicle used for the delivery of biomolecules. By incorporating microspheres into the network, we create an independent mechanism to tune drug delivery, while maintaining the structure of the scaffold. Drug delivery from microspheres can be easily controlled by composition and size as has been described before [96-98]. Furthermore, by using the spraying technique it is conceivable that more than one composition of microsphere may be introduced for delivery of multiple drugs. The controlled delivery of biomolecules from electro-spun/spayed scaffolds will be the subject of future research.

2.5. Conclusions

Herein, we ventured to investigate the influence of scaffold architecture on mechanical properties and on cell response and to develop means of sustained delivery of bioactive molecules. Our data indicate that aligned orientated fibres exhibit high stress at break values, whilst random orientated fibres exhibit high strain at break values. We identified that bovine tenocytes aligned perpendicularly to the substrate topography. We speculate that the lack of mechanical loading is responsible for this; having run the experiment under tension, tenocytes may have aligned parallel to the substrate topography. We have also successfully incorporated microspheres into the three dimensional scaffold by slightly modifying the electro-spinning set-up.

2.6. References

[1] Zeugolis DI, Chan JCY, Pandit A. Tendons: Engineering of Functional Tissues. In: Pallua N, Suscheck CV, editors. Tissue Engineering: Springer Berlin Heidelberg; 2011. p. 537-572.

[2] Ionescu LC, Lee GC, Sennett BJ, Burdick JA, Mauck RL. An anisotropic nanofiber/microsphere composite with controlled release of biomolecules for fibrous tissue engineering. Biomaterials 2010;31:4113-4120.

[3] Pot SA, Liliensiek SJ, Myrna KE, Bentley E, Jester JV, Nealey PF, Murphy CJ. Nanoscale Topography–Induced Modulation of Fundamental Cell Behaviors of Rabbit Corneal Keratocytes, Fibroblasts, and Myofibroblasts. Investigative Ophthalmology & Visual Science 2010;51:1373-1381.

[4] Hutmacher DW. Scaffold design and fabrication technologies for engineering tissues-state of the art and future prespectives. Journal of Biomaterials Science Polymer Edition 2001;12:107-124.

[5] Khademhosseini A, Langer R, Borenstein J, Vacanti JP. Microscale technologies for tissue engineering and biology. PNAS 2006;103:2480-2487.

[6] Yang L, Fitie CFC, van der Werf KO, Bennink ML, Dijkstra PJ, Feijen J. Mechanical properties of single electrospun collagen type I fibers. Biomaterials 2008;29:955-962.

[7] Zeugolis DI, Khew ST, Yew ESY, Ekaputra AK, Tong YW, Yung L-YL, Hutmacher DW, Sheppard C, Raghunath M. Electro-spinning of pure collagen nano-fibres - Just an expensive way to make gelatin? Biomaterials 2008;29:2293-2305.

[8] Jiang X, Lim SH, Mao H-Q, Chew SY. Current applications and future perspectives of artificial nerve conduits. Experimental Neurology 2010;223:86-101.

[9] Yao L, O'Brien N, Windebank A, Pandit A. Orienting neurite growth in electrospun fibrous neural conduits. J Biomed Mater Res B Appl Biomater 2009;90:483-491.

[10] Ladd MR, Lee SJ, Stitzel JD, Atala A, Yoo JJ. Co-electrospun dual scaffolding system with potential for muscle-tendon junction tissue engineering. Biomaterials 2011;32:1549-1559.

[11] Nerurkar NL, Sen S, Baker BM, Elliott DM, Mauck RL. Dynamic culture enhances stem cell infiltration and modulates extracellular matrix production on aligned electrospun nanofibrous scaffolds. Acta Biomaterialia 2011;7:485-491.

[12] Gupta D, Venugopal J, Mitra S, Giri Dev VR, Ramakrishna S. Nanostructured biocomposite substrates by electrospinning and electrospraying for the mineralization of osteoblasts. Biomaterials 2009;30:2085-2094.

[13] Li X, Xie J, Yuan X, Xia Y. Coating Electrospun Poly(ε-caprolactone) Fibers with Gelatin and Calcium Phosphate and Their Use as Biomimetic Scaffolds for Bone Tissue Engineering. Langmuir 2008;24:14145-14150.

[14] Shields KJ, Beckman MJ, Bowlin GL, Wayne JS. Mechanical Properties and Cellular Proliferation of Electrospun Collagen Type II. Tissue Engineering 2004;10:1510 -1517.

[15] Toyokawa N, Fujioka H, Kokubu T, Nagura I, Inui A, Sakata R, Satake M, Kaneko H, Kurosaka M. Electrospun Synthetic Polymer Scaffold for Cartilage Repair Without Cultured Cells in an Animal Model. Arthroscopy: The Journal of Arthroscopic & Related Surgery 2010;26:375-383.

[16] Stitzel J, Liu J, Lee SJ, Komura M, Berry J, Soker S, Lim G, Van Dyke M, Czerw R, Yoo JJ, Atala A. Controlled fabrication of a biological vascular substitute. Biomaterials 2006;27:1088-1094.

[17] Heydarkhan-Hagvall S, Schenke-Layland K, Dhanasopon AP, Rofail F, Smith H, Wu BM, Shemin R, Beygui RE, MacLellan WR. Three-dimensional electrospun ECM-based hybrid scaffolds for cardiovascular tissue engineering. Biomaterials 2008;29:2907-2914.

[18] Chai C, Leong KW. Biomaterials Approach to Expand and Direct Differentiation of Stem Cells. Mol Ther 2007;15:467-480.

[19] Laporte LD, Shea LD. Matrices and Scaffolds for DNA Delivery in Tissue Engineering. Adv Drug Deliv Rev 2007;59:292-307.

[20] Barras F, Pasche P, Bouche N, Aebischer P, Zurn A. Glial cell line-derived neurotrophic factor released by synthetic guidance channels promotes facial nerve regeneration in the rat. J Neurosci Res 2002;70:746-755.

[21] Tornqvist N, Bjorklund L, Almqvist P, Wahlberg L, Stromberg I. Implantation of bioactive growth factor-secreting rods enhances fetal dopaminergic graft survival, outgrowth density, and functional recovery in a rat model of Parkinson's disease. Exp Neurol 2000;164:130-138.

[22] Bensadoun J, Pereira de Almeida L, Fine E, Tseng J, Deglon N, Aebischer P. Comparative study of GDNF delivery systems for the CNS: polymer rods, encapsulated cells, and lentiviral vectors. J Controlled Release 2003;87:107-115.

[23] Liao I, Chew S, Leong K. Aligned core-shell nanofibers delivering bioactive proteins. Nanomedicine 2006;1:465-471.

[24] Huang Z-M, He C-L, Yang A, Zhang Y, Han X-J, Yin J, Wu Q. Encapsulating drugs in biodegradable ultrafine fibers through co-axial electrospinning. Journal of Biomedical Materials Research Part A 2006;77A:169-179.

[25] Mundargi RC, Babu VR, Rangaswamy V, Patel P, Aminabhavi TM. Nano/micro technologies for delivering macromolecular therapeutics using poly(d,l-lactide-co-glycolide) and its derivatives. Journal of Controlled Release 2008;125:193-209.

[26] Meng ZX, Wang YS, Ma C, Zheng W, Li L, Zheng YF. Electrospinning of PLGA/gelatin randomly-oriented and aligned nanofibers as potential scaffold in tissue engineering. Materials Science and Engineering: C 2010;30:1204-1210.

[27] McManus MC, Boland ED, Koo HP, Barnes CP, Pawlowski KJ, Wnek GE, Simpson DG, Bowlin GL. Mechanical Properties of Electrospun Fibrinogen Structures. Acta Biomaterialia 2006;2:19-28.

[28] Wang SD, Zhang YZ, Yin GB, Wang HW, Dong ZH. Fabrication of a Composite Vascular Scaffold Using Electrospinning Technology. Materials Science and Engineering: C 2010;30:670-676.

[29] Li W-J, Cooper JAJ, Mauck RL, Tuan RS. Fabrication and characterization of six electrospun poly(a-hydroxy-ester)-based fibrous scaffolds for tissue engineering applications. Acta Biomaterialia 2006;2:377-385.

[30] Kato YP, Christiansen DL, Hahn RA, Shieh S-J, Goldstein JD, Silver FH. Mechanical properties of collagen fibres: a comparison of reconstituted and rat tail tendon fibres. Biomaterials 1989;10:38-42.

[31] Huang Z-M, Zhang YZ, Ramakrishna S, Lim CT. Electrospinning and mechanical characterization of gelatin nanofibers. Polymer 2004;45:5361-5368.

[32] Shortkroff S, Spector M. Isolation and In Vitro Proliferation of Chondrocytes, Tenocytes, and Ligament Cells. In: Morgan JR, Yarmush ML, editors. Tissue Engineering Methods and Protocols: Humana Press; 1999. p. 195-203.

[33] Xia Y. Nanomaterials at work in biomedical research. Nature Materials 2008;7:758-760.

[34] Weiss P. Experiments on cell and axon and orientation in vitro: the role of colloidal exudates in tissue organization. J Exp Zool 1945;100:353-386.

[35] Rosenberg M. Cell guidance by alterations in monomolecular films. Science 1963;139:411-412.

[36] Curtis A, Varde M. Control of cell behavior: topological factors. J Natl Cancer Inst 1964;33:15-26.

[37] Saino E, Focarete ML, Gualandi C, Emanuele E, Cornaglia AI, Imbriani M, Visai L. Effect of Electrospun Fiber Diameter and Alignment on Macrophage Activation and Secretion of Proinflammatory Cytokines and Chemokines. Biomacromolecules 2011;12:1900-1911.

[38] Bauer AL, Jackson TL, Jiang Y. Topography of Extracellular Matrix Mediates Vascular Morphogenesis and Migration Speeds in Angiogenesis. PLoS Comput Biol 2009;5:e1000445.

[39] Ridley AJ, Schwartz MA, Burridge K, Firtel RA, Ginsberg MH, Borisy G, Parsons JT, Horwitz AR. Cell migration: integrating signals from front to back. Science 2003;302:1704-1709.

[40] Cai K, Kong T, Wang L, Liu P, Yang W, Chen C. Regulation of endothelial cells migration on poly(d, l-lactic acid) films immobilized with collagen gradients. Colloids and Surfaces B: Biointerfaces 2010;79:291-297.

[41] Xia N, Thodeti CK, Hunt TP, Xu Q, Ho M, Whitesides GM, Westervelt R, Ingber DE. Directional control of cell motility through focal adhesion positioning and spatial control of Rac activation. The FASEB Journal 2008;22:1649-1659.

[42] Teixeira A, Abrams G, Bertics P, Murphy C, Nealey P. Epithelial contact guidance on well-defined micro- and nanostructured substrates. J Cell Sci 2003;116:1881-1892.

[43] Teixeira A, McKie G, Foley J, Bertics P, Nealey P, Murphy C. The effect of environmental factors on the response of human corneal epithelial cells to nanoscale substrate topography. Biomaterials 2006;27:3945-3954.

[44] Yim E, Reano R, Pang S, Yee A, Chen C, Leong K. Nanopattern-induced changes in morphology and motility of smooth muscle cells. Biomaterials 2005;26:5405-5413.

[45] Curtis A, Gadegaard N, Dalby M, Riehle M, Wilkinson C, Aitchison G. Cells react to nanoscale order and symmetry in their surroundings. IEEE Trans Nanobiosci 2004;3:61-65.

[46] Mitragotri S, Lahann J. Physical approaches to biomaterial design. Nat Mater 2009;8:15-23.

[47] Nel AE, Madler L, Velegol D, Xia T, Hoek EMV, Somasundaran P, Klaessig F, Castranova V, Thompson M. Understanding biophysicochemical interactions at the nano-bio interface. Nat Mater 2009;8:543-557.

[48] Holladay C, Keeney M, Greiser U, Murphy M, O'Brien T, Pandit A. A matrix reservoir for improved control of non-viral gene delivery. J Control Release 2009;136:220-225.

[49] Setton L. Reservoir Drugs. Peptide-functionalized polymer nanoparticles target and bind to articular cartilage tissue, making them promising drug-delivery vehicles. Nature Materials 2008;7:172-174.

[50] Kopecek J. Biomaterials and Drug Delivery: Past, Present, and Future. Molecular Pharmaceutics 2010;7:922-925.

[51] Attenburrow GE, Bassett DC. Compliances and failure modes of oriented chain-extended polyethylene. Journal of Materials Science 1979;14:2679-2687.

[52] Rigby BJ, Hirai N, Spikes JD, Eyring H. The mechanical properties of rat tail tendon. The Journal of General Physiology 1959;43:265-283.

[53] Hepworth DG, Smith JP. The mechanical properties of composites manufactured from tendon fibres and pearl glue (animal glue). Composites Part A: Applied Science and Manufacturing 2002;33:797-803.

[54] Garcia Paez JM, Jorge Herrero E, Carrera Sanmartin A, Millan I, Cordon A, Martin Maestro M, Rocha A, Arenaz B, Castillo-Olivares JL. Comparison of the mechanical behaviors of biological tissues subjected to uniaxial tensile testing: pig, calf and ostrich pericardium sutured with Gore-Tex. Biomaterials 2003;24:1671-1679.

[55] Knight DP, Nash L, Hu XW, Haffegee J, Ho MW. In vitro formation by reverse dialysis of collagen gels containing highly oriented arrays of fibrils. Journal of Biomedical Materials Research 1998;41:185-191.

[56] Attenburrow GE. The rheology of leather - A review. Journal of the Society of Leather Technologists and Chemists 1993;77:107-114.

[57] Wang MC, Pins GD, Silver FH. Collagen fibres with improved strength for the repair of soft tissue injuries. Biomaterials 1994;15:507-512.

[58] Fratzl P, Misof K, Zizak I, Rapp G, Amenitsch H, Bernstorff S. Fibrillar structure and mechanical properties of collagen. Journal of Structural Biology 1997;122:119-122.

[59] Zeugolis DI, Paul GR, Attenburrow G. Cross-linking of extruded collagen fibres - A biomimetic three-dimensional scaffold for tissue engineering applications. Journal of Biomedical Materials Research Part A 2009;89:895-908.

[60] Pins GD, Christiansen DL, Patel R, Silver FH. Self-assembly of collagen fibers. Influence of fibrillar alignment and decorin on mechanical properties. Biophysical Journal 1997;73:2164-2172.

[61] Cavallaro JF, Kemp PD, Kraus KH. Collagen Fabrics as Biomaterials. Biotechnology and Bioengineering 1994;43:781-791.

[62] Gentleman E, Lay AN, Dickerson DA, Nauman EA, Livesay GA, Dee KC. Mechanical characterization of collagen fibers and scaffolds for tissue engineering. Biomaterials 2003;24:3805-3813.

[63] He W, Ma Z, Yong T, Teo WE, Ramakrishna S. Fabrication of collagen-coated biodegradable polymer nanofiber mesh and its potential for endothelial cells growth. Biomaterials 2005;26:7606-7615.

[64] He W, Yong T, Ma ZW, Inai R, Teo WE, Ramakrishna S. Biodegradable Polymer Nanofiber Mesh to Maintain Functions of Endothelial Cells. Tissue Engineering 2006;12:2457 -2466.

[65] Kwon IK, Matsuda T. Co-Electrospun Nanofiber Fabrics of Poly(L-lactide-co-*e*-caprolactone) with Type I Collagen or Heparin. Biomacromolecules 2005;6:2096-2105.

[66] Dunn MG, Avasarala PN, Zawadsky JP. Optimization of extruded collagen fibers for ACL reconstruction. Journal of Biomedical Materials Research 1993;27:1545-1552.

[67] Moutos FT, Freed LE, Guilak F. A biomimetic three-dimensional woven composite scaffold for functional tissue engineering of cartilage. Nature Materials 2007;6:162-167.

[68] Pins G, Huang E, Christiansen D, Silver F. Effects of static axial strain on the tensile properties and failure mechanisms of self-assembled collagen fibers. Journal of Applied Polymer Science 1997;63:1429-1440.

[69] Kato YP, Christiansen D, Hahn RA, Shieh S-J, Goldstein JD, Silver FH. Mechanical properties of collagen fibres: A comparison of reconstituted and rat tail tendon fibres. Biomaterials 1989;10:38-42.

[70] Pins GD, Silver FH. A self-assembled collagen scaffold suitable for use in soft and hard tissue replacement. Materials Science and Engineering: C 1995;3:101-107.

[71] Koob TJ, Hernandez DJ. Material properties of polymerized NDGA-collagen composite fibers: development of biologically based tendon constructs. Biomaterials 2002;23:203-212.

[72] Kato YP, Dunn MG, Zawadsky JP, Tria AJ, Silver FH. Regeneration of Achilles tendon with a collagen tendon prosthesis. Results of a one-year implantation study. The Journal of Bone and Joint Surgery American Volume 1991;73:561-574.

[73] Kato YP, Silver FH. Formation of continuous collagen fibres: Evaluation of biocompatibilily and mechanical properties. Biomaterials 1990;11:169-175.

[74] Goldstein JD, Tria AJ, Zawadsky JP, Kato KY, Christiansen D, Silver FH. Development of a reconstituted collagen tendon prosthesis. The Journal of Bone and Joint Surgery 1989;71A:1183-1191.

[75] Chen X, Wang Z, Qin T-W, Liu C-J, Yang Z-M. Effects of micropatterned surfaces coated with type I collagen on the proliferation and morphology of tenocytes. Applied Surface Science 2008;255:368-370.

[76] Riboh J, Chong AKS, Pham H, Longaker M, Jacobs C, Chang J. Optimization of Flexor Tendon Tissue Engineering With a Cyclic Strain Bioreactor. The Journal of Hand Surgery 2008;33:1388-1396.

[77] Wang B, Liu W, Zhang Y, Jiang Y, Zhang WJ, Zhou G, Cui L, Cao Y. Engineering of extensor tendon complex by an ex vivo approach. Biomaterials 2008;29:2954-2961.

[78] Cao D, Liu W, Wei X, Xu F, Cui L, Cao Y. In vitro tendon engineering with avian tenocytes and polyglycolic acids: a preliminary report. Tissue Eng 2006;12:1369-1377.

[79] Hess G, Cappiello W, Poole R, Hunter S. Prevention and treatment of overuse tendon injuries. Sports Med 1989;8:371-384.

[80] Kannus P. Structure of the tendon connective tissue. Scandinavian Journal of Medicine & Science in Sports 2000;10:312-320.

[81] Chaplin DM, Greenlee TKJ. The development of human digital tendons. J Anat 1975;120:253-274.

[82] Chuen FS, Chuk CY, Ping WY, Nar WW, Kim HL, Ming CK. Immunohistochemical Characterization of Cells in Adult Human Patellar Tendons. J Histochem Cytochem 2004;52:1151-1157.

[83] Boote C, Dennis S, Huang Y, Quantock AJ, Meek KM. Lamellar orientation in human cornea in relation to mechanical properties. Journal of Structural Biology 2005;149:1-6.

[84] Canty EG, Kadler KE. Collagen fibril biosynthesis in tendon: a review and recent insights. Comparative Biochemistry and Physiology - Part A: Molecular & Integrative Physiology 2002;133:979-985.

[85] Osborne CS, Barbenel JC, Smith D, Savakis M, Grant MH. Investigation into the tensile properties of collagen/chondroitin-6-sulphate gels: the effect of crosslinking agents and diamines. Medical & Biological Engineering & Computing 1998;36:129-134.

[86] Damink LHHO, Dijkstra PJ, van Luyn MJA, van Wachem PB, Nieuwenhuis P, Feijen J. Crosslinking of dermal sheep collagen using hexamethylene diisocyanate. Journal of Materials Science: Materials in Medicine 1995;6:429-434.

[87] Holmes DF, Graham HK, Kadler KE. Collagen Fibrils Forming in Developing Tendon Show an Early and Abrupt Limitation in Diameter at the Growing Tips. Journal of Molecular Biology 1998;283:1049-1058.

[88] Douglas T, Hempel U, Mietrach C, Viola M, Vigetti D, Heinemann S, Bierbaum S, Scharnweber D, Worch H. Influence of collagen-fibril-based coatings containing decorin and biglycan on osteoblast behavior. Journal of Biomedical Materials Research Part A 2008;84A:805-816.

[89] Cao H, Xu S-Y. EDC/NHS-crosslinked type II collagen-chondroitin sulfate scaffold: characterization and in vitro evaluation. J Mater Sci: Mater Med 2008;19:567-575.

[90] Wright KT, El Masri W, Osman A, Roberts S, Chamberlain G, Ashton BA, Johnson WEB. Bone marrow stromal cells stimulate neurite outgrowth over neural proteoglycans (CSPG), myelin associated glycoprotein and Nogo-A. Biochemical and Biophysical Research Communications 2007;354:559-566.

[91] Yao C, Markowicz M, Pallua N, Magnus Noah E, Steffens G. The effect of cross-linking of collagen matrices on their angiogenic capability. Biomaterials 2008;29:66-74.

[92] Fontana A, Spolaore B, Mero A, Veronese FM. Site-specific modification and PEGylation of pharmaceutical proteins mediated by transglutaminase. Advanced Drug Delivery Reviews 2008;60:13-28.

[93] Shen YH, Shoichet MS, Radisic M. Vascular endothelial growth factor immobilized in collagen scaffold promotes penetration and proliferation of endothelial cells. Acta Biomaterialia 2008;4:477-489.

[94] Liman ST, Kara CO, Bir F, Yildirim B, Topcu S, Sahin B. The effects of estradiol and progesterone on the synthesis of collagen in tracheal surgery. International Journal of Pediatric Otorhinolaryngology 2005;69:1327-1331.

[95] Chen R, Mooney D. Polymeric growth factor delivery strategies for tissue engineering. Pharm Res 2003;20:1103-1112.

[96] Chen L, Apte RN, Cohen S. Characterization of PLGA microspheres for the controlled delivery of IL-1[alpha] for tumor immunotherapy. Journal of Controlled Release 1997;43:261-272.

[97] Mundargi RC, Srirangarajan S, Agnihotri SA, Patil SA, Ravindra S, Setty SB, Aminabhavi TM. Development and evaluation of novel biodegradable microspheres based on poly(d,l-lactide-co-glycolide) and poly([epsilon]-caprolactone) for controlled delivery of doxycycline in the treatment of human periodontal pocket: In vitro and in vivo studies. Journal of Controlled Release 2007;119:59-68.

[98] Chung H, Kim H, Yoon J, Park T. Heparin Immobilized Porous PLGA Microspheres for Angiogenic Growth Factor Delivery. Pharmaceutical Research 2006;23:1835-1841.

Chapter 3

Anisotropic Imprinted Substrates for Directional Cell and Tissue Growth

Sections of this chapter have been published at:

English, A., Azeem, A., Biggs, M., Jones, E., Tripathi, B., Basu, N., Rooney, N., Riley, G., O'Riordan, A., Cross, G., Hutmacher, D., Pandit, A., Zeugolis, D.I. *Substrate topography: Dimension-dependent contact guidance is not translated into a tenogenic preclinical host response*. Acta Biomateriala, Submitted

Azeem, A., **English, A.**, Kumar, P., Satyam, A., Biggs, M., Jones, E., Tripathi, B., Basu, N., Henkel, J., Vaquette, C., Rooney, N., Riley, G., O'Riordan, A., Cross, G., Ivanovski, S., Hutmacher, D., Pandit, A., Zeugolis, D.I. *The influence of anisotropic nano- to micro- topography on in vitro and in vivo osteogenesis*. Nanomedicine (Future in Medicine), 10:5, 677-680

3.1. Introduction

The ever-increased active lifestyle has resulted in an unprecedented increase of tendon injuries, whilst the increased life amplifies the financial strain of tendon injuries on healthcare systems. Given the poor inherent regeneration capability of tendons, largely attributed to low vascularity and low activity cellular content, intervention strategies should be develop to promote functional repair and regeneration. Given that surgical therapies, based on tissue grafts, have failed to restore native tendon function, it is anticipated that the tissue-engineering arpeggio (scaffolds, cells, biologics), alone or in combination, will provide a functional therapy in the years to come [1-13].

Two- and three- dimensional scaffold fabrication technologies (e.g. electro-spinning [14-19], fibre extrusion [20-23], isoelectric focusing [24, 25] and imprinting [26-28]) have been at the forefront of scientific and technological research and innovation to recapitulate native tendon extracellular matrix (ECM) supramolecular assemblies. Although fibrous constructs (e.g. electro-spun polymeric fibres, extruded collagen fibres and isoelectrically focused collagen fibres) have been shown to maintain tenocyte phenotype and to differentiate stem cells towards tenogenic lineage *in vitro* and to induce acceptable regeneration in preclinical models, none of these technologies offers precise control over the spatial distribution of the fibres. Imprinting technologies, on the other hand, have demonstrated a diverse effect on a range of permanently differentiated and stem cell functions, including adhesion, orientation, secretome expression and lineage commitment [29-36]. Specifically to tendon repair, such technologies have maintained tenocyte phenotype and have restored lost tenocyte phenotype [26], have promoted aligned tendon-specific ECM deposition [27] and have differentiated stem cells towards tenogenic lineage [28]. Despite these advancements, a comprehensive study on the influence of surface

topography over different scales, ranging from nano- to micron-level, on tenocyte function *in vitro* and on tissue response *in vivo* has yet to be elucidated.

In the present study, we employed imprinting lithography technologies to create anisotropically grooved substrates with constant width and spacing and varying depth and we subsequently assessed the influence of anisotropic topography, as opposed to isotropic topography, on tenocyte function *in vitro* and host tissue response *in vivo*.

3.2. Materials and Methods

3.2.1. Anisotropic Substrate Fabrication

The process of substrate fabrication has been described previously [37]. Briefly, Si master moulds with anisotropic topographies were fabricated via a photolithography process, followed by reactive ion etching (RIE). 1.5 x 1.5 cm^2 regions were patterned with lines / gratings of 2101.78 ± 35.21 nm and 1911.42 ± 37.50 nm widths respectively, and variable groove depths (37.48 ± 3.4 nm, 317.29 ± 7.05 nm and 1988.2 ± 195.3 nm). Silicon wafers (3.0 x 3.0 cm^2) were spin-coated with a positive photoresist (S1813 PR, Shipley) and then exposed using OAI Mask Aligner (Model MBA800). Following photoresist development, the master mould was etched by RIE (Oxford ICP etcher) using CHF3 + SF6 ionised gas. The moulds were silanised with 5 mM octadecyltrichlorosilane (OTS, Sigma Aldrich, Ireland) solution to facilitate imprint release. A thermal imprinting process was used to transfer the master pattern into a 2.0 x 2.0 cm^2 PLGA substrate (85:15, Sigma Aldrich, Ireland) using a Specac Hydraulic Press (15 T & 25 T) at 120 °C and a pressure of 5 MPa, for 5 min. The imprinted gratings on polymer were subsequently analysed by SEM and AFM. Planar non-imprinted PLGA substrates were used as control.

3.2.2. Human Tenocyte Culture

Human tenocytes (Cambridge Biosciences, UK) were cultured in Dulbecco's Modified Eagle's Medium (DMEM) supplemented 10 % foetal bovine serum and 1 % penicillin/streptomycin (all Sigma Aldrich, Ireland). Cells were maintained at 37 °C and 5 % carbon dioxide, with the media being changed every 3 days. Tenocytes were sub-cultured when 80 % confluency was reached. Tenocytes were detached from the culture flask with trypsin-EDTA solution (Sigma Aldrich, Ireland) and then seeded on

the imprinted and isotropic substrates in 8-well (Lab-Tek^{TM}, Thermo Scientific, UK) and 12-well (Ibidi$^{®}$, Germany) chamber slides at a cell density of 2 x 10^4 cells per 0.8 cm^2 and 7 x 10^3 cells per 0.35 cm^2, respectively. All *in vitro* experiments were conducted for 1, 5, and 10 days.

3.2.3. Human Tenocyte Morphometric Analysis

Immunofluorescent images were used to evaluated cell morphology and alignment. At the end of culture points, the substrates were washed three times with Hanks Balanced Salt Solution (HBSS, Sigma Aldrich, Ireland) and the cells were fixed with 4 % paraformaldehyde (Sigma Aldrich, Ireland) for 15 min at room temperature (RT). The cells were washed again in HBSS three times and then permeabilised with 0.2 % Triton X (Sigma Aldrich, Ireland) for 5 min. The cells were then exposed to 4',6-diamidino-2-phenylindole (DAPI, Molecular Probes, Ireland) in phosphate buffer saline (PBS) for 5 min, washed with HBSS and then exposed to rhodamine-conjugated phalloidin (Molecular Probes, Ireland) in PBS for 1 h. Images were captured with a 10X objective, using an inverted BX51 Olympus fluorescence microscope (Olympus, Japan).

Immunofluorescent micrographs of tenocytes were quantitatively analysed using ImageJ software (NIH). Briefly, images were converted to 8-bit grey scale and threshold to distinguish cellular outlines from the non-cellular background signal; the program detected cells on the basis of contrast and fitted the cellular outlines to equivalent ellipses. The following cell shape characteristics were measured for each fitted ellipse: major axis, minor axis, aspect ratio (major axis / minor axis), perimeter, area, and orientation angle with respect to the direction of grooves. Cellular orientation / alignment was determined by the angle between the major axis of the cell and the

groove direction. The angle for each cell was converted such that 0° represented cell orientation along the direction of the grooves and 90° represented a perpendicular orientation, with respect to the direction of the grooves. Cells within 10° of the groove direction were considered aligned. Cell morphology was quantified using aspect ratio (major axis/minor axis). Aspect ratio was used to evaluate cellular elongation, with a higher aspect ratio indicating increased elongation. Cells that overlapped or aggregated together or wherever boundaries of contacting cells could not be distinguished clearly were not used for quantitative analysis. Approximately, two hundred cells were used to assess the influence of surface topography on cellular morphology.

3.2.4. Human Tenocyte Viability, Metabolic Activity and Proliferation

Live/Dead® assay (BioSource International, Invitrogen, Ireland) was performed on days 1, 5 and 10 to assess cellular viability, as per manufacturer's protocol. Briefly, cells were washed 3 times with HBSS and exposed to the staining solution of calcein and ethidium homodimer. The cells were incubated at 37 °C for 45 min. Following staining, the cells were viewed using the BX51 Olympus fluorescence microscope and analysed using ImageJ.

Cell metabolic activity was determined using alamarBlue® assay on days 1, 5, and 10, as per manufacturer's protocol. Briefly, alamarBlue® dye was diluted with HBSS to make a 10 % (v/v) alamarBlue® solution. Media was removed from each well and 0.5 ml alamarBlue® solution was added to each well. Cell were incubated for 3 h at 37 °C; the absorbance of the alamarBlue® was measured at wavelengths of 550 nm and 595 nm using a micro plate reader (Varioskan Flash, Thermo Scientific, UK). The level of

metabolic activity was calculated using the simplified method of calculating % reduction, according to the supplier's protocol.

Cell proliferation was assessed on days 1, 5, and 10, by counting DAPI stained cell nuclei, using the BX51 Olympus fluorescence microscope.

3.2.5. Human Tenocyte Gene Expression Analysis

A comprehensive gene expression analysis was conducted using TaqMan® Low Density Array (TLDA; Applied Biosystems, UK), grouping genes of interest as collagenous, non-collagenous, adhesion and housekeepers (**Table 3.1**).

Cell density of 2 x 10^4 per 0.8 cm^2 was seeded on the substrates and total RNA was extracted from human tenocytes on days 0, 1, 5 and 10. Total RNA was extracted using Trizol reagent method. Briefly, Trizol (400 µg/well, Sigma Aldrich, UK) was added to the cells for 15 min to disrupt the cellular membranes. Then, the Trizol solution was collected and chloroform (Sigma Aldrich, UK) was added to the solution and shaken vigorously for 15 sec. RT incubation for 5 min was followed. Then the upper aqueous phase containing the RNA was removed and mixed with isopropanol (Sigma Aldrich, UK) to obtain a pure RNA pellet. Subsequently, the RNA was used for the reverse-transcriptase reaction to synthesize the first strand of cDNA. cDNA (100 ng) and universal PCR mastermix (50 µl) were loaded into the fill reservoirs (100 µl / reservoir) and the plate was run according to manufacturer's instructions, using the Applied Biosystems 7900HT Real-Time PCR System and Applied Biosystems Sequence Detection Systems (SDS 2.3 and RQ manager 1.2) software. The thermal cycles were as follows: 50 °C for 2 min, 94.5 °C for 10 min, followed by 40 cycles of 97 °C for 30 sec and 59.7 °C for 1 min. Using the $2^{-\Delta Ct}$ method, mean Ct values of each target gene was normalised to the housekeeping gene values. To analyse the

changes in gene expression between the isotropic control and the anisotropic substrates for each day, $2^{-\Delta\Delta Ct}$ method was used. The gene expression was then evaluated using hierarchical clustering software (IPA software of complex 'omics data, Ingenuity® systems, Qiagen, USA) with the fold change compared to the time point control and a threshold set at 1.4.

Table 3.1: Genes and their transcripts, grouped as collagenous, non-collagenous, adhesion and housekeepers.

Gene Name	Gene Symbol	NCBI Ref. Seq.	TaqMan® Transcript
Collagenous			
Collagen I	COL1A1	NM_000088.3	Hs00164004_m1
Collagen III	COL3A1	NM_000090.3	Hs00943809_m1
Collagen IV	COL4A1	NM_001845.4	Hs00266237_m1
Collagen V	COL5A1	NM_000093.3	Hs00609088_m1
Collagen VI	COL6A1	NM_001848.2	Hs00242448_m1
Collagen XI	COL11A1	NM_001854.3	Hs01097664_m1
Collagen XII	COL12A1	NM_004370.5	Hs00189184_m1
Collagen XIV	COL14A1	NM_021110.1	Hs00966234_m1
Non-collagenous			
Scleraxis Homolog A	SCXA	NM_001008271.1	Hs03054634_g1
Tenascin C	TNC	NM_002160.3	Hs01115665_m1
Biglycan	BGN	NM_001711.4	Hs00156076_m1
Decorin	DCN	NM_001920.3	Hs00370384_m1
Osteopontin	SPP1	NM_00058.2	Hs00959010_m1
Alkaline Phosphatase	ALPL	NM_000478.4	Hs01029144_m1
Bone Sialoprotein	IBSP	NM_004967.3	Hs00173720_m1
Osteonectin	SPARC	NM_003118.2	Hs00234160_m1

Runt-related transcription factor 2	RUNX2	NM_001015051.3	Hs00231692_m1
Cartilage oligomeric protein	COMP	NM_001920.3	Hs00164359_m1
Matrix gla protein	MGP	NM_000900.3	Hs00969490_m1
Thrombospondin 4	THBS4	NM_003248.4	Hs00170261_m1
Fibromodulin	FMOD	NM_002203.3	Hs00158127_m1
Fibronectin	FN1	NM_212482.1	Hs00277509_m1
Laminin	LAMA	NM_005559.3	Hs00300550_m1
Aggrecan	ACAN	NM_0011353.3	Hs00153936_m1
Versican	VCAN	NM_001126336.2	Hs01007933_m1
Adhesion			
Integrin α1	ITGA1	NM_181501.1	Hs00235006_m1
Integrin α2	ITGA2	NM_002203.3	Hs00201927_m1
Integrin α3	ITGA3	NM_002204.2	Hs01076873_m1
Integrin α4	ITGA4	NM_000885.4	Hs00168433_m1
Integrin α5	ITGA5	NM_002205.2	Hs01547673_m1
Integrin α6	ITGA6	NM_000210.2	Hs01041011_m1
Integrin α10	ITGA10	NM_003637.3	Hs00174623_m1
Integrin α11	ITGA11	NM_001004439.1	Hs00201927_m1
Integrin β1	ITGB1	NM_002211.3	Hs00559595_m1
Integrin β2	ITGB2	NM_000211.3	Hs00164957_m1
Integrin β3	ITGB3	NM_000212.2	Hs01001469_m1

Integrin β5	ITGB5	NM_002213.3	Hs00174435_m1
CD44	CD44	NM_000610.3	Hs01075861_m1
Housekeeping			
18S ribosomal RNA	18S rRNA		Hs99999901_s1
Topoisomerase (DNA) I	TOP1	NM_003286.2	Hs00243257_m1
Eukaryotic translation initiation factor 4α	EIF4α		Hs00756996_g1

3.2.6. *In vivo* Study and Analysis

The Animal Care Research Ethics Committee of NUI Galway approved all experimental protocols. For the tendon model, female Lewis rats (200g – 250g) were used, following a protocol described previously [38]. Briefly, surgery was performed under general anaesthesia. A small incision was made to the side of the knee, exposing the patellar tendon by moving the skin and opening the fascia. Using a punch biopsy, a 2mm circular defect was created at the centre of the tendon, allowing creation of a consistent and reproducible injury, without compromising the mechanical integrity of the tendon. The tendon was wiped dry using sterile gauze. Circular sections of the structured substrates were secured at the injury site using a PLGA film, secured in place with sutures. The grooved substrates were aligned parallel to the tendon orientation (**Figure 3.1**). Following euthanisation, tissue samples were harvested at weeks 2, 4 and 12, fixed in 4% paraformaldehyde (Sigma Aldrich, Ireland), stored in sucrose (Sigma Aldrich, Ireland) and then fixed in freezing compound (Sigma Aldrich, Ireland). Cryo-sectioning was performed at Histotech (University of York, UK0. Sections (10 μm thick) were cut using a Leica CM 1950 cryostat (Leica Microsystems, Germany) on manual setting, operating at -20 °C and collected onto Superfrost® Plus glass slides (Thermo Scientific, UK). Sections were air dried at ambient temperature for 1 hour and stored desiccated at -80ºC until use. Tissue sections were then stained with haematoxylin-eosin (Sigma Aldrich, Ireland) and images were captured with an Olympus IX-81 inverted microscope (Olympus Corporation, Tokyo, Japan). For the subcutaneous study, female Lewis rats (200g – 250g) were used, following a protocol described previously [39]. Briefly, surgery was performed on rats under general anaesthesia. Incisions were made at the back of each animal, allowing insertion of a 0.5 cm x 0.5 cm structured substrate. The wound was then closed, using biodegradable

sutures (**Figure 3.2**). Following euthanisation, the substrates were harvested at days 2 and 14 and were stained using DAPI and rhodamine-conjugated phalloidin. Images were captured with an Olympus IX-81 inverted microscope (Olympus Corporation, Tokyo, Japan).

Figure 3.1: For the tendon model, we induced an incision to the side of the leg (A) to expose the tendon by moving the skin (B). Using a 2 mm in diameter punch biopsy, we created a wound at the centre of the tendon, where the structured substrates were then inserted (C). The implants were secured using a PLGA film (D) and wounds were closed using biodegradable sutures (E).

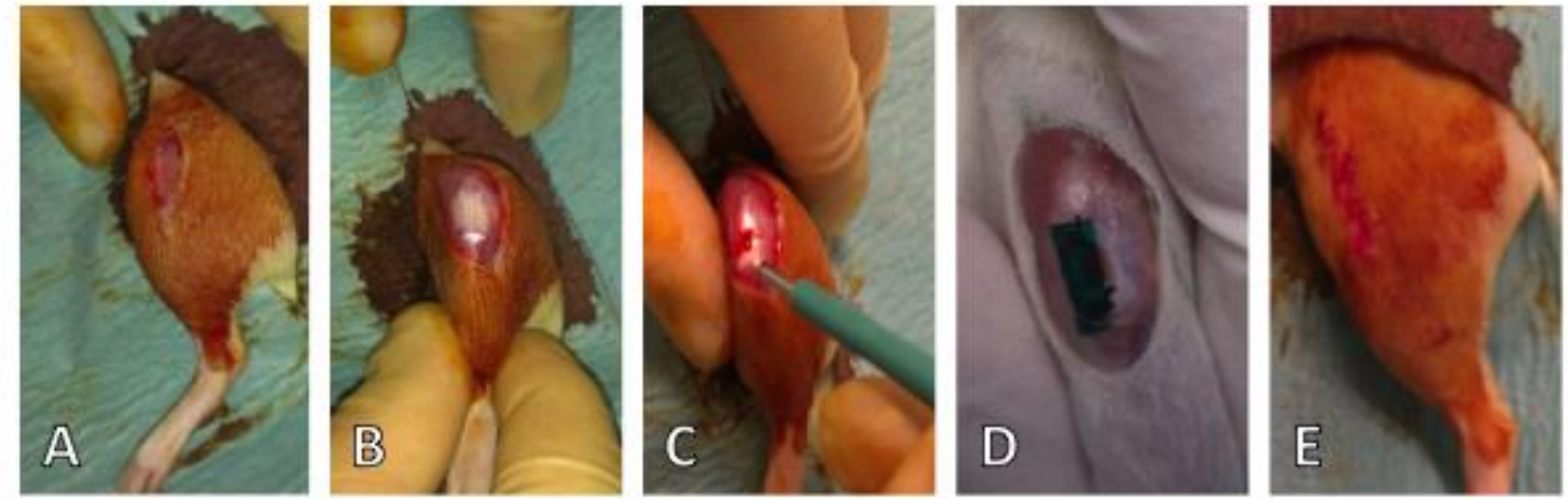

Figure 3.2: For the subcutaneous model, incisions were created on the back. The substrates were then inserted subcutaneously and wounds were closed using biodegradable sutures.

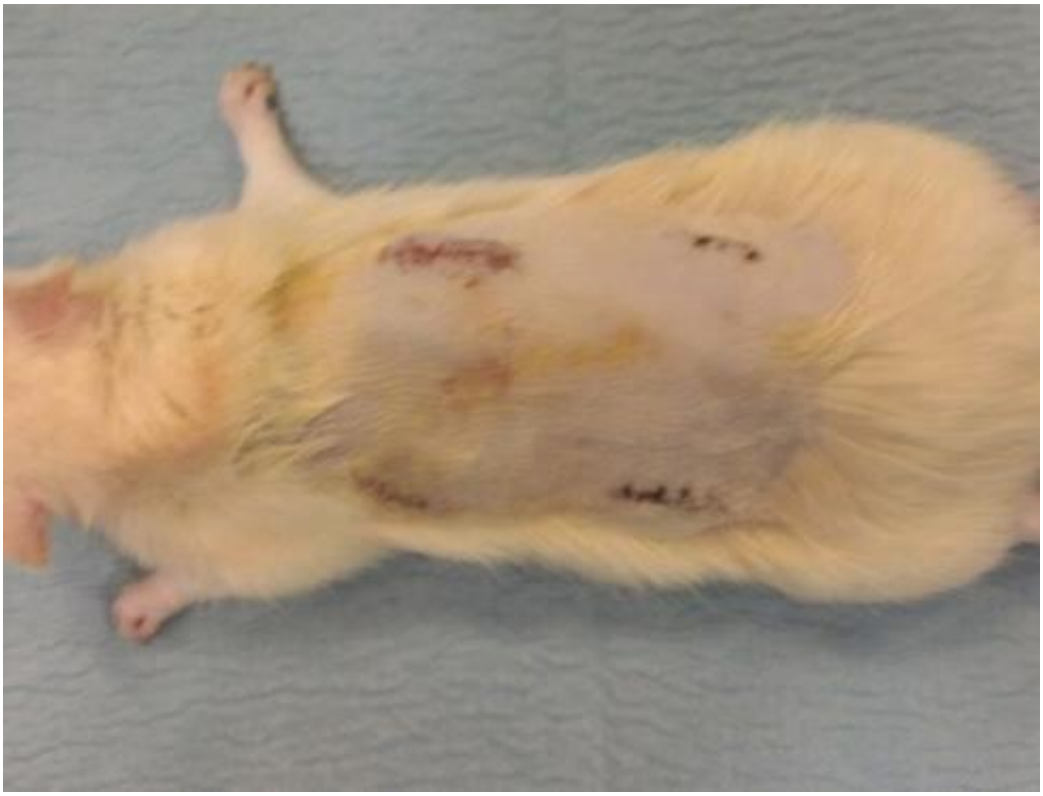

3.2.7. Statistical Analysis

All data were analysed using GraphPad Prism® 5 (GraphPad Software, USA) and/or PASW Statistics 17.0 (SPSS Inc, IL). Analysis of variance (ANOVA) and Tukey's multiple comparison post-hoc tests were performed. Statistical significance was accepted at $p < 0.05$.

3.3. Results

3.3.1. Substrate Analysis

Anisotropic PLGA substrates with constant groove and line width of 1911.42 ± 37.50 nm and 2101.78 ± 35.21 nm respectively and variable groove depth of 37.48 ± 3.4 nm, 317.29 ± 7.05 nm and 1988.2 ± 195.3 nm were fabricated using standard photolithography followed by imprinting lithography. Isotropic / planar PLGA substrates were used as control, with an inherent Ra of 80.17 ± 28.92 nm over 10 μm^2 (**Figure 3.3**).

Figure 3.3: AFM analysis of isotropic (A) and structured (B, C, D) substrates. Quantification of isotropic control roughness, groove width, line width and groove depth (E).

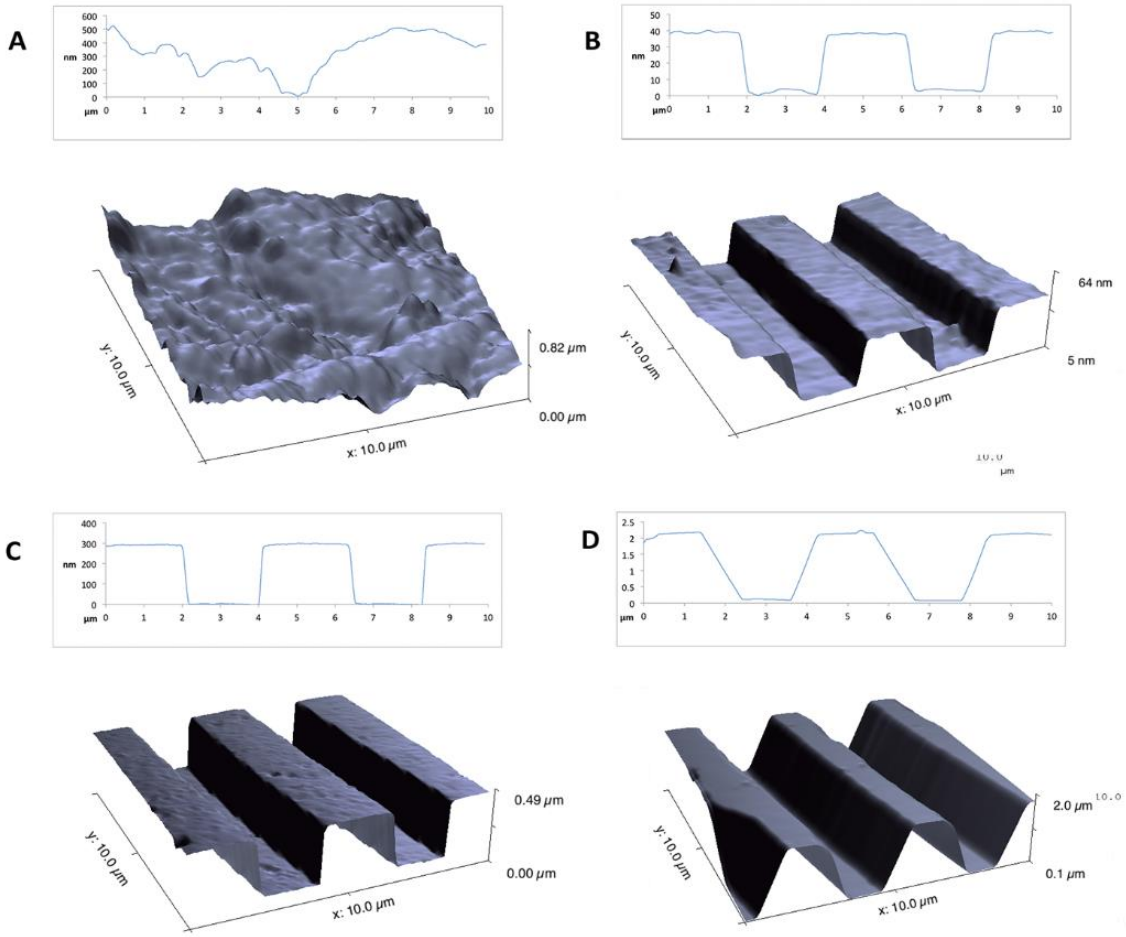

E

AFM analysis of imprinted PLGA substrates			
Roughness (R_a) of isotropic control over 10 µm^2 (A) 80.168 ± 28.92 nm			
Groove Width (nm)	1911.42 ± 37.50	Line Width (nm)	2101.78 ± 35.21
Groove Depth (nm)	(B) 37.48 ± 3.4	(C) 317.29 ± 7.05	(D) 1988.2 ±195.3

3.3.2. Human Tenocyte Morphometric Analysis as a Function of Topography

Gross visual analysis of immunofluorescent images revealed that at all time points (1, 5 and 10 days), human tenocytes exhibited spread morphology on isotropic and imprinted substrates with groove depth of ~37 nm (**Figure 3.4**). An aligned orientation and an elongated morphology, parallel to the substrate topography, was observed as early as 24 h in culture and was maintained for up to 10 days (longer culture time point assessed) on imprinted substrates with groove depth of ~317 nm and ~1988 nm (**Figure 3.4**).

Figure 3.4: DAPI (blue) and rhodamine-conjugated phalloidin (red) indicates that tenocytes aligned parallel to the substrate topography of groove depths of ~317 nm and ~1988 nm, whilst a random morphology was observed on isotropic substrates and substrates with groove depth of ~37 nm.

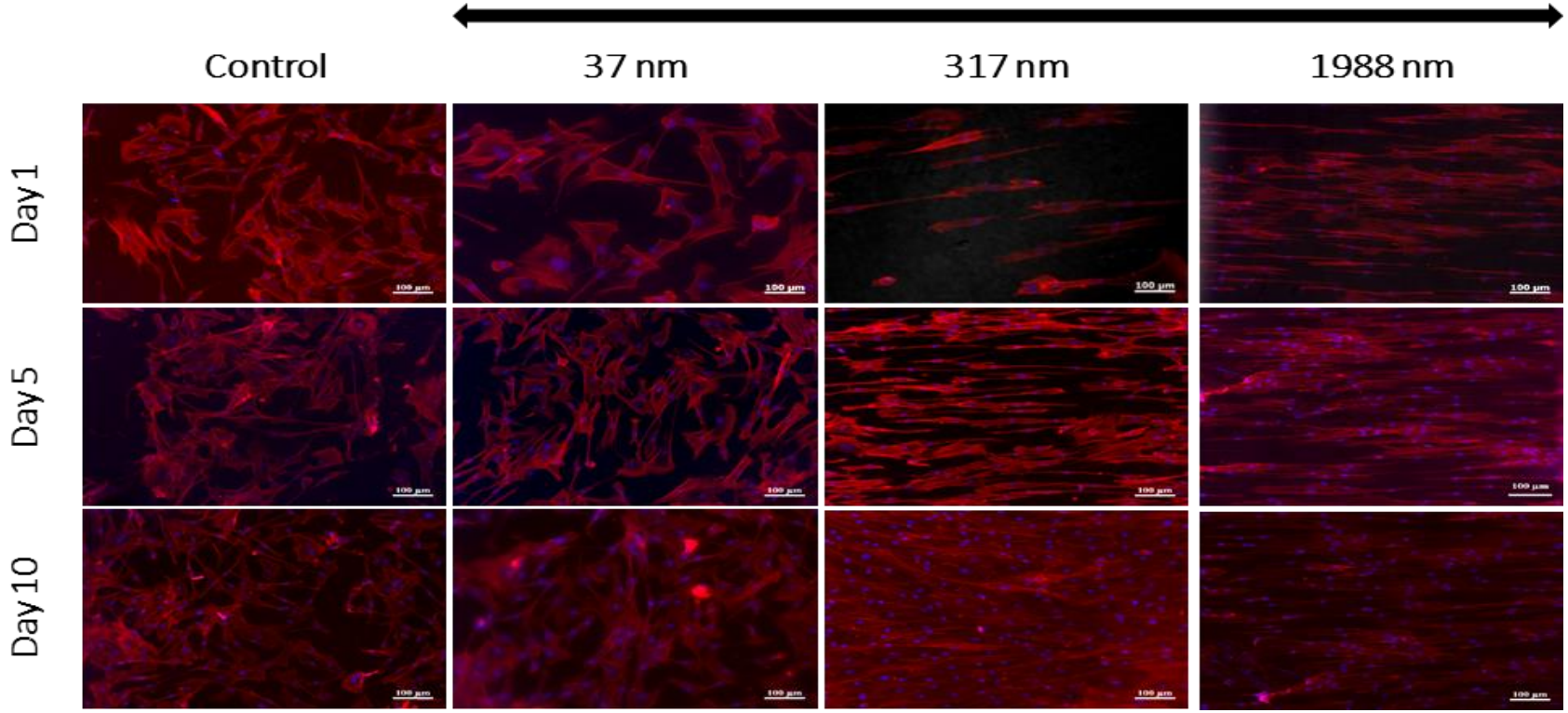

Subsequently, a detailed quantitative analysis was carried out to assess the influence of the various topographies, including planar, on cellular morphometry. Tenocytes on planar and ~37 nm in depth substrates exhibited random alignment / orientation, with the major axis of the cells evenly distributed over 90 °. Whereas by increasing the groove depth to ~317 nm and ~1988 nm, 80 % and 100 % respectively cellular alignment / elongation parallel to the substrate topography was evidenced (**Figure 3.5A**). Although cellular area (**Figure 3.5B**) and nuclei aspect ratio (**Figure 3.5D**) were not affected as a function of the substrate topography, cellular aspect ratio was significantly increased ($p < 0.005$; **Figure 3.5C**) as a function of ascending groove depth, resulting in increasingly fusiform tenocytes. Indeed, tenocytes seeded on the isotropic and ~37 nm in depth substrates exhibited cellular aspect ratio of approximately 4, whereas by increasing the groove depth to ~317 nm and ~1988 nm, the aspect ratio was increased to approximately 11 and 16 respectively.

Figure 3.5: Tenocyte alignment to the substrate topography further confirmed when the angle of cells parallel to the underlying topography was between 0 – 20 ° on substrates with groove depth of ~317 nm and ~1988 nm (A). Substrates with groove depth of ~317 nm and ~1988 nm induced the highest cytoskeleton elongation (C). No significant difference was observed in cellular area (B) and nuclei aspect ratio (D) as a function of surface topography.

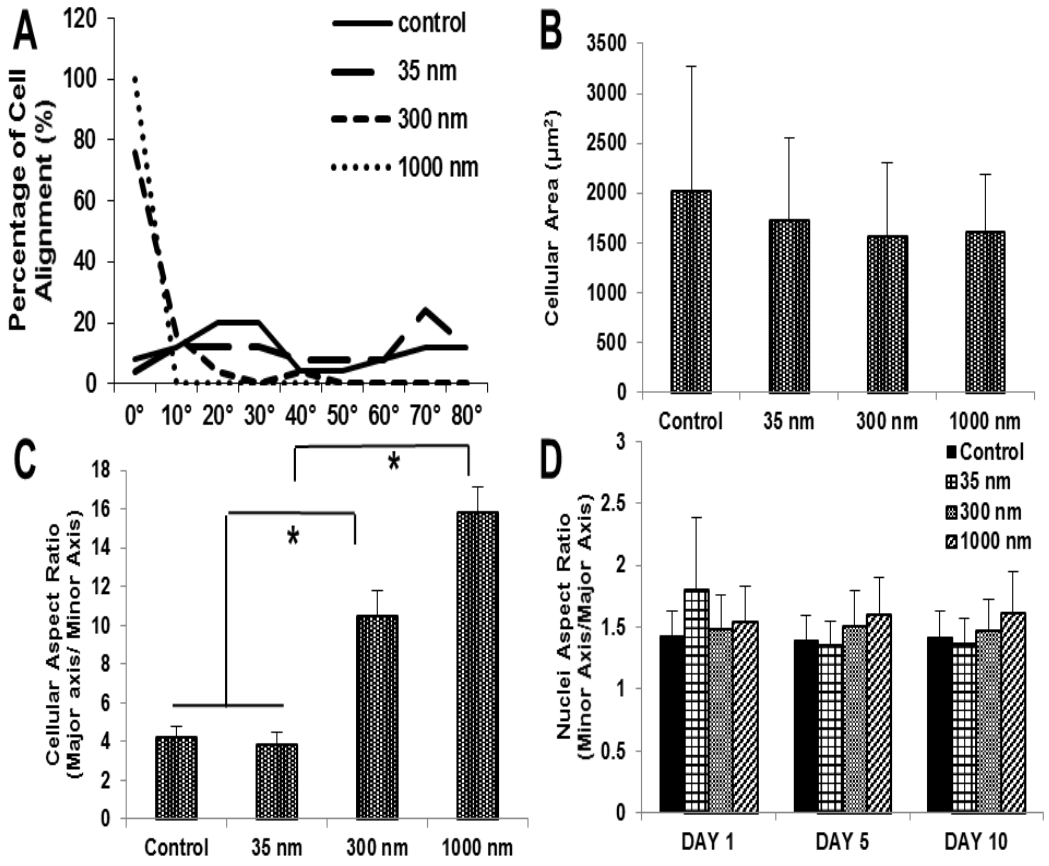

3.3.3. Human Tenocyte Viability, Metabolic Activity and Proliferation Analysis as a Function of Topography

No significant differences ($p > 0.05$) in human tenocyte viability (**Figure 3.6**), metabolic activity (**Figure 3.7**) and proliferation (**Figure 3.8**) were observed at any time point (1, 5 and 10 days), as a function of the different topographies.

Figure 3.6: No significant difference in cell viability was detected as a function of topography and time in culture.

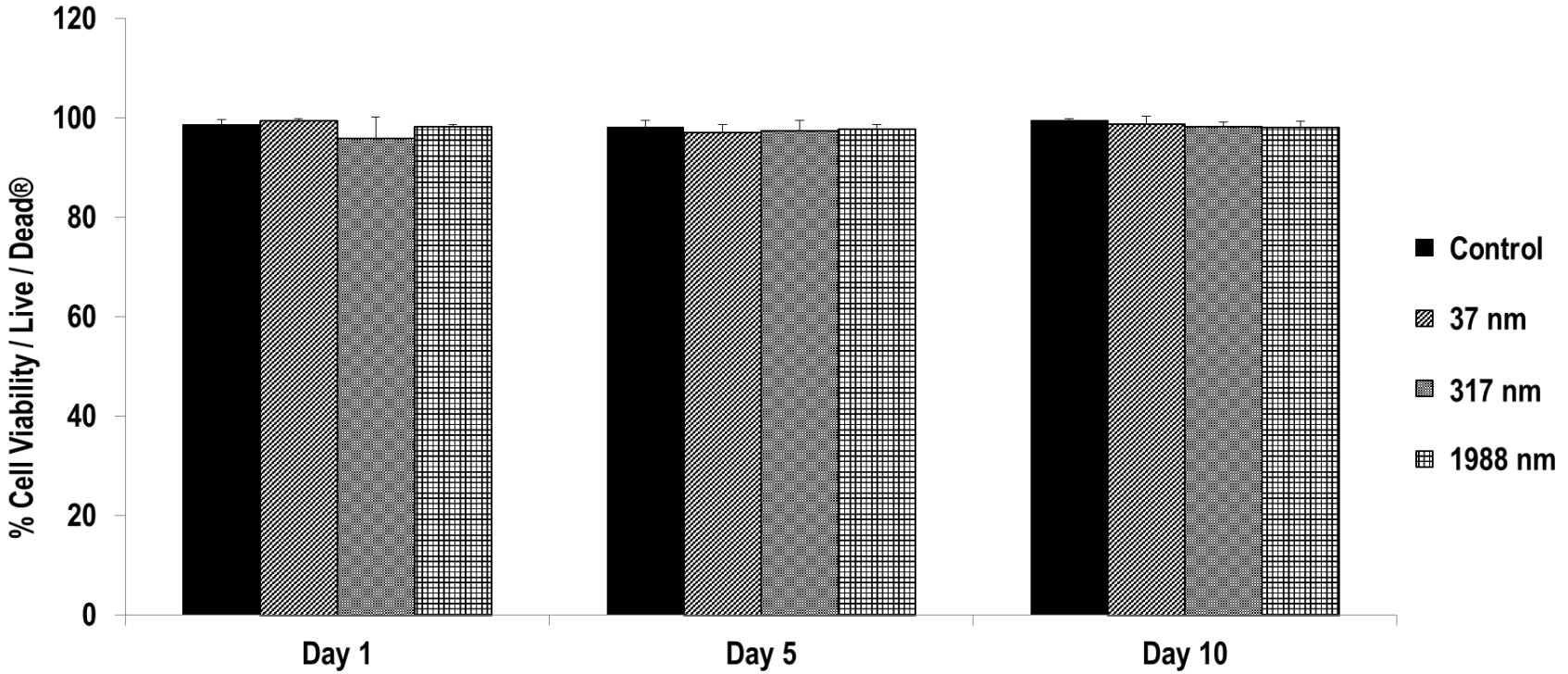

Figure 3.7: No significant difference in cell metabolic activity was detected as a function of topography and time in culture.

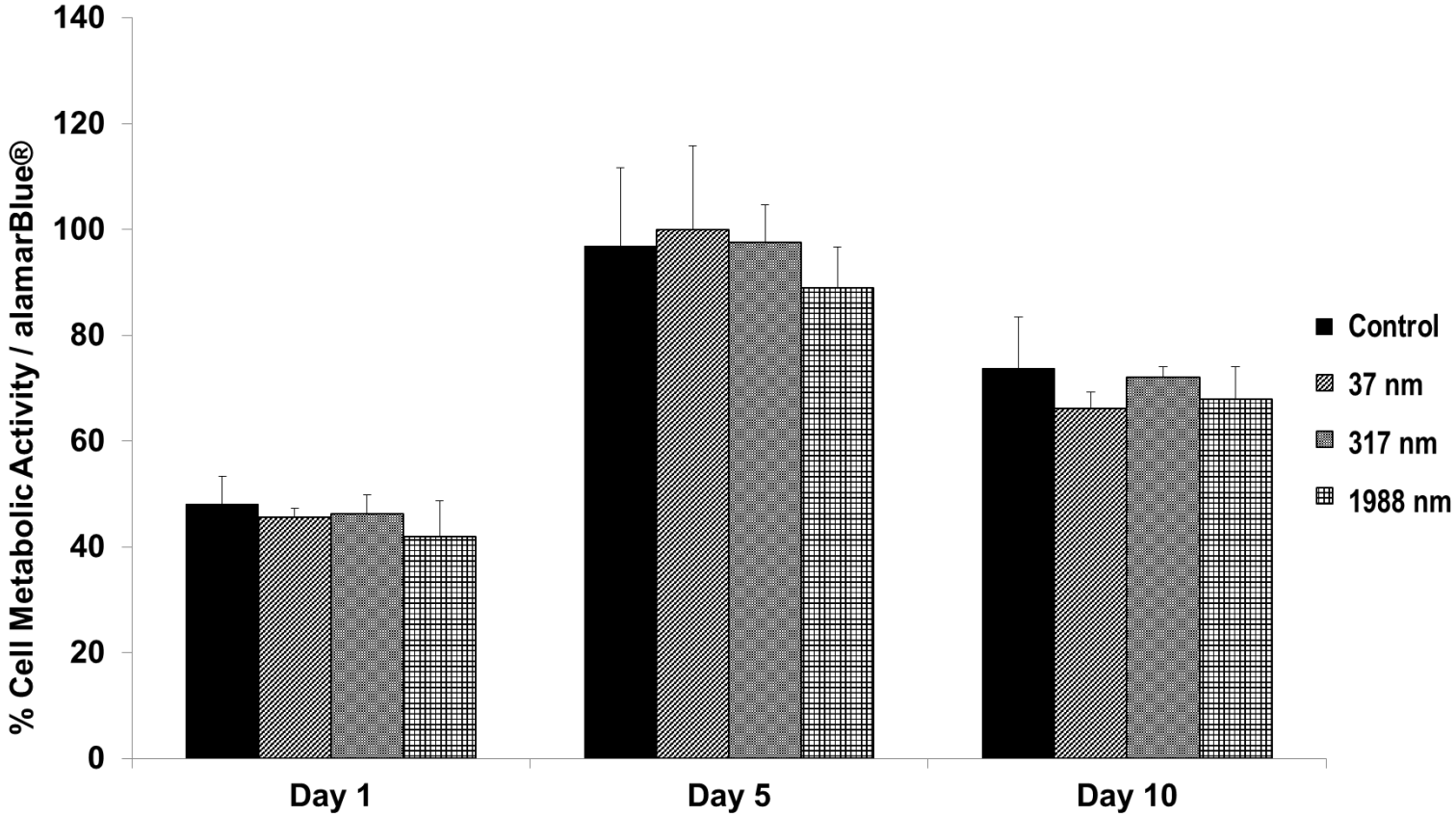

Figure 3.8: No significant difference in cell proliferation was detected as a function of topography and time in culture.

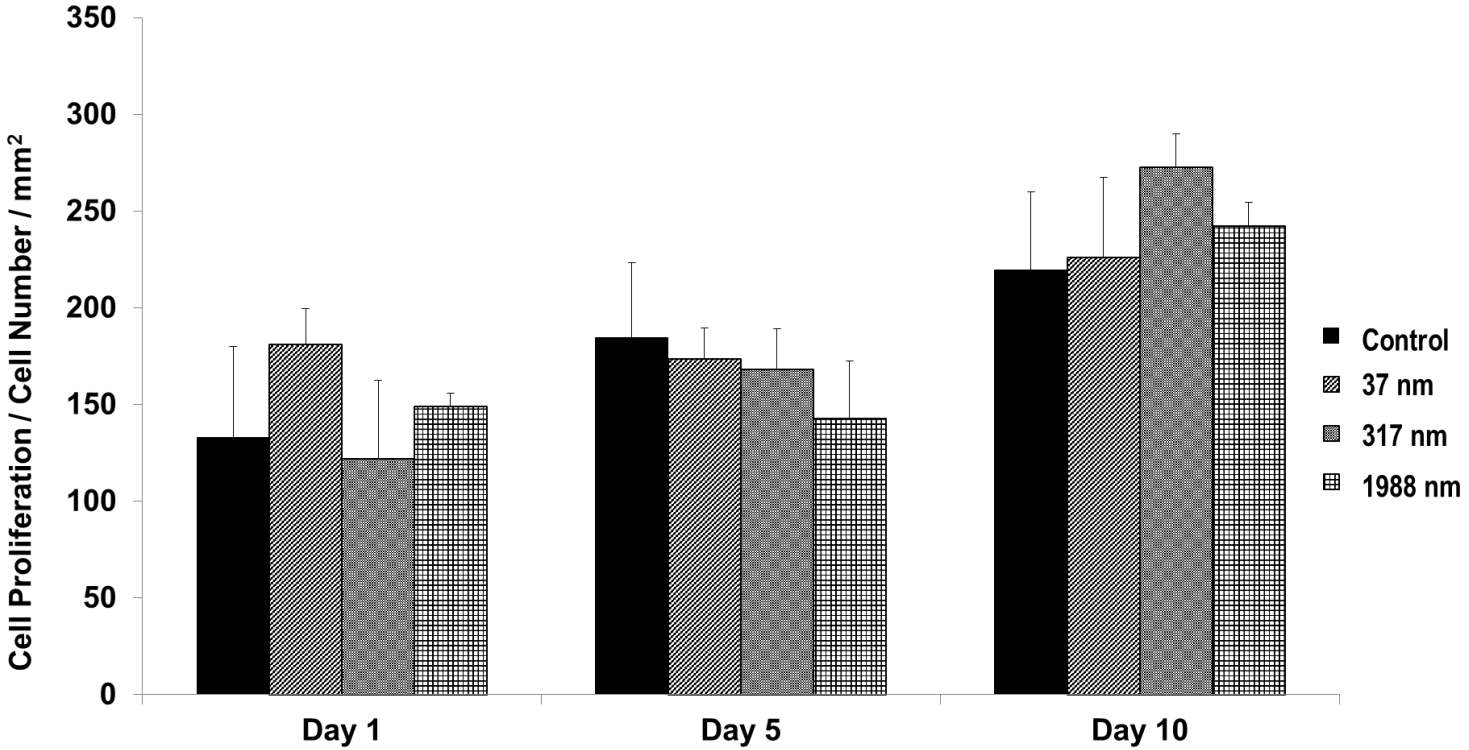

3.3.4. Human Tenocyte Gene Analysis as a Function of Topography

Hierarchal clustering of the fold change (threshold of 1.4) in gene expression of human tenocytes on the anisotropic substrates, as compared to the isotropic control substrates, at the corresponding time points (day 1, 5 and 10) is presented in **Figure 3.9**. At day 1, an overall gene upregulation was observed only on substrates with groove depth of 1988 nm, whilst at day 10 substrates with groove depth ~317 nm and ~1988 nm had more upregulated genes than substrates with groove depth ~37 nm. At day 10, IBSP (bone sialoprotein) and ACAN (aggrecan) were upregulated on all substrates.

Figure 3.9: Gene analysis demonstrates an overall gene upregulation at day 1 only on cells seeded on ~1988 nm in depth substrates, whilst at day 10 substrates with groove depth ~317 nm and ~1988 nm had more upregulated genes than substrates with groove depth of ~37 nm. At day 10, bone sialoprotein and aggrecan were upregulated on all substrates.

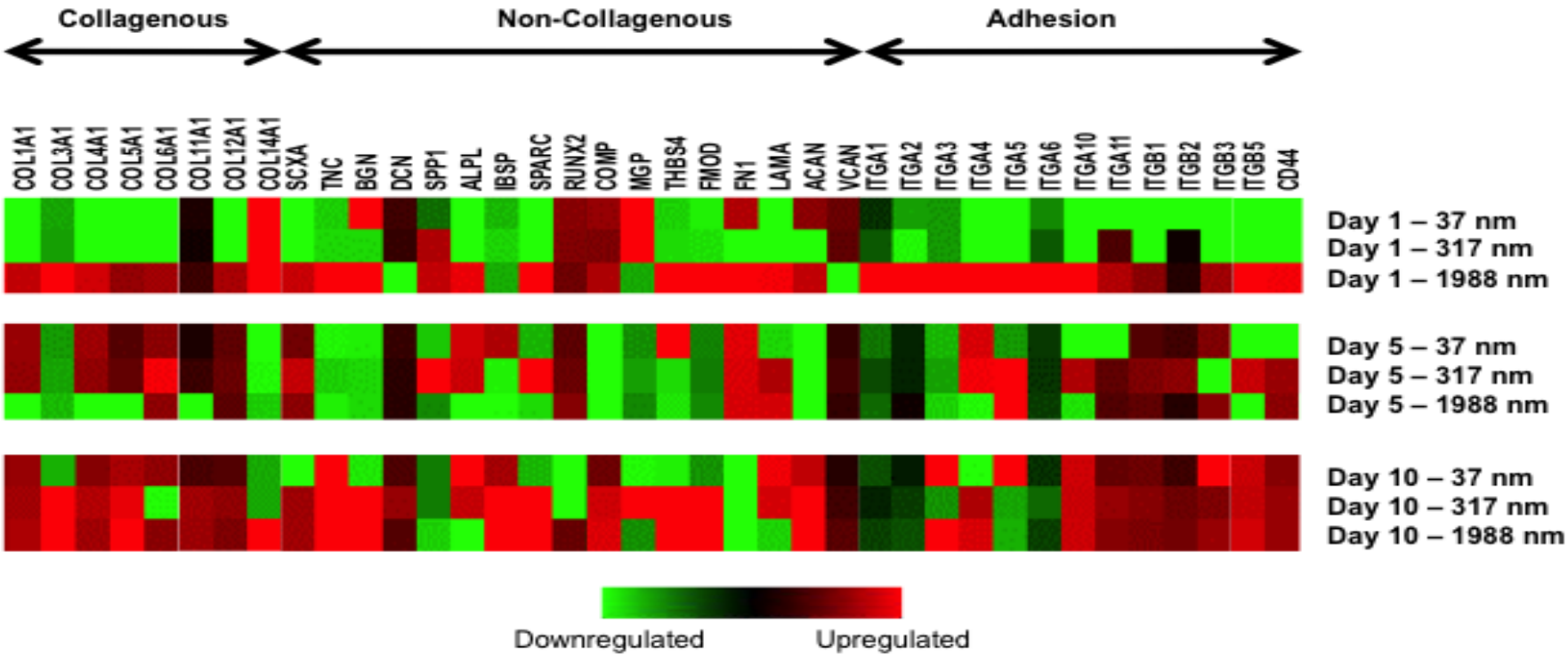

3.3.5. Host Tissue Response as a Function of Topography

Histological examination at the tendon repair site showed a disorganised collagen fibre pattern for all anisotropic substrates (**Figure 3.10**). In a subcutaneous model, when structured substrates were explanted and stained for DAPI and rhodamine-conjugated phalloidin, no apparent cellular alignment was evidenced (**Figure 3.11**).

Figure 3.10: Histological examination at the tendon repair site showed a disorganised collagen fibre pattern for all implanted anisotropic substrates.

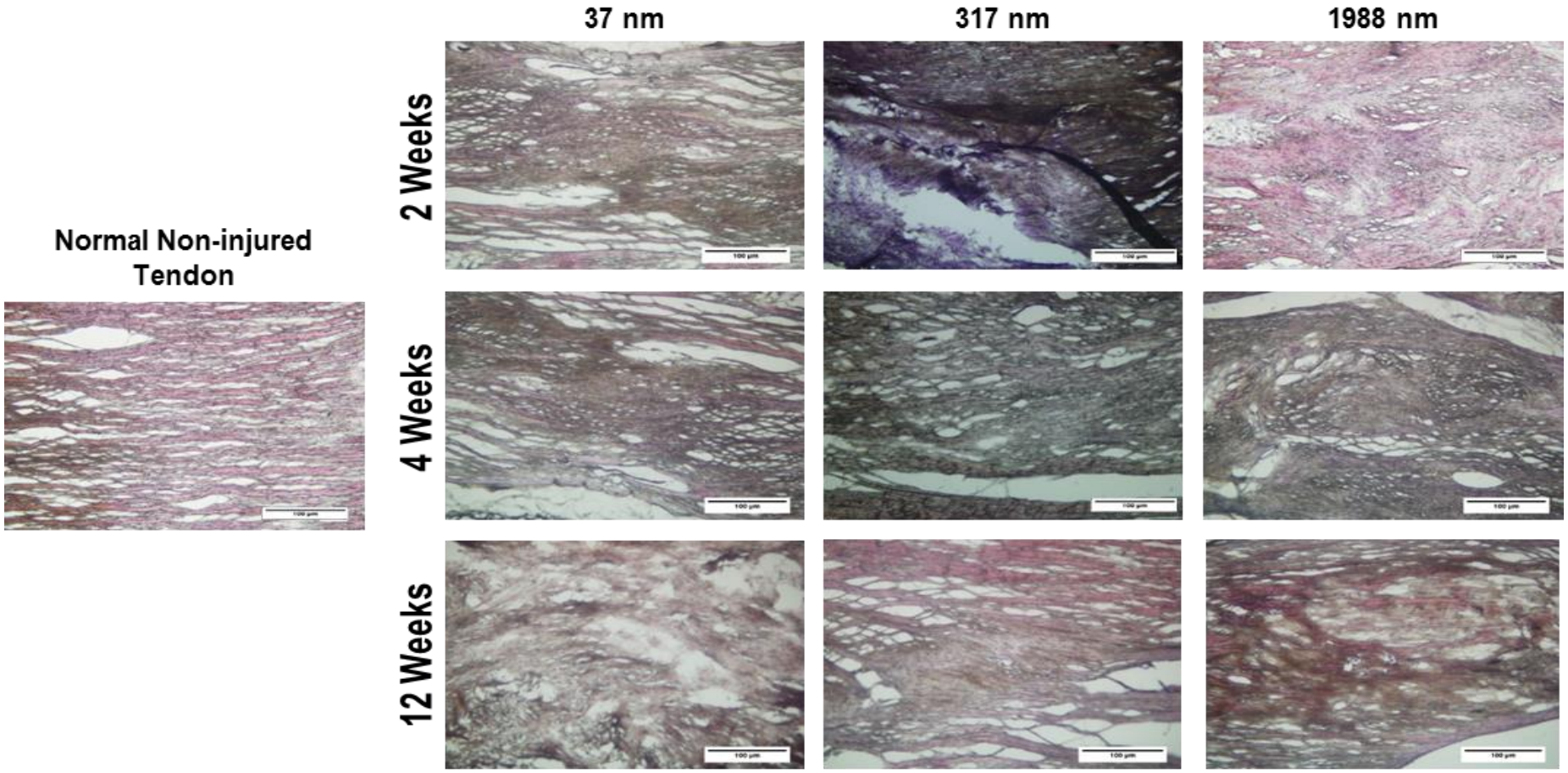

Figure 3.11: In a subcutaneous model, the structured substrates did not induce parallel to the substrate topography host cell orientation.

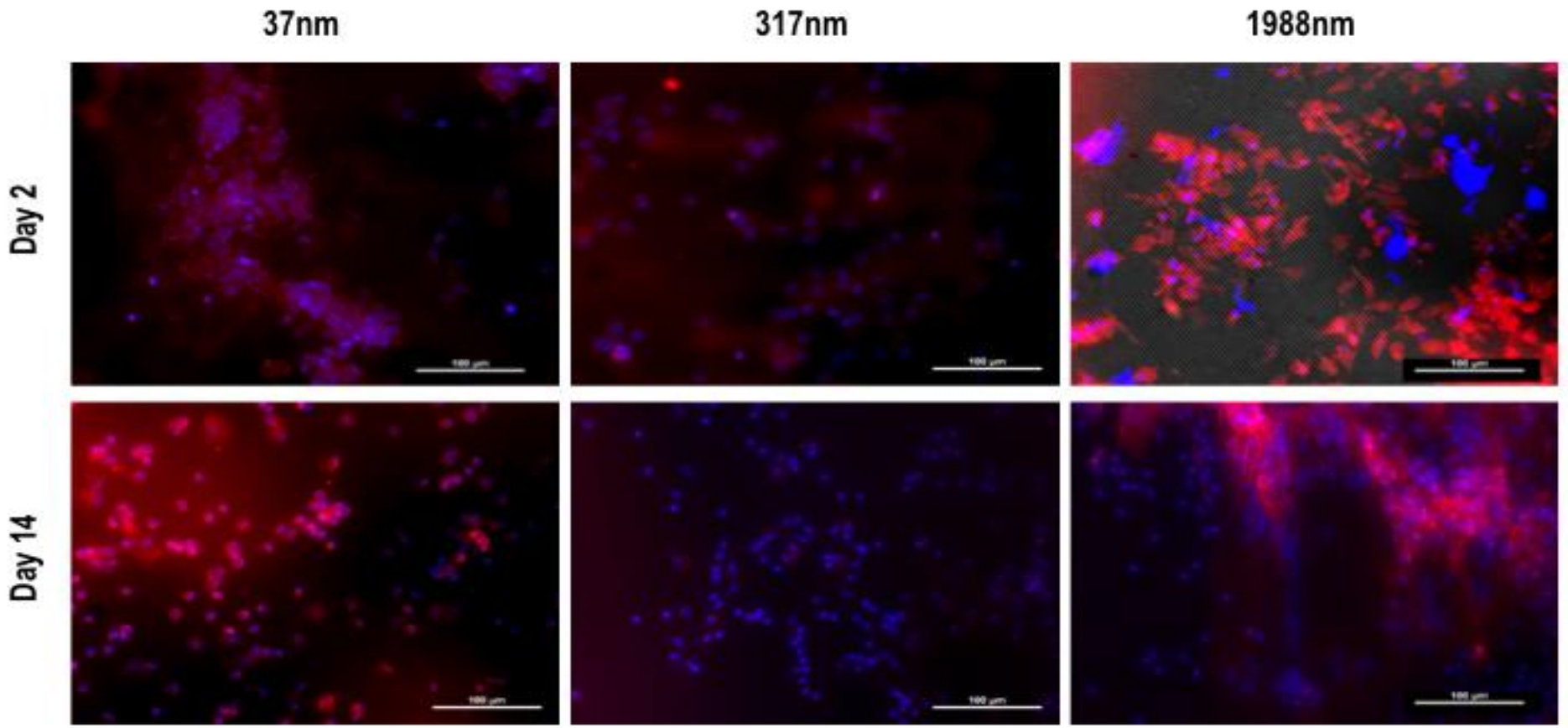

3.4. Discussion

Biomaterials' design and development is coming ever closer in mimicking native ECM assemblies, as advancements in engineering have allowed development of two- and three-dimensional substrates with precise architectural features. Indeed, current biomaterial fabrication technologies not only achieve structural support, but also provide means for permanently differentiated cell phenotype maintenance and directional lineage commitment of stem cells. However, the optimal presentation / dimensionality of such topographical features remains elusive, despite significant scientific achievements and technological innovations [32]. Herein, we ventured to investigate the impact of groove depth (~37 nm, ~317 nm and ~1988 nm), whilst maintain groove width (~1911 nm) and line width (~2102 nm) constant, on human tenocyte morphology and gene expression *in vitro* and on directional neotissue formation *in vivo*. The groove depths were selected on the basis that closely represent the topographical cues (dimensionality of collagen fibrils, fibres and fibre bundles) that tenocytes are exposed to *in vivo*. The micro-scale groove depth was selected based on previous publications, where authors supported that pitch dimensionality in the range of 4000 nm induces efficient cellular contact guidance [28, 30, 40]. Furthermore, the cellular response to underlying topographies is enhanced when the feature pitch is similar to or smaller than the dimensions of the cell type being studied [41], facilitating contact with more than one discontinuity. This approach allows for directional alignment of the cells without physically restricting cells within individual groove features [42].

Starting with the morphometric analysis, we observed that isotropic (control) substrates and substrates with groove depth of ~37 nm, being to shallow, failed to induce any morphological changes to the cells tested. On the other hand, substrates

with deeper grooves (~317 nm and ~1988 nm) induced cytoskeleton morphometric changes, but not obvious nuclei differences. Although, the mechano-transduction theory proposes that intracellular tension in elongated and aligned cytoskeleton actin filaments is transferred to the nucleus through cytoskeletal elements [43-48], this indifference in nuclei morphology may be attributed to the short time after culture on grooved substrates that nuclei aspect ratio was assessed.

No significant difference was observed in cell metabolic activity, viability and proliferation, between the groups. This observation indicates that although both topography and mechanical stretching can induce bidirectional cell growth, only mechanical loading, in excessive form, can activate apoptotic pathways [49-52].

Gene analysis clearly indicates that only substrates with groove depth of ~1988 nm had an immediate (day 1) upregulation effect on cultured tenocytes, which was maintained for all cultured time points. However, by day 10, bone sialoprotein, osteonectin, runt-related transcription factor 2, cartilage oligomeric protein and aggrecan were upregulated on substrates with groove depth ~1988 nm and bone sialoprotein and aggrecan were upregulated on all substrates. These observations indicate trans-differentiation of tenocytes towards osteogenic / chondrogenic lineage. Indeed, bone sialoprotein encodes non-collagenous components of bone ECM; runt-related transcription factor 2 promotes osteogenic differentiation; and osteonectin is a bone-specific protein that binds selectively to hydroxyapatite and collagen [53-56]. Similarly, cartilage oligomeric protein and aggrecan, although they are encountered in tendon, they are primarily considered cartilage-specific molecules, mutations of which are associated with skeletal pathophysiologies [57-60]. We attribute this indicative trans-differentiation to the far from physiological substrate stiffness of the PLGA material used. Indeed, substrate stiffness has been shown to strongly regulate protein

expression, cell phenotype maintenance and stem cell differentiation, with soft substrates to be neurogenic and rigid substrates to be chondrogenic / osteogenic [61-64]. This implies that multifactorial, rather than mono-domain, approaches should be assessed and is in accordance to previous observations, where it was suggested that topography should be combined with mechanical loading for physiological bovine tenocyte morphology maintenance [15].

Critically, herein, the *in vitro* work was followed up with two *in vivo* studies. None of the structured substrates induced parallel to the substrate topography neotissue formation in a tendon model. Further, in a subcutaneous model, none of the substrates induced parallel to the direction of the substrate topography cellular orientation. This observation indicates that three-dimensional fibrous constructs that allow cell growth, motility, matrix deposition and neotissue growth within this contained environment, are more effective for directional neural [65-67], tendon [17, 23, 68], bone [69-71] and skin [72-74] neotissue formation, rather than the two-dimensional imprinted substrates that are overwhelmed with body fluids upon implantation, prohibiting favourable cell / material interaction at the substrate-tissue nano-bio-interface.

3.5. Conclusions

Herein, we demonstrated that low nano topographical features (~37 nm groove depth) were not sufficient to induce physiological tenocyte morphology, as compared to ~317 nm and ~1988 nm groove depth substrates. In two different animal models, the structured substrates failed to induce parallel to the underlined topography directional host cell growth and neotissue formation. Further, the rigid substrate induced tenocyte trans-differentiation towards chondrogenic / osteogenic lineage. Collectively, these data indicate that three-dimensional fibrous constructs are more promising for directional neotissue formation, whilst two-dimensional imprinted substrates can be used for optimal cell expansion in vitro, should multifactorial approaches be established.

3.6. References

[1] Liu C, Aschbacher-Smith L, Barthelery N, Dyment N, Butler D, Wylie C. What we should know before using tissue engineering techniques to repair injured tendons: A developmental biology perspective. Tissue Eng Part B Rev 2011;17:165-176.

[2] Zhang X, Bogdanowicz D, Erisken C, Lee N, Lu H. Biomimetic scaffold design for functional and integrative tendon repair. J Should Elb Surg 2012;21:266-277.

[3] Longo U, Lamberti A, Petrillo S, Maffulli N, Denaro V. Scaffolds in tendon tissue engineering. Stem Cells Intern 2012;2012:517165.

[4] Liu Y, Ramanath H, Wang D. Tendon tissue engineering using scaffold enhancing strategies. Trends Biotechnol 2008;26:201-209.

[5] Cigognini D, Lomas A, Kumar P, Satyam A, English A, Azeem A, Pandit A, Zeugolis D. Engineering in vitro microenvironments for cell based therapies and drug discovery. Drug Discov Tod 2013;18:1099-1108.

[6] Bagnaninchi P, Yang Y, Haj A, Maffulli N. Tissue engineeering for tendon repair. Br J Sports Med 2007;41:1-5.

[7] James R, Kesturu G, Balian G, Chhabra A. Tendon: Biology, biomechanics, repair, growth factors, and evolving treatment options. Journal Hand Surg 2008;33:102-112.

[8] Butler D, Juncosa-Melvin N, Boivin G, Galloway M, Shearn J, Gooch C, Awad H. Functional tissue engineering for tendon repair: A multidisciplinary strategy using mesenchymal stem cells, bioscaffolds, and mechanical stimulation. J Orthop Res 2008;26:1-9.

[9] Gaspar D, Spanoudes K, Holladay C, Pandit A, Zeugolis D. Progress in cell-based therapies for tendon repair. Adv Drug Deliv Rev In Press.

[10] Lomas A, Ryan C, Sorushanova A, Shologu N, Sideri A, Tsioli V, Fthenakis G, Tzora A, Skoufos I, Quinlan L, O'Laighin G, Mullen A, Kelly J, Kearns S, Biggs M,

Pandit A, Zeugolis D. The past, present and future in scaffold-based tendon treatments. Adv Drug Deliv Rev In Press.

[11] Abbah S, Spanoudes K, O'Brien T, Pandit A, Zeugolis D. Assessment of stem cell carriers for tendon tissue engineering in pre-clinical models. Stem Cell Res Ther 2014;5:38.

[12] Spanoudes K, Gaspar D, Pandit A, Zeugolis D. The biophysical, biochemical, and biological toolbox for tenogenic phenotype maintenance in vitro. Trends Biotechnol 2014;32:474-482.

[13] Docheva D, Müller S, Majewski M, Evans C. Biologics for tendon repair. Adv Drug Deliv Rev In Press.

[14] Ladd M, Lee S, Stitzel J, Atala A, Yoo J. Co-electrospun dual scaffolding system with potential for muscle-tendon junction tissue engineering. Biomater 2011;32:1549-1559.

[15] English A, Azeem A, Gaspar D, Keane K, Kumar P, Keeney M, Rooney N, Pandit A, Zeugolis D. Preferential cell response to anisotropic electro-spun fibrous scaffolds under tension-free conditions. J Mater Sci Mater Med 2012;23:137-148.

[16] Chen B, Wang B, Zhang W, Zhou G, Cao Y, Liu W. In vivo tendon engineering with skeletal muscle derived cells in a mouse model. Biomater 2012;33:6086-6097.

[17] Liu W, Chen B, Deng D, Xu F, Cui L, Cao Y. Repair of tendon defect with dermal fibroblast engineered tendon in a porcine model. Tissue Eng 2006;12:775-788.

[18] Sahoo S, Toh S, Goh J. A bFGF-releasing silk/PLGA-based biohybrid scaffold for ligament/tendon tissue engineering using mesenchymal progenitor cells. Biomater 2010;31:2990-2998.

[19] Yin Z, Chen X, Chen J, Shen W, Hieu-Nguyen T, Gao L, Ouyang H. The regulation of tendon stem cell differentiation by the alignment of nanofibers. Biomater 2010;31:2163-2175.

[20] Zeugolis D, Paul G, Attenburrow G. Cross-linking of extruded collagen fibres - A biomimetic three-dimensional scaffold for tissue engineering applications. J Biomed Mater Res - Part A 2009;89:895-908.

[21] Kato Y, Dunn M, Zawadsky J, Tria A, Silver F. Regeneration of Achilles tendon with a collagen tendon prosthesis. Results of a one-year implantation study. J Bone Joint Surg 1991;73:561-574.

[22] Cavallaro J, Kemp P, Kraus K. Collagen fabrics as biomaterials. Biotechn Bioeng 1994;43:781-791.

[23] Enea D, Gwynne J, Kew S, Arumugam M, Shepherd J, Brooks R, Ghose S, Best S, Cameron R, Rushton N. Collagen fibre implant for tendon and ligament biological augmentation. in vivo study in an ovine model. Knee Surg Sports Traumatol Arthrosc 2013;21:1783-1793.

[24] Kishore V, Bullock W, Sun X, VanDyke W, Akkus O. Tenogenic differentiation of human MSCs induced by the topography of electrochemically aligned collagen threads. Biomater 2012;33:2137-2144.

[25] Cheng X, Gurkan U, Dehen C, Tate M, Hillhouse H, Simpson G, Akkus O. An electrochemical fabrication process for the assembly of anisotropically oriented collagen bundles. Biomater 2008;29:3278-3288.

[26] Zhu J, Li J, Wang B, Zhang W, Zhou G, Cao Y, Liu W. The regulation of phenotype of cultured tenocytes by microgrooved surface structure. Biomater 2010;31:6952-6958.

[27] Kapoor A, Caporali E, Kenis P, Stewart M. Microtopographically patterned surfaces promote the alignment of tenocytes and extracellular collagen. Acta Biomater 2010;6:2580-2589.

[28] Tong W, Shen W, Yeung C, Zhao Y, Cheng S, Chu P, Chan D, Chan G, Cheung K, Yeung K, Lam Y. Functional replication of the tendon tissue microenvironment by a bioimprinted substrate and the support of tenocytic differentiation of mesenchymal stem cells. Biomater 2012;33:7686-7698.

[29] Dalby M, Riehle M, Yarwood S, Wilkinson C, Curtis A. Nucleus alignment and cell signaling in fibroblasts: response to a micro-grooved topography. Experim Cell Res 2003;284:272-280.

[30] Biggs M, Richards R, McFarlane S, Wilkinson C, Oreffo R, Dalby M. Adhesion formation of primary human osteoblasts and the functional response of mesenchymal stem cells to 330nm deep microgrooves. J Royal Soc Interf 2008;5:1231-1242.

[31] Chen W, Villa-Diaz L, Sun Y, Weng S, Kim J, Lam R, Han L, Fan R, Krebsbach P, Fu J. Nanotopography influences adhesion, spreading, and self-renewal of human embryonic stem cells. ACS Nano 2012;6:4094-4103.

[32] Unadkat H, Hulsman M, Cornelissen K, Papenburg B, Truckenmuller R, Post G, Uetz M, Reinders M, Stamatialis D, van Blitterswijk C, de Boer J. An algorithm-based topographical biomaterials library to instruct cell fate. Proc Natl Acad Sci USA 2011;108:16565-16570.

[33] Chen S, Jones J, Xu Y, Low H, Anderson J, Leong K. Characterization of topographical effects on macrophage behavior in a foreign body response model. Biomater 2010;31:3479-3491.

[34] Fisher O, Khademhosseini A, Langer R, Peppas N. Bioinspired materials for controlling stem cell fate. Acc Chem Res 2009;43:419-428.

[35] Brunetti V, Maiorano G, Rizzello L, Sorce B, Sabella S, Cingolani R, Pompa P. Neurons sense nanoscale roughness with nanometer sensitivity. Proc Natl Acad Sci USA 2010;107:6264-6269.

[36] Bauer A, Jackson T, Jiang Y. Topography of extracellular matrix mediates vascular morphogenesis and migration speeds in angiogenesis. PLoS Comput Biol 2009;5:e1000445.

[37] Azeem A, English A, Kumar P, Satyam A, Biggs M, Jones E, Tripathi B, Basu N, Henkel J, Vaquette C, Rooney N, Riley G, O'Riordan A, Cross G, Ivanovski S, Hutmacher D, Pandit A, Zeugolis D. The influence of anisotropic nano- to micro-topography on in vitro and in vivo osteogenesis. Nanomedicine (Future in Medicine) In Press.

[38] Zhang J, Li B, Wang J. The role of engineered tendon matrix in the stemness of tendon stem cells in vitro and the promotion of tendon-like tissue formation in vivo. Biomater 2011;32:6972-6981.

[39] Keeney M, van den Beucken J, van der Kraan P, Jansen J, Pandit A. The ability of a collagen/calcium phosphate scaffold to act as its own vector for gene delivery and to promote bone formation via transfection with VEGF(165). Biomater 2010;31:2893-2902.

[40] Cassidy J, Roberts J, Smith C, Robertson M, White K, Biggs M, Oreffo R, Dalby M. Osteogenic lineage restriction by osteoprogenitors cultured on nanometric grooved surfaces: The role of focal adhesion maturation. Acta Biomater 2014;10:651-660.

[41] Clark P, Connolly P, Curtis A, Dow J, Wilkinson C. Topographical control of cell behaviour. I. Simple step cues. Development 1987;99:439-448.

[42] Clark P, Connolly P, Moores G. Cell guidance by micropatterned adhesiveness in vitro. J Cell Sc 1992;103:287-292.

[43] Ingber D. Tensegrity: The architectural basis of cellular mechanotransduction. Annu Rev Physiol 1997;59:575-599.

[44] Pierres A, Benoliel A, Bongrand P. Cell fitting to adhesive surfaces: A prerequisite to firm attachment and subsequent events. Eur Cell Mater 2002;3:31-45.

[45] Pavalko F, Norvell S, Burr D, Turner C, Duncan R, Bidwell J. A model for mechanotransduction in bone cells: The load-bearing mechanosomes. J Cell Biochem 2003;88:104-112.

[46] Orr A, Helmke B, Blackman B, Schwartz M. Mechanisms of mechanotransduction. Dev Cell 2006;10:11-20.

[47] Dalby M, Biggs M, Gadegaard N, Kalna G, Wilkinson C, Curtis A. Nanotopographical stimulation of mechanotransduction and changes in interphase centromere positioning. J Cell Biochem 2007;100:326-338.

[48] Ingber D. From cellular mechanotransduction to biologically inspired engineering: 2009 Pritzker Award Lecture, BMES Annual Meeting October 10, 2009. Ann Biomed Eng 2010;38:1148-1161.

[49] Noble B, Peet N, Stevens H, Brabbs A, Mosley J, Reilly G, Reeve J, Skerry T, Lanyon L. Mechanical loading: Biphasic osteocyte survival and targeting of osteoclasts for bone destruction in rat cortical bone. Am J Physiol Cell Physiol 2003;284:C934–C943.

[50] Scott A, Khan K, Heer J, Cook J, Lian O, Duronio V. High strain mechanical loading rapidly induces tendon apoptosis: An ex vivo rat tibialis anterior model. Br J Sports Med 2005;39:1-4.

[51] Egerbacher M, Arnoczky S, Caballero O, Lavagnino M, Gardner K. Loss of homeostatic tension induces apoptosis in tendon cells: An in vitro study. Clin Orthop Relat Res 2008;466:1562-1568.

[52] Kuo Y, Wu L, Sun J, Chen M, Sun M, Tsuang Y. Mechanical stress-induced apoptosis of nucleus pulposus cells: An in vitro and in vivo rat model. J Orthop Sci 2014;19:313-322.

[53] Fowlkes J, Bunn R, Liu L, Wahl E, Coleman H, Cockrell G, Perrien D, Lumpkin C, Thrailkill K. Runt-related transcription factor 2 (RUNX2) and RUNX2-related osteogenic genes are down-regulated throughout osteogenesis in type 1 diabetes mellitus. Endocrinology 2008;149:1697-1704.

[54] Wu C, Miron R, Sculean A, Kaskel S, Doert T, Schulze R, Zhang Y. Proliferation, differentiation and gene expression of osteoblasts in boron-containing associated with dexamethasone deliver from mesoporous bioactive glass scaffolds. Biomater 2011;32:7068-7078.

[55] Khan M, Donos N, Salih V, Brett P. The enhanced modulation of key bone matrix components by modified titanium implant surfaces. Bone 2012;50:1-8.

[56] Termine J, Kleinman H, Whitson S, Conn K, McGarvey M, Martin G. Osteonectin, a bone-specific protein linking mineral to collagen. Cell 1981;26:95-105.

[57] Posey K, Hecht J. The role of cartilage oligomeric matrix protein (COMP) in skeletal disease. Curr Drug Targets 2008;9:869-877.

[58] Geng H, Carlsen S, Nandakumar K, Holmdahl R, Aspberg A, Oldberg A, Mattsson R. Cartilage oligomeric matrix protein deficiency promotes early onset and the chronic development of collagen-induced arthritis. Arthr Res & Ther 2008;10:R134.

[59] Kiani C, Chen L, Wu Y, Yee A, Yang B. Structure and function of aggrecan. Cell Res 2002;12:19-32.

[60] Hardingham T, Fosang A, Dudhia J. The structure, function and turnover of aggrecan, the large aggregating proteoglycan from cartilage. Eur J Clin Chem Clin Biochem 1994;32:249-257.

[61] Engler A, Sen S, Sweeney H, Discher D. Matrix elasticity directs stem cell lineage specification. Cell 2006;126:677-689.

[62] Evans N, Minelli C, Gentleman E, LaPointe V, Patankar S, Kallivretaki M, Chen X, Roberts C, Stevens M. Substrate stiffness affects early differentiation events in embryonic stem cells. Eur Cell Mater 2009;18:1-14.

[63] Keogh M, O'Brien F, Daly J. Substrate stiffness and contractile behaviour modulate the functional maturation of osteoblasts on a collagen–GAG scaffold. Acta Biomater 2010;6:4305-4313.

[64] Mullen C, Haugh M, Schaffler M, Majeska R, McNamara L. Osteocyte differentiation is regulated by extracellular matrix stiffness and intercellular separation. J Mech Behav Biomed Mater 2013;28:183-194.

[65] Gelain F, Panseri S, Antonini S, Cunha C, Donega M, Lowery J, Taraballi F, Cerri G, Montagna M, Baldissera F, Vescovi A. Transplantation of nanostructured composite scaffolds results in the regeneration of chronically injured spinal cords. ACS Nano 2011;5:227-236.

[66] Weightman A, Jenkins S, Pickard M, Chari D, Yang Y. Alignment of multiple glial cell populations in 3D nanofiber scaffolds: Toward the development of multicellular implantable scaffolds for repair of neural injury. Nanomedicine 2014;10:291-295.

[67] Binan L, Tendey C, De Crescenzo G, El Ayoubi R, Ajji A, Jolicoeur M. Differentiation of neuronal stem cells into motor neurons using electrospun poly-L-lactic acid/gelatin scaffold. Biomater 2014;35:664-674.

[68] Xu L, Cao D, Liu W, Zhou G, Zhang W, Cao Y. In vivo engineering of a functional tendon sheath in a hen model. Biomater 2010;31:3894-3902.

[69] Ngiam M, Liao S, Patil A, Cheng Z, Chan C, Ramakrishna S. The fabrication of nano-hydroxyapatite on PLGA and PLGA/collagen nanofibrous composite scaffolds and their effects in osteoblastic behavior for bone tissue engineering. Bone 2009;45:4-16.

[70] Prabhakaran M, Venugopal J, Ramakrishna S. Electrospun nanostructured scaffolds for bone tissue engineering. Acta Biomater 2009;5:2884-2893.

[71] Cipitria A, Lange C, Schell H, Wagermaier W, Reichert J, Hutmacher D, Fratzl P, Duda G. Porous scaffold architecture guides tissue formation. J Bone Miner Res 2012;27:1275-1288.

[72] Chen H, Huang J, Yu J, Liu S, Gu P. Electrospun chitosan-graft-poly (ε -caprolactone)/poly (ε-caprolactone) cationic nanofibrous mats as potential scaffolds for skin tissue engineering. Int J Biol Macromol 2011;48:13-19.

[73] Yang Y, Xia T, Chen F, Wei W, Liu C, He S, Li X. Electrospun fibers with plasmid bFGF polyplex loadings promote skin wound healing in diabetic rats. Mol Pharm 2011;9:48-58.

[74] Vatankhah E, Prabhakaran M, Jin G, Ghasemi-Mobarakeh L, Ramakrishna S. Development of nanofibrous cellulose acetate/gelatin skin substitutes for variety wound treatment applications. J Biomater Appl 2014;28:909-921.

Chapter 4

Summary and Future Studies

4.1. Introduction

Implantable devices are developing rapidly from their once primitive form of merely providing similar mechanical properties to the tissue to be replaced, to devices that closely imitate native tissue supramolecular assemblies and provide control over cellular functions. Cells, *in vivo*, are exposed to a wide variety of topographical features (e.g. fibres with diameter range from nano- to micro- scale), with each tissue niche providing an entirely unique topography profile. Cell shape is vital for a number of functions, including phenotype maintenance, differentiation, tissue organisation and ECM remodelling [1-3]. Therefore, engineering an *in vitro* environment, which promotes physiological cell morphology is essential for tissue engineering and regenerative medicine applications.

Cell-substrate interactions at the substrate interface are becoming increasingly important in our understanding of a range of physiological processes [4]. For example, textured substrates have been shown to favourably promote cell attachment, migration and differentiation, since they closely imitate the *in vivo* niche [5-7]. However, to facilitate clinical translation of such technologies, it is important to fully comprehend the influence of topography at cellular and molecular level, and to use this knowledge to design the next generation of textured biomaterials. With advances in fabrication techniques, there is an increasing ability to create biomaterials with precise topographical features from nano- to micro- scale that will interact with cells and provide physical cues.

This project aimed to developed two- and three- dimensional constructs from commercially available biomaterials to provide control over cellular functions in *vitro* and *in vivo*. This project investigated two nano-technology processing techniques, electro-spinning and imprinting lithography. Both of these techniques demonstrated

the ability to support cellular attachment, proliferation and directional cell growth *in vitro*. Imprinting failed to induce directional tissue formation *in vivo*.

4.2. Summary

In chapter 2, electro-spinning was used to create anisotropic PLGA fibrous mats, due to the versatility of the process [8]. The influence of the fibrous meshes on bovine tenocytes was subsequently assessed. Strikingly, tenocytes orientated perpendicularly to the substrate topography, when they were seeded onto aligned orientated electro-spun mats, suggesting that multifactorial approaches (e.g. topography and mechanical loading) should be introduced to fully control cellular functions.

In chapter 3, imprinting lithography was employed to assess the influence of precise topographical features on tenocyte response. Cell morphometric analysis revealed that anisotropic substrates with groove depth of ~317 nm and ~1988 nm promoted human tenocyte alignment parallel to underlined topography *in vitro*, whilst substrates with groove depth of ~37 nm were too shallow to induce morphological changes. Gene analysis indicated that chondrogenic and osteogenic genes were upregulated, most likely due to the rigidity mismatch between the tendon tissue and the PLGA substrates, once more suggesting that multifactorial approaches (e.g. substrate rigidity and surface stiffness) should be employed introduced to fully control cellular functions *in vitro*. The most significant finding herein was that none of the imprinted substrates was able to induce directional neotissue growth. This finding indicates that three-dimensional nano- and micro-fibrous constructs that allow cell penetration within the three-dimensional fibrous matrix induce cell-guidance and neotissue growth within this contained / restricted architecture / environment, whilst two-dimensional constructs are only suitable for *in vitro* studies.

4.3. Future Studies

The following section is dedicated to the possible future projects that may follow up based on the outcomes and limitation encountered during this work.

4.3.1. Dynamic Environment

In this thesis, the influence of anisotropic topographies on tenocyte growth was evaluated under no mechanical tension; thus bovine tenocytes may have aligned perpendicular to the substrate topography. Recent studies clearly demonstrate that mechanical loading is necessary to maintain tenocyte phenotype *in vitro* [9-11]. Therefore, future studies need to investigate the influence of dynamic environment on cell phenotype maintenance.

4.3.2. Substrate Rigidity

In this thesis, we also assessed the influence of surface topography on tenocyte function. However, we identified that very rigid substrates induce trans-differentiation of tenocytes towards chondrogenic / osteogenic lineage. This is not surprisingly, given that substrate rigidity is an important modulator of the *in vitro* microenvironment [22, 23]. Thus, it is imperative to identify the optimal substrate rigidity for tenocyte phenotype maintenance *in vitro*.

4.3.3. Macromolecular Crowding

This research has demonstrated that anisotropic substrates with features significantly smaller than tenocytes can influence the growth and morphology of the seeded cells, creating confluent aligned and elongated cultures of tenocytes. However, in traditional culture conditions, extracellular matrix deposition is very slow. Therefore, the next stage of this research could combine topography with the recent advancement in macromolecular crowding (MMC) to aid in the development of scaffold-free constructs for tendon tissue engineering [12-15].

4.4. References

[1] Singhvi R, Kumar A, Lopez G, Stephanopoulos G, Wang D, Whitesides G, Ingber D. Engineering cell shape and function. Science 1994;264:696-698.

[2] Von Der Mark K, Gauss V, Von Der Mark H, Muller P. Relationship between cell shape and type of collagen synthesised as chondrocytes lose their cartilage phenotype in culture. Nature 1977;267:531-532.

[3] McBeath R, Pirone DM, Nelson CM, Bhadriraju K, Chen CS. Cell Shape, Cytoskeletal Tension, and RhoA Regulate Stem Cell Lineage Commitment. Developmental Cell 2004;6:483-495.

[4] Stevens MM. Exploring and Engineering the Cell Surface Interface. Science 2005;310:1135-1138.

[5] Woo KM, Chen VJ, Ma PX. Nano-fibrous scaffolding architecture selectively enhances protein adsorption contributing to cell attachment. Journal of Biomedical Materials Research Part A 2003;67A:531-537.

[6] Tambasco de Oliveira P, Nanci A. Nanotexturing of titanium-based surfaces upregulates expression of bone sialoprotein and osteopontin by cultured osteogenic cells. Biomaterials 2004;25:403-413.

[7] Yim EKF, Leong KW. Significance of synthetic nanostructures in dictating cellular response. Nanomedicine: Nanotechnology, Biology and Medicine 2005;1:10-21.

[8] Liao S, Murugan R, Chan C, Ramakrishna S. Processing nanoengineered scaffolds through electrospinning and mineralization suitable for biomimetic bone tissue engineering. Journal of the Mechanical Behavior of Biomedical Materials 2008;1:252-260.

[9] Jiang Y, Liu H, Li H, Wang F, Cheng K, Zhou G, Zhang W, Ye M, Cao Y, Liu W, Zou H. A proteomic analysis of engineered tendon formation under dynamic mechanical loading in vitro. Biomaterials 2011;32:4085-4095.

[10] Garvin J, Qi J, Maloney M, Banes AJ. Novel system for engineering bioartificial tendons and application of mechanical load. Tissue Eng 2003;9:967-979.

[11] Zhu J, Li J, Wang B, Zhang WJ, Zhou G, Cao Y, Liu W. The regulation of phenotype of cultured tenocytes by microgrooved surface structure. Biomaterials 2010;31:6952-6958.

[12] Chen C, Loe F, Blocki A, Peng Y, Raghunath M. Applying macromolecular crowding to enhance extracellular matrix deposition and its remodeling in vitro for tissue engineering and cell-based therapies. Advanced Drug Delivery Reviews 2011;63:277-290.

[13] Lareu RR, Subramhanya KH, Peng Y, Benny P, Chen C, Wang Z, Rajagopalan R, Raghunath M. Collagen matrix deposition is dramatically enhanced in vitro when crowded with charged macromolecules: The biological relevance of the excluded volume effect. FEBS Letters 2007;581:2709-2714.

[14] Lareu RR, Arsianti I, Subramhanya HK, Yanxian P, Raghunath M. In vitro enhancement of collagen matrix formation and crosslinking for applications in tissue engineering: A preliminary study. Tissue Eng Part A 2007;13:385-391.

[15] Satyam A, Kumar P, Fan X, Gorelov A, Rochev Y, Joshi L, Peinado H, Lyden D, Thomas B, Rodriguez B, Raghunath M, Pandit A, Zeugolis D. Macromolecular crowding meets tissue engineering by self-assembly: A paradigm shift in regenerative medicine. Adv Mater 2014;26:3024-3034.

Appendix

A. Electro-spinning

Materials and Equipment

1. Personal protective equipment
2. Laboratory coat, powder free gloves, face-mask and eye goggles must be used when preparing the solution.
3. All solutions must be prepared inside the fume hood.
4. 50ml centrifuge tubes.
5. Parafilm.
6. Laboratory tube rotator (suitable for 50ml tube).
7. Leur-lock syringes.
8. Leur-lock blunt tip needles.
9. Permitted solvents: Chloroform, Trichloromethane, Dichloromethane, Hexafluoroisopropanol, Tetrahydrofuran.
10. Permitted Biomaterials: Fibrin, collagen, carbon, starch, NIPAM, biodegradable polyesters, composites of the above, proprietary biomaterials.

Procedure

1. Preparing the solution.
2. Weigh the polymer.
3. Place it in a 50ml tube.
4. Add required amount of solvent to the polymer using a Pasteur pipette (to be done in fume hood).
5. Secure cap on tube.
6. Cover with tube cap with Parafilm™.
7. Place in rotating mixer until completely dissolved.

8. Using electro-spinning Rig.

9. Turn on the fume hood.

10. Select the desired mandrel geometry.

11. Cover the mandrel with aluminium foil.

12. Connect the mandrel securely to the rotating motor by completely closing the mandrel chamber.

13. Under a fume hood fill the syringe with the desired amount of polymer solution.

14. Place the syringe in the syringe pump and lock in place.

15. Set the displacement of the syringe pump by adjusting the distance between the two limit switches on the linear table. Set the distance between the tip of the needle and the mandrel by moving the syringe pump platform (the platform should be placed in such a way that the linear table is parallel to the mandrel's longitudinal).

16. Turn the syringe pump on.

17. Set the pump's parameters (syringe diameter, flow rate).

18. Start the syringe pump.

19. Close the fume hood (Verify that the inter-lock on the left of the fume hood is completely closed).

20. Over on the control panel, start the linear table, high voltage supply and rotating motor (never touch any cables, the alligator clip or the needle when the electro-spinning rig is on).

21. In case of formation of any clot of solution on the tip of the syringe stop the entire process (linear table, high voltage supply, rotating motor and syringe pump), clean the tip of the needle and repeat steps 6.11-6.12.

B. Fibre Collection

1. When processing is complete, stop all elements (linear table, high voltage supply, rotating motor and syringe pump).
2. Open the mandrel chamber and remove the mandrel.
3. With a blade, cut the processed construct and aluminium foil along the longitudinal axis of the mandrel.
4. Place the mandrel back in its chamber and close it completely.
5. Remove the syringe from the pump.
6. Dispose of the blunt tipped needle in the sharps bin and place the spent syringe in the sharps disposal bin – do not cover the used needle.
7. Make sure that the electrical supply is turned off at the mains, that the Electro-spinning Rig is cleaned and close the fume-hood before leaving.
8. Substrate prep and sterilisation
9. Cell culture aseptic technique
10. To ensure that the interior of the hood was sprayed with Virkon for 5 minutes and then with 70% IMS.
11. Everything entering the hood was sprayed with 70 IMS
12. Any containers must only be opened within the hood. Any containers opened outside the hood was considered contaminated.

C. Changing Media

1. Tenocytes media was changed every three days.
2. Media and HBSS were placed in the water bath to warm to 37°C.
3. To speed this up first, under the hood, poor out media and HBSS in to 50ml falcon tubes and place these into the water bath.

4. Aseptic technique was used, the flask were removed from the incubator and sprayed with IMS.

5. The cells were viewed with the microscope to check how confluent the cells were and to ensure no contamination.

6. The media was removed from the flask and placed in the waste container, which had Virkon in it.

7. The cells were washed with HBSS and the fresh media was added.

8. The flasks were then returned to the incubator.

D. Passaging Cells

1. When cells reached approximately 80% confluency, they were split into two or more flasks or frozen for later use.

2. Media, HBSS and were placed in the water bath to warm to 37°C.

3. Aseptic technique was used, the flask were removed from the incubator and sprayed with IMS.

4. The media was removed from the flask and placed in the waste container, which had Virkon in it.

5. The cells were washed with HBSS.

6. Trypsin-EDTA (T/E) was added to the flask, ensuring complete coverage of the flask.

7. The flask was returned to the incubator for 5 minutes (enzyme is active at 37°C).

8. The flask was examined under the microscope to see if cells had detached from the surface.

9. Cells should be rounded and floating in the media, if not lightly tapping the flask may remove the remaining cells or replace in the incubator for another 5 minutes. It is not recommended to have the cells in the incubator for longer than 10 minutes.

10. Once cells were detached from the surface the flask is placed back into the incubator

11. Equal volume of media supplemented with 10% serum was added to the flask. This deactivates the trypsin.

12. All of the liquid was then removed and put into a sterile centrifuge tube and centrifuged for 5 minutes at 1200 rpm (placing a counter weight in the centrifuge to ensure it is balanced.

13. The tubes are removed. The cells form a pellet at the bottom of the tube.

14. The supernatant is removed and the pellet is re-suspended in fresh media

a. Use 1ml pipettes to re-suspend the pellet and then add more media if required.

b. Try to minimise the formation of air bubbles when re-suspending cells

15. The cells are then counted and seeded into new flasks.

E. Freezing Cells

1. To freeze cell carry out the passaging protocol.

2. However instead of re-suspending the pellet in to media pen/strp, cells are re-suspended in freezing media. Freezing media consists of media supplemented with 10% FBS and 1% and 10% filtered DMSO. (DMSO is a cryo-protective agent)

3. Generally there is 1 ml per vial, containing 500,000 to 2 million cells.

4. Cells were placed in Mr. Frosty container and placed in the -80°C freezer.

5. Wear protective gloves and face shield when adding cryo-vials from liquid nitrogen cylinder

6. Cells were then put into liquid nitrogen after 24 hours.

F. Thawing Cells

1. Wear protective gloves and face shield when removing cryo-vials from liquid nitrogen cylinder
2. Remove the required number of vials from the liquid nitrogen container.
3. Place the vial in the water bath, just long enough to thaw the solution. Do not cover the vial as this can lead to contamination.
4. Spray the vial with IMS before placing into the hood.
5. DMSO needs to be removed, as it is toxic.
6. Cells are immediately placed in to pre-warmed media in a sterile centrifuge tube.
7. The cells were centrifuged for 5 minutes at 1200 rpm.
8. The supernatant media was aspirated leaving the cell pellet at the bottom of the tube.
9. The cells were re-suspended in media.
10. The cells were counted and plated out at 4000 cells/cm^2.

G. Cell Counting

1. 50 µl of cell suspension was mixed with 50 µl trypan blue
2. 10 µl of the cell/trypan blue solution was added to each side of the haemocytometer
3. Trypan blue is excluded by the live cells and penetrates the dead cells due to their damaged membranes – blue cells are dead, clear cells are alive.

H. Cell Seeding

Please see respectful sections in the thesis.

I. Staining for rhodamine phalloidin and DAPI

Materials

1. HBSS
2. 1x PBS
3. DAPI (0.1% ddH_2O)
4. Rhodamine Phalloidin (1:100)
5. 4% Paraformaldehyde (PFA)
6. TritonX-100 (0.2% PBS)
7. Blocking solution (1% BSA (1x PBS))

Methods

1. Remove media from the cells.
2. Wash the cells twice with HBSS.
3. Fix the cells with 4% PFA for 15mins at room temperature.
4. Wash the cells 3 times with 1x PBS.
5. Permeabilise the cells with Triton X for 5mins at room temperature.
6. Block with the blocking solution for 30 minutes at room temperature. (Optional)
7. Wash the cells 3 times with 1x PBS.
8. Incubate with the rhodamine-phalloidin solution for 30 minutes to one hour, at room temperature, protected from light.
9. Wash the cells 3 times with 1x PBS.

10. Stain the nuclei with DAPI for 5mins at room temperature.

11. Wash the cells four times with 1x PBS and observe using an inverted fluorescence microscope.

J. alamarBlue® Cell Metabolic Activity Assay

Materials:

1. Hank's balanced salt solution
2. AlamarBlue

Methods:

1. Add 1000 μl of Hank's balanced salt solution into the required number of wells in the sterile 24 well plate i.e. same number as samples to be tested.
2. Make up the solution of AlamarBlue® in Hank's balanced salt solution (ratio 1:9 respectively). 500 μl is required per well.
3. Transfer the seeded scaffolds/tissue culture inserts from their original well plate to the Hanks solution well plate using the sterile tweezers.
4. Remove the Hanks solution from each well.
5. Cover the scaffolds and positive control (empty wells washed with Hanks) with 500µl of the alamarBlue® in Hank's balanced salt solution (ratio 1:9).
6. Incubate for 2 hours at 37°C
7. After incubating for 2 hours, transfer 200 µl of the dye into the clear 96 well plate
8. Measure the absorbance at 550 nm and 595 nm (0.5 seconds per well).
9. Calculate a viability value according to 'simplified method of calculating % reduction' available in the alamarBlue® handbook.

10. Subtract the absorbance values of Hank's balanced salt solution only from the absorbance values of the alamarBlue® in Hank's balanced salt solution (ratio 1:9). AO_{LW} = absorbance of oxidized form at lower wavelength, and AO_{HW} = absorbance of oxidized form at higher wavelength.

11. Calculate correlation factor: R_O.

12. $R_O = AO_{LW}/AO_{HW}$

13. To calculate the % of reduced alamarBlue™:

14. $AR_{LW} = A_{LW} – (A_{HW} \times R_O) \times 100$

K. Live/Dead Assay

1. Take kit out of freezer, defrost tubes

2. Place in the centrifuge for a few seconds to ensure contents are at the bottom of the tube

3. Media was removed from chamber/wells and cells were was washed with HBSS

4. For a dead control immerse cells in 70 % Methanol

5. Prepare staining solution

a. Calcein (live) is at 4 mM concentration in the tube. Use 4 μl

b. Dilute 1:1000 – 5 μl in 5 ml

6. Ethidium homoimer-1 (dead) is at 2 mM. Use at 2 μM

a. Dilute 1:1000 – 5 μl in 5 ml

7. Protect from light

8. Add enough stain to cover the substrates

9. Incubate for 30 minutes

10. The live cells were imaged using FITC filter and the dead cells were imaged using the Texas red filter.

11. Proliferation Protocol

L. RNA Extraction Protocol

1. At the predefined time to analyse cells for RNA content, wash scaffold/cells with Hanks balanced Salt solution.

2. Microbiology Hood Ground Floor Lab

3. Add 0.250 μl (12-well chamber slide, double for 8well chamber slide) of TRI Reagent® to wells containing scaffolds/cells.

4. Homogenize samples using the tip of a pipette (using a scrapping motion on entire surface, then aspirate 4-6 times) being careful not to contaminate adjacent wells. Make sure scaffolds have been completely homogenized.

5. Using a 1 ml pipette tip, aspirate the solution repetitively.

6. Store homogenate for 5 minutes at room temperature to dissociate nucleoprotein complexes.

7. Remove the TRI Reagent® solution to a sterile 1.5 ml eppendorf.

8. Note: Tri/Lysate solution can be frozen at this point at -80 °C for approximately a month.

9. Add 50 μl of chloroform per 0.25 ml of TRI Reagent®.

10. Sake vigorously for 15 seconds by inversion.

11. Incubate for 15 minutes at room temperature.

12. Centrifuge at 12,000 g for 15 minutes at 4 °C. Following the centrifugation, 3 phases will appear; -a lower red phenol-chloroform phase, an inter-phase, and an aqueous phase (translucent). mRNA is located within the aqueous phase.

13. Remove the clear upper aqueous phase (~ 100 μl) to a sterile eppendorf. Be careful not to touch the interface. Leave a little of the upper phase to avoid contact with the interface.

14. Slowly add 1 volume of 70% ethanol and mix by inversion.

15. Add sample from step 12 to RNeasy column.

16. Centrifuge at 8,000 g for 15 seconds and discard the collected solution.

17. Repeat step 13 and 14 for remaining sample.

18. Add 350 μl of RW1 buffer to centre of column, centrifuge at 8,000 g for 15 seconds. Discard the collected solution.

19. Transfer column to new collection tube. Add 500 μl RPE to centre of column, centrifuge at 8,000 g for 15 seconds. Discard the collected solution.

20. Add 500 μl RPE to centre of column, centrifuge at 8,000 g for 2 seconds. Discard the collected solution.

21. Transfer column to a new 1.5 ml eppendorf. Add 20 μl RNase-free water onto the column, incubate at room temperature for 1 minute and centrifuge for 1 minute at 8,000 g.

22. Place the flow through solution onto the column again, incubate at room temperature for 1 minute and centrifuge at 8,000 g for 1 minute.

23. MDRG Lab NanoDrop

24. Determine the concentration using the NanoDrop and freeze at -80 °C.

25. Calibrate the spectrometer with water.

26. Place 1-1.2 μl on the nanodrop. The purity is determined from the ratio between A260 and A280. The ratio A260/A280 should be above 1.8 to indicate a pure form of RNA.

27. Print of report and place in lab book comment on any irregularities.

M. Surgery Protocols

Equipment needed:

1. Scalpel handle
2. Toothed forceps
3. Fine tip forceps
4. Scissors
5. Sutures holders
6. Biopsy punches
7. Metal bowls
8. Cotton swabs
9. 2 mm biopsy punch

Surgery room Prep

1. Wipe down surgery table with Virkon and IMS.
2. Ensuring not to touch the surgical side place two green surgical drapes on the table.
3. Place a heating pad under the drape intended for surgery. (These turn off automatically, ensure they stay on throughout the surgeries.
4. Place surgical equipment on the table without touching with gloves.
5. Place iodine and IMS in to the two metal bowls.
6. Cut up a surgical drape to cover the animal during surgery.
7. Ensure adequate clean cages are prepared for after surgery.

Animals

1. Species: Rats
2. Strain: Lewis
3. Specifications: 200-350 g of weight
4. Sex: female

Surgery

1. At time 0, rats will be weighed and a health check conducted.
2. Anaesthetize animal using isoflorane (5% reducing to 1-2%).
3. Shave both legs.
4. Clean both legs with iodine solution.
5. Place animal on the surgery table and secure the anaesthetic mask and cove the rest of the animal.
6. Put on the surgical gloves.
7. Create an incision through the skin (~1 cm) by the side of the right knee.
8. Open the fascia above the patellar tendon carefully, avoiding creating injury.
9. Clean wound area once patellar tendon is exposed
10. Using a biopsy punch (2 mm) an injury will be made in the centre of the patellar tendon
11. The construct will be inserted into or over the injured area and sutured.
12. The wound area will be closed in layers
13. A second construct may be inserted subcutaneously before closing the skin in order to compare the effects of the construct in the tendon to the effects of the construct in unloaded tissue.
14. On the left side, the same surgery will be done inserting the removed biopsy from the first as an autograft control.

N. Post-operative Care

1. The health of the animals will be monitored daily immediately following surgery and a comprehensive analysis will be conducted and recorded weekly. This analysis will consist of functional evaluation of the tendon to ensure that it has not ruptured and to compare the relative efficacies of the various constructs.
2. At each time point, the animals will be euthanized and the samples explanted for analysis.

O. Picro Sirius Red Staining

1. Wash cryosection slides in ddH_2O
2. Place in Weigerts Haemotoxylin for 8 minutes
3. Rinse in running tap water for 5 minutes
4. Stain in 0.2% phosphomolybdic acid hydrate for 2 minutes (make fresh)
5. Rinse in distilled water
6. Stain in Picro-Sirius red for 1 hour
7. Wash in acidified water
8. Place in 80%, 95%, 100% ethanol for 10 seconds in each bath
9. Dehydrate in two changes of xylene

P. Haematoxylin and Eosin Staining

1. Wash in $H_2O$for 30 seconds
2. Mayer hematoxylin for 5 minutes
3. Rinse in running water for 1-10 minutes
4. To optimize start of low and increase if needed
5. 1% eosin y for 10 -30 seconds
6. Wash 3 times in h_2o
7. Place in 70% EtOH 30 sec
8. Place in 90% EtOH 30 sec
9. Place in100% EtOH 30 sec
10. Dehydrate in two changes of xylene

Q. Outputs

Manuscripts

1. Azeem, A., **English, A.**, Kumar, P., Satyam, A., Biggs, M., Jones, E., Tripathi, B., Basu, N., Henkel, J., Vaquette, C., Rooney, N., Riley, G., O'Riordan, A., Cross, G., Ivanovski, S., Hutmacher, D., Pandit, A., Zeugolis, D.I. The influence of anisotropic nano- to micro- topography on in vitro and in vivo osteogenesis. Nanomedicine (Future in Medicine), In Press. Impact Factor 2013: 5.26.

2. Cigognini, D., Lomas, A., Kumar, P., Satyam, A., **English, A.**, Azeem, A., Pandit, A., Zeugolis, D. Engineering in vitro microenvironments for cell-based therapies and drug discovery. Drug Discovery Today, Vol. 18, No. 21-22, pp. 1099-1108 (2013). Impact Factor 2011: 6.828.

3. **English, A.**, Azeem, A., Gaspar, D.A., Keane, K., Kumar, P., Keeney, M., Rooney, N., Pandit, A., Zeugolis, D.I. Preferential cell response to anisotropic electro-spun fibrous scaffolds under tension-free conditions. Journal of Materials Science: Materials in Medicine, Vol. 23, No. 1, pp. 137-148 (2012). Impact Factor 2011: 2.316.

4. **English, A.**, Azeem, A., Biggs, M., Jones, E., Tripathi, B., Basu, N., Rooney, N., Riley, G., O'Riordan, A., Cross, G., Hutmacher, D., Pandit, A., Zeugolis, D.I. Substrate topography: Dimension-dependent contact guidance is not translated into a tenogenic preclinical host response. Biomaterials, Submitted. Impact Factor 2012: 7.404.

Book Chapters

1. Lomas, A., **English, A.**, Biggs, M., Pandit, A., Zeugolis, D.I. Engineering anisotropic 2D and 3D structures for tendon repair, in Tendon regeneration: Understanding tissue physiology and development to engineer functional substitutes. Elsevier Science. Editors: Reis, R.L., Gomes, M.E., Rodrigues, M.T. Submitted.

Abstract Publications

1. **English, A.**, Azeem, A., Tripathi, B., Jones, E., Legerlotz, K., Riley, G., Cross, G., Rooney, N., Pandit, A., Zeugolis, D. Human tenocyte response to nano-topographic interfaces and implications on medical device design. Journal of Tissue Engineering and Regenerative Medicine, Vol. 6, pp. 229-229 (2012).

Conference Papers

1. 10/2013: **English, A.**, Gaspar, D., Sweeney, I., Satyam, A., Holladay, C., Lomas, A., Abbah, S.A., Miraftab, M., O'Dowd, C., Pandit, A., Zeugolis, D.I. Scaffold and scaffold-free strategies towards tendon repair. Podium Presentation at 8th Combined Meeting of Orthopaedic Research Societies (CORS), 13th to 16th of October 2013, Venice, Italy.
2. 09/2013: **English, A.**, Gaspar, D., Sweeney, I., Satyam, A., Holladay, C., Lomas, A., Miraftab, M., O'Dowd, C., Pandit, A., Zeugolis, D. Scaffold and scaffold-free strategies towards tendon repair. Podium Presentation at European Society for Biomaterials, 8th to 12th of September 2013, Madrid, Spain.
3. 06/2013: **English, A.**, Gaspar, D., Sweeney, I., Satyam, A., Holladay, C., Lomas, A., Abbah, S., Miraftab, M., O'Dowd, C., Pandit, A., Zeugolis, D.I. Scaffold

and scaffold-free strategies towards tendon repair. Podium Presentation at TERMIS, EU Meeting, 17-20 of June 2013, Istanbul, Turkey.

4. 06/2013: **English, A.**, Gaspar, D., Sweeney, I., Satyam, A., Holladay, C., Lomas, A., Abbah, S., Miraftab, M., O'Dowd, C., Pandit, A., Zeugolis, D.I. Scaffold and scaffold-free strategies towards tendon repair. Poster Presentation at TERMIS, EU Meeting, 17-20 of June 2013, Istanbul, Turkey.

5. 09/2012: **English, A.**, Azeem, A., Holladay, C., Tripathi, B., Jones, E., Legerlotz, K., Cross, G., Rooney, N., Riley, G., Hutmacher, D., Pandit, A., Zeugolis, D. Preferential cell response to anisotropic nano-topography. Poster presentation at Nanoweek, 14th to 21st of September 2012, Dublin, Ireland.

6. 09/2012: **English, A.**, Azeem, A., Tripathi, B., Jones, E., Legerlotz, K., Riley, G., Cross, G., Rooney, N., Pandit, A., Zeugolis, D. Human tenocyte response to nano-topographic interfaces and implications on medical device design. Podium Presentation at 3rd TERMIS World Congress 2012, 5th to 8th of September 2012, Hofburg Congress Centre, Vienna, Austria.

7. 09/2012: **English, A.**, Satyam, A., Holladay, C., Meirovitch, S., Tripathi, B., Jones, E., Legerlotz, K., Shoseyov, O., Cross, G., O'Dowd, C., Rooney, N., Rodriguez, B., Riley, G., Pandit, A., Zeugolis, D. Scaffold and scaffold-free strategies towards tendon repair. Podium Presentation at Tendinopathy: From basic science to treatment, British Society for Matrix Biology meeting, 3rd to 4th of September 2012, Norwich, UK.

8. 06/2012: Azeem, A., **English, A.**, Tripathi, B., Jones, E., Rooney, N., Legerlotz, K., Riley, G., Cross, G., Hutmacher, D., Pandit, A., Zeugolis, D. Guiding osteoblast behaviour at the nano-bio-interface by anisotropically ordered surfaces. Poster Presentation at Royal Academy of Medicine in Ireland (RAMI), Section of

Biomedical Sciences, Bailey Allen Hall, National University of Ireland Galway, 14th of June 2012, Galway, Ireland.

9. 06/2012: **English, A.**, Azeem, A., Jones, E., Legerlotz, K., Rooney, N., Riley, G., Pandit, A., Zeugolis, D. Tenocytes align perpendicular to the substrate topography in the absence of mechanical loading. Podium Presentation at 9th World Biomaterials Congress, Chengdu, China, 1-5 June, 2012.

10. 06/2012: Azeem, A., **English, A.**, Jones, E., Rooney, N., Legerlotz, K., Riley, G., Hutmacher, D., Pandit, A., Zeugolis, D. The influence of nano-topographical cues on cellular behaviour of bone-like cells. Podium Presentation at 9th World Biomaterials Congress, Chengdu, China, 1-5 June, 2012.

11. 09/2011: **English, A.**, Azeem, A., Rooney, N., Pandit, A. and Zeugolis, D.I. Guiding bone-like cellular behaviour at the nano-bio-interface. Poster Presentation at the 24th European Society for Biomaterials, 4th-8th of September, Dublin, Ireland, 2011.

12. 09/2011: **English, A.**, Rooney, N., Pandit, A. and Zeugolis, D.I. Nano-textured biomaterials and cell interaction at the nano-bio-interface. Rapid Fire Podium Presentation at the 24th European Society for Biomaterials, 4th-8th of September, Dublin, Ireland, 2011.

13. 09/2011: Raj, J., **English, A.**, D'Sa, R.A., Dickinson, P.J., Zeugolis, D.I., Brown, A. and Meenan, B.J. Response of endothelial cells to poly (L-lactide-co-ε-caprolactone) (PLCL) membranes. Rapid Fire Podium Presentation at the 24th European Society for Biomaterials, 4th-8th of September, Dublin, Ireland, 2011.

14. 04/2011: **English, A.**, Rooney, N., Pandit, A. and Zeugolis, D.I. Topographical cues – Controlling cellular behaviour. Poster Presentation at 2011 Joint Research Day between NUI Galway and University of Limerick, Galway, Ireland

15. 06/2011: **English, A.**, Rooney, N., Pandit, A. and Zeugolis, D.I. Soft tissue cell behaviour influenced by the nano-bio-interface. Poster Presentation at the 7th NanoBio-Europe Conference, 21st-23rd of June, Cork, Ireland, 2011.

16. 06/2011: **English, A.**, Rooney, N., Pandit, A. and Zeugolis, D.I. Soft tissue cell behaviour influenced by the nano-bio-interface. Podium Presentation as part of the Young Researcher Session, at the 7th NanoBio-Europe Conference, 21st-23rd of June, Cork, Ireland, 2011.

17. 06/2011: **English, A.**, Azeem, A., Rooney, N., Pandit, A. and Zeugolis, D.I. Surface functionalisation: Human bone-like cell response to a range of nano-topographies. Poster Presentation at the 7th NanoBio-Europe Conference, 21st-23rd of June, Cork, Ireland, 2011.

18. 06/2011: **English, A.**, Rooney, N., Pandit, A., Zeugolis, D.I. Evaluation of cellular functions at the nano-bio-interface. Podium Presentation at the Tissue Engineering Regenerative Medicine International Society - EU Meeting, 7th-10th of June, Granada, Spain, 2011.

19. 04/2011: **English, A.**, Rooney, N., Pandit, A. and Zeugolis, D.I. Topographical cues – Controlling cellular behaviour. Poster Presentation at the 2011 Joint Research Day between NUI Galway and University of Limerick, 5th of April, Galway, Ireland, 2011.

20. 01/2011: **English, A.**, Rooney, N., Pandit, A. and Zeugolis, D.I. Topographical cues for cellular guidance. Poster Presentation at the Nanoweek 2011 Conference, 31st of January to 1st of February, Kildare, Ireland, 2011.

21. 10/2010**: English, A.**, Keeney, M., Rooney, N., Pandit, A. and Zeugolis, D.I. Topographical cues for cellular guidance. Poster Presentation at the 12th Surface

Science of Biologically Important Interfaces Conference, 27th of October, Belfast, Northern Ireland, 2010.

Patents

1. Zeugolis, D.I., **English, A.**, Azeem, A. Identifying optimal topography to control cellular function and neotissue formation. Publication Number: WO2012168466 A1, Publication Date: 13/12/2012, Application Number: PCT/EP2012/060946.

Awards

1. Second Best Podium Presentation at Tissue Engineering and Regenerative Medicine World Congress, Vienna, Austria, 5^{th} – 8^{th} September2012.
2. Winner of Young Investigator Travel Award for Tissue Engineering and Regenerative Medicine World Congress, Vienna, Austria, 5^{th} – 8^{th} September2012.
3. Winner of Best Poster Presentation at the Scientific Surfaces for Biologically Important Interfaces Conference, Belfast, Northern Ireland 27^{th} October 2010
4. Winner of Best Poster Presentation at the NanoBio Europe Conference, Cork, Ireland June 2011

Courses

1. Completed a course on Nanotechnology Entrepreneurship, 19th April 2012, University of Nottingham, Funded by CANN.
2. Completed LAST course, January 2011, Trinity College Dublin.